ILLUMINATING THE STRUCTURE AND FUNCTION OF BCE ANTIMICROBIAL PEPTIDE RESISTANCE MODULES THROUGH CRYO-EM

By

Natasha George

A DISSERTATION

Submitted to
Michigan State University
in partial fulfillment of the requirements
for the degree of

Microbiology and Molecular Genetics – Doctor of Philosophy

2024

ABSTRACT

The bacterial cell envelope is critical for maintaining cell structure and providing a barrier against environmental stressors, necessitating diverse strategies for repairing and defending these layers from external threats. In Firmicutes, one widespread strategy is to use Bce modules - membrane protein complexes that unite a peptide-detoxifying ABC transporter with a stress response coordinating two-component system. These modules provide specific, front-line defense for a wide variety of antimicrobial peptides and small molecule antibiotics as well as coordinate responses for heat, acid, and oxidative stress. Because of these abilities, Bce modules play important roles in virulence and the development of antibiotic resistance in a variety of pathogens. Despite their importance, Bce modules are still poorly understood, with scattered functional data in only a small number of species.

In this work, I investigated Bce module function from a structural biology angle, using cryo-electron microscopy to capture snapshots of the *B. subtilis* BceABRS bacitracin resistance system. Chapter 2 describes acquisition of structures of the BceAB transporter in multiple conformations, which revealed unique features of this unusual ABC transporter that may underlie removal of antimicrobial peptides from the cell membrane. This work was followed up by studies of the full BceAB-S transporter-histidine kinase complex (Chapter 3) that revealed how the two halves of the membrane-bound portion of Bce module interact and regulate each other's function. While many questions remain about Bce module function, the structures and biochemical assays in these studies provide a framework with which to interpret earlier mutational studies and reveal new mechanistic details of Bce-mediate antimicrobial peptide resistance. Finally, Chapters 1 and 4 are adapted from a review that provides a much-needed synthesis of functional data on Bce modules across all the species in which they have been studied. Understanding these multifunctional membrane complexes will enhance our understanding of bacterial stress sensing and may point toward new therapeutic targets for highly resistant pathogens.

TABLE OF CONTENTS

CHAPTER 1: INTRODUCTION

This chapter is adapted from a review published as: **George, N. L**., Bennett, E.C. & Orlando, B. J. Guarding the Walls: The Multifaceted Roles of Bce Modules in Cell Envelope Stress Sensing and Antimicrobial Resistance. *J Bacteriol* 0:e00123-24 (2024).

Cell Wall Synthesis As A Major Target for Antimicrobial Peptides

As the outermost layer of the gram-positive cell, the cell wall is critical for protection from environmental stressors and maintenance of cell homeostasis. However, these characteristics also make the cell wall an accessible and valuable target for antimicrobial peptides (AMPs). To maintain this critical layer of "armor," bacteria carefully regulate cell wall synthesis and coordinate an array of cell envelope stress sensing systems to ensure that cell wall construction, remodeling, and repair are unhindered by external stressors.

At the heart of cell wall maintenance is the lipid II cycle, the process by which peptidoglycan subunits are constructed and carried across the cytoplasmic membrane for addition onto the wall. In this process, N-acetyl muramic acid pentapeptide and N-acetylglucosamine are added to the lipid undecaprenyl phosphate (UP) sequentially to produce lipid II, which is flipped across the membrane to expose the peptidoglycan subunit to the cell wall (1). From here, transglycosylases and transpeptidases connect the new unit to the existing meshwork of peptidoglycan, and the lipid II carrier, now undecaprenyl pyrophosphate (UPP), is dephosphorylated back to UP and returned to the cytoplasmic face of the membrane for the next round of the cycle. The undecaprenyl lipids for cell wall synthesis are in limited supply, necessitating regulation of peptidoglycan synthesis and defense mechanisms to protect this highly sensitive process from damage (2).

Despite the cell's defense mechanisms, many antimicrobial peptides (AMPs) target key intermediates of the cell envelope. Antimicrobial peptides that attack each step along the lipid II pathway have been identified, from lipid-II binding vancomycin to UPP-binding bacitracin (Fig. 1.1A). Some of these cell envelope-targeting AMPs, such as bacitracin, nisin, vancomycin, and daptomycin have already found clinical or industrial applications, while many more have gone into clinical trials or been proposed as potential therapeutics (3,4). AMPs such as teixobactin, malacidin, and clovibactin that target the critical peptidoglycan carrier lipid II have been highlighted for their ability to bind a highly-conserved target and efficacy against highly-resistant pathogens (5-8).

Antimicrobial peptides that target the cell envelope are highly diverse in structure and synthesis. Many, but not all cell-wall targeting antimicrobial peptides are cationic, encouraging interaction with negatively-charged phospholipids on the cell membrane (9). AMPs adopt a variety of three-dimensional structures, and often contain unusual amino acids or modifications,

such as the glycopeptides vancomycin and teicoplanin; enduracididine-containing enduracidin, ramoplanin and teixobactin; and lantibiotics, which are characterized by post-translational modification of Cys residues to form lanthionine and 3-methyllanthionine (10-13). AMPs are also produced either ribosomally (such as nisin) or non-ribosomally (such as bacitracin), and can be produced by bacteria (including the diverse group of bacteriocins produced by gram-positive bacteria) or by eukaryotes as part of the innate immune system. Some AMPs produced by host innate immune systems include the structurally-diverse cathelicidins (such as human LL-37) and the disulfide-bonded defensins (such as hBD3)**.** Both families of host-produced innate immune peptides are produced as propeptides that undergo processing to their mature forms, which can have both antimicrobial and immune-modulatory functions (14,15).

Mechanisms of action of AMPs depends on their structure and primary cell envelope target. AMPs such as bacitracin and vancomycin, which bind to lipid II-cycle intermediates UPP and lipid II respectively, cause cell damage by blocking these lipids from downstream recycling, stalling cell wall synthesis and repair through depletion of the free lipid pool. Other AMPs work primarily by reducing membrane integrity directly. These peptides form pores through entry of the peptide structure into the lipid bilayer, by "carpeting" the membrane to restrict lipid movement, or by causing aggregation of membrane and cell wall components (9). Some AMPs may have dual functions. For example, nisin binds to lipid II to prevent incorporation of peptidoglycan subunits into the cell wall and is also able to form pores in the membrane (16). Similarly, host-derived defensins such as hBD3 and plectasin may have efficacy against both gram-positive and gram-negative bacteria by both disrupting membrane integrity and targeting lipid II (15). In many cases, these effects are concentration-dependent, with AMPs killing cells through different mechanisms depending on the amount of peptide on the cell membrane.

Resistance to AMPs is predicted to develop more slowly than to small molecule antibiotics, making these molecules valuable alternatives to traditional therapeutics (3). However, the development of resistance does occur, as seen with vancomycin resistant *Staphylococcus* and *Enterococcus* species (17,18). Many bacteria possess innate defenses to specific AMPs and have been observed to evolve increased resistance to antimicrobial peptides over time, necessitating further study into the mechanisms of AMP defenses and resistance potential for future AMP therapeutics (19).

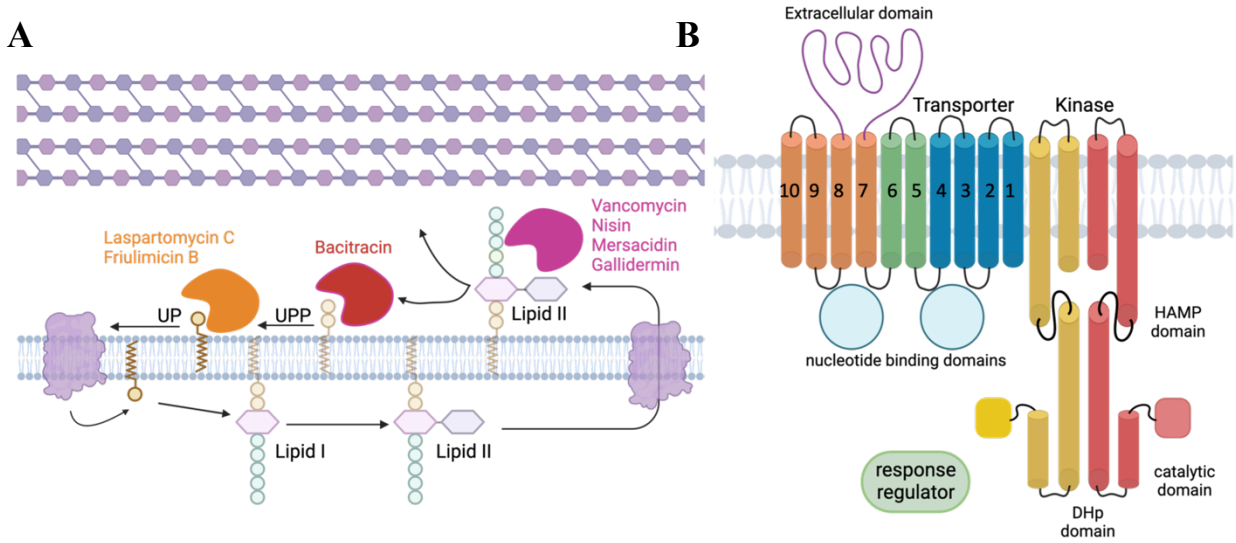

Figure 1.1: A variety of antimicrobial peptides bind to lipid II cycle intermediates to impair cell wall synthesis (A). Bce modules at their simplest consist of a 10-TM helix ABC transporter with a large extracellular domain and a two-component system that includes an intramembrane histidine kinase (B).

Bce Modules: Widespread All-In-One Sensing and Resistance Machines

In Firmicutes, a common strategy to resist cell envelope-targeting AMPs involves membrane protein complexes called Bce modules. These complexes, pairing an ABC transporter with a two-component system that are typically encoded together (Fig. 1.1B), function as frontline defenders of the cell wall and coordinators of cell envelope stress response (CESR) networks (20-23). Bce modules respond to structurally and mechanistically diverse antimicrobial peptides that target both cell wall synthesis and membrane integrity, and are also implicated in regulation of heat, pH and oxidative stress responses (22,24-27). As a result, these modules contribute significantly to virulence of pathogenic strains (25, 28-35). In addition, directed evolution experiments reveal a high propensity for mutation in Bce proteins to increase cell survival under adverse conditions in a variety of species, and Bce-like proteins have been identified on integrative conjugative elements, suggesting a potential for horizontal gene transfer (36-42).

From these findings, it is clear that Bce modules are integral to our understanding of pathogenesis and antimicrobial resistance in many gram-positive species, however many gaps remain in our knowledge of Bce module mechanisms of action in clinically and environmentally important species. Of the hundreds of Bce-like sequences identified across the Firmicutes, less than two dozen have published functional data (Table 1.1) (43,44). A major challenge in Bce module research has been the architecture of the complex itself: many early studies focused on either the Bce transporter or kinase without drawing connections to the other half of the module. In the rest of the chapter, I will describe what is known about Bce module function, focusing on the modules listed in Table 1.1.

SPECIES	*Bacillus licheniformis*		*Bacillus subtilis*			*Bacillus cereus group*
MODULE	YxdJKLM	YtsABCD	BceABRS	PsdABRS	ApeABRS	YvcPQRS
OTHER NAMES	YxdK2, YxdL2, YxdM2		YtsABCD	YvcPQRS	YxdJKLM	
SENSING TRANSPORTER	YxdLM	YtsAB	BceAB	YvcRS	ApeAB/YxdLM	YvcPQ
RESISTANCE TRANSPORTER						
OTHER FUNCTIONS						Regulation of sporulation via expression of KapD?
REFERENCES	60	60	20,21,43,44,49–51,54,55,61,76,77,79,81,84,85,110,133–143, 229	76,77,81,134, 140,141, 229	61,62,76,110 ,141,144, 229	145–147

SPECIES	*Enterococcus faecalis*	*Enterococcus faecium*	*Lactobacillus casei*		*Lactococcus lactis*
MODULE	SapABRS-RapAB	SapABRS-RapAB	ApsABRS-DerAB	PsdABRS	YsaABCD-KinG-LlrG
OTHER NAMES	YxdJKLM-YvcRS/MadABRS-MadLM	YxdJKLM-YvcRS/ChtRS	ApsRS = TCS12	PsdRS = Tcs09 = YvcRS	KinG-LlrG = TCS7
SENSING TRANSPORTER	SapAB	SapAB	ApsAB	PsdAB	YsaBC
RESISTANCE TRANSPORTER	RapAB	RapAB	ApsAB/DerAB?		
OTHER FUNCTIONS	Cell wall modification	Cell wall modification	Acid, temperature, bile stress		Cell wall modification, acid stress, lysozyme resistance
REFERENCES	23,41,80,108,148,149,231	111,118,150	22,120,151,152	22,151,152	39,40,57,64,153–156

Table 1.1: Bce modules that have been functionally characterized. Under module name, two-component systems are underlined. For systems with two transporters, the predominant role of each transporter is indicated.

Table 1.1 (cont'd)

SPECIES	*Listeria monocytogenes*	*Staphylococcus aureus*		*Staphylococcus epidermidis*
MODULE	VirABRS-AnrAB	BraDERS-VraDEH	VraFG-GraRSX	VraFG-GraRSX
OTHER NAMES		BraDERS = BceABRS = NsaABRS	GraRSX = ApsRSX	GraRSX = ApsRSX
SENSING TRANSPORTER	VirAB	BraDE	VraFG	VraFG
RESISTANCE TRANSPORTER	AnrAB	VraDE		
OTHER FUNCTIONS	Biofilm formation, motility, virulence, cell wall modification, acid stress	Adhesion and biofilm formation, metal transport	Acid stress, biofilm formation, lysozyme resistance, quorum sensing, virulence, cell wall modification	Cell wall modification, acid stress
REFERENCES	35,71,72,112,113,129–131,135,157–163, 233	52,59,73,74,82, 96,107,116,117, 137,164–178	25,27,32–34,36, 53,56, 75,89,91–95,107, 114–117,119,121, 122,124,125,136,165,167, 169,173,174,179–208, 234	83,90, 136,195, 232

SPECIES	*Streptococcus mutans*	*Streptococcus pneumoniae*	*Streptococcus thermophilus*	*Streptococcus suis*	*Streptococcus agalactiae*
MODULE	MbrABCD	BceAB-SirRH	BceABRS	BceABRS	SaNsrFPRK-Nsr
OTHER NAMES	BceABRS	SirRH = TCS01	BceRS = TCS07		NsaAB-GraRS, BceABRS
SENSING TRANSPORTER	MbrAB	BceAB	BceAB	BceAB	NsrFP
RESISTANCE TRANSPORTER					
OTHER FUNCTIONS	Biofilm formation	Virulence, acid and oxidative stress		Virulence	Biofilm formation, oxidative stress, virulence
REFERENCES	88,98,126,127,136,218–222	26,28,29,31,37,136, 223–226,230	227,228	30	65–69,86,97,128, 137,209–217

Core Bce Module Architecture

The core Bce module components are an ABC transporter and a two-component system which are united in a single AMP resistance and signaling complex. Both halves of the module are required for function: the Bce transporter mediates AMP sensing and detoxification and the two-component system tunes expression of additional transporter and often other stress-related genes in response to the Bce transporter's activity.

Bce transporters are similar to the type VII ABC transporters, which include the gram-negative MacAB and FtsEX transporters involved in macrolide resistance and cell division (45,46). The typical Bce transporter has ten transmembrane (TM) helices, eight of which form two pseudosymmetric bundles with FtsX-domain folds, with a ~200 residue extracellular domain between TM7 and TM8. The extracellular domain is the least conserved region of the Bce transporter, with less than ~10% sequence identity compared to ~25-40% identity across the entire sequences (43,44). Bce transporters were previously classified into subgroups based on the predicted secondary structure of their extracellular domains, however sequence alignments and AlphaFold models suggest that there is significant variation even within these subgroups (Fig. 1.2A,B) (43).

Bce kinases are intramembrane histidine kinases (IM-HKs) lacking a distinct extracellular signal sensing domain and are buried in the membrane with only a short linker connecting the two transmembrane helices (47,48). IM-HKs make up ~2-3% of known two-component system histidine kinases, and most either belong to the Bce family or are related to the general cell envelope stress sensor LiaS (48). Lacking an input domain, Bce kinases, rely on their paired Bce transporter for signal sensing and activation (49,50). The catalytic and DHp domains of Bce kinases are usually separated from the transmembrane domain by a HAMP domain and stalk helix, though two kinases, BraS of *Staphylococcus aureus* and KinG of *Lactococcus lactis* are predicted to lack a HAMP domain (51).

Bce transporters and kinases work together to mediate resistance and signal transduction by forming stable complexes with each other. Evidence for complex formation comes from bacterial two-hybrid experiments (50, 52-54). In addition, sequence co-evolution underscores the tight relationship between transporters and kinases (43). The general architecture of Bce modules is likely to be conserved, as AlphaFold models of distantly-related Bce complexes closely match each other and the BceABRS cryo-EM structures that will be described in Chapter 3 (55).

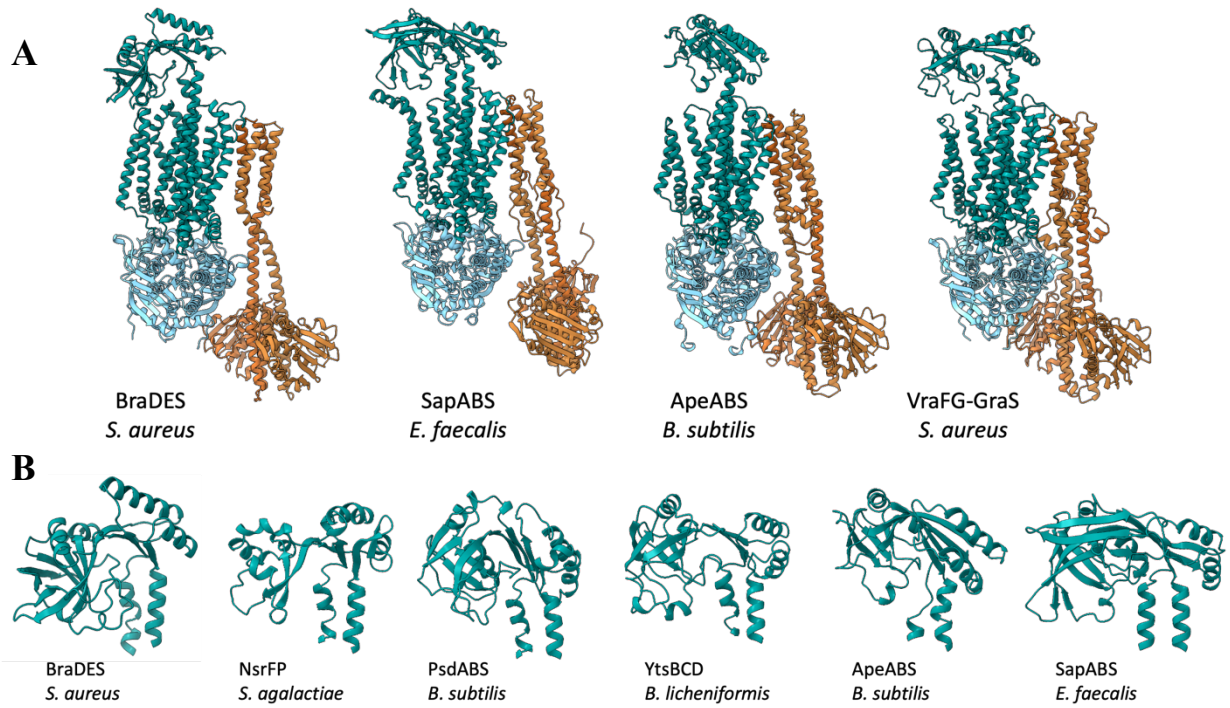

Figure 1.2: AlphaFold models of four Bce transporter-kinase complexes (A) show conserved architecture, though extracellular domains (B) vary widely. Transporters are colored in teal and light blue, while the kinases are colored orange.

Bce Accessory Proteins

In addition to the core transporter and two-component system components, Bce modules are sometimes encoded alongside genes which may represent module accessory proteins. Several of these proteins are expressed alongside core Bce genes and may play a role in module function. A few general groupings of these accessory proteins and what is known about them are described below and summarized in Table 1.2.

GraX (Fig. 1.3A) is an auxiliary protein associated with the VraFG-GraRS module in *Staphylococcus* species. Encoded in the GraRS two-component system operon, GraX is required for GraRS-dependent transcriptional activation in both *S. aureus* and *S. epidermidis* (25,33). Through localization analysis with a pho-lac reporter system and BACTH assays, GraX was determined to be a cytosolic protein that can interact with all three cytoplasm-exposed module components GraS, GraR and VraF (53,56). BLAST searches reveal similarity between GraX and NAD-binding dehydrogenases or sugar epimerases, which is supported by a predicted Rossmann-like fold at the N terminus of GraX (25). Despite these insights, the mechanism by which GraX contributes to cationic AMP-induced signaling in the VraFG-GraRSX module remains unclear. A GraX homolog is also slightly upregulated by the VirABRS-AnrAB module of *Listeria monocytogenes*, though its relationship to the Bce module is unknown (35).

The *Lactococcus lactis* YsaABCD-KinG-LlrG module encodes a VanZ-like membrane protein, YsaA (Fig. 1.3B) alongside the transporter YsaBC (57). A VanZ-like protein is also upregulated by VirR in *L. monocytogenes* (35). VanZ homologs are typically encoded in Van resistance cassettes and are involved in resistance to teicoplanin (58). The contribution of these proteins to Bce module function, however, has not been investigated.

In some species, small predicted-helical peptides are encoded near Bce module genes, however only in *Staphylococcus* has one of these been experimentally linked to module function. The *S. aureus* VraH protein (Fig. 1.3C) is associated with the two-transporter BraDERS-VraDE module and contributes to resistance to gallidermin, daptomycin, and NAI-107 (59). BACTH analysis suggests that this peptide interacts with the VraDE transporter, which serves as the resistance-mediating component of the BraDERS-VraDE module, and resistance enhancement by VraH appears to depend on the C-terminal motif YYKRREEKGK (59). This motif, however, is not conserved in other Bce-associated peptides, such as *spr0811* encoded in an operon with the transporter of the *Streptococcus pneumoniae* BceAB-SirRH module (37).

YxeA (Figure 3D) proteins are a widespread group of small Bce accessory proteins with N-terminal signal sequences. The eponymous YxeA protein in *Bacillus* species is associated with the ApeABRS (formerly YxdJKLM) module. YxeA appears to be transcribed alongside the ApeAB transporter and is upregulated in response to AMPs in *B. subtilis* and *B. licheniformis* (60-62). Evidence for YxeA involvement in module function can be found in *L. monocytogenes,* where a YxeA homolog may contribute to cefuroxime resistance, and in *L. lactis,* where the YxeA homolog YsaD may play a role in modulating signal transduction between the transporter YsaBC and kinase KinG (35,57,63,64).

Finally, Nsr proteins (Fig. 1.3E) are S41 family peptidases found primarily in *Streptococcus* and *Lactococcus* species as part of conserved operons alongside Bce modules (65). Mechanistic studies show *Streptococcus agalactiae* Nsr, encoded in the same operon as the *Sa*NsrFPRK Bce module, enhances nisin resistance by cleaving off the last six residues of nisin to render the peptide nonfunctional (66). Crystal structures and MD simulations of *Sa*Nsr reveal a central substrate binding tunnel bordered by a conserved TASSAEM motif that is predicted to recognize the last lanthionine ring of nisin (66). These data have supported efforts to develop nisin derivatives that can evade recognition by Nsr as well as inhibitors of Nsr function (67-69).

While most work on Bce modules to date has focused on the core transporter and kinase components, it appears that the involvement of additional proteins is much more common in Bce modules than previously realized. Future work on Bce module function should consider potential involvement of accessory proteins, and the contribution of known accessories to Bce-mediated resistance must be further investigated.

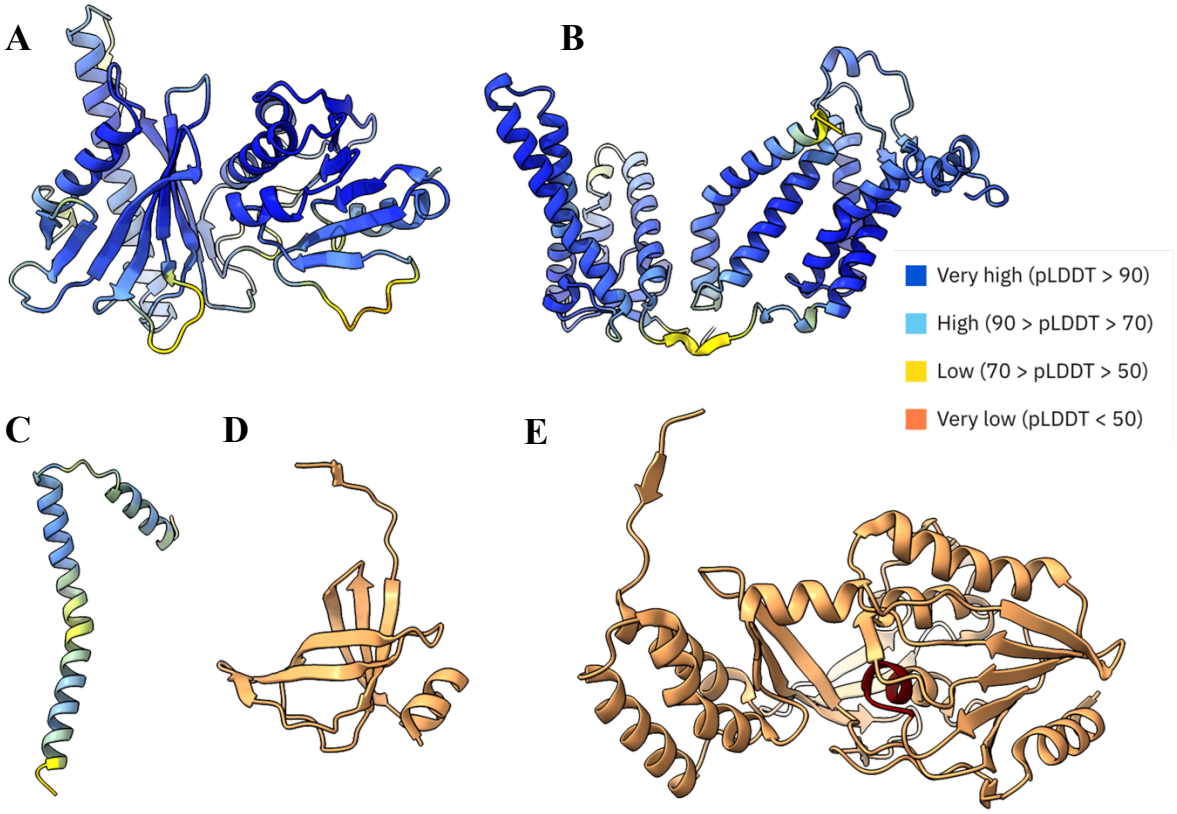

Figure 1.3: AlphaFold models of Bce module accessory proteins colored by pLDDT score: *S. aureus* GraX (A), *L. lactis* YsaA (B), *S. aureus* VraH (C). Crystallographic structures of accessory proteins *B. subtilis* YxeA (D, PDB 3NPP) and *S. agalactiae* Nsr (E, PDB 4Y68). The Nsr catalytic motif TASSAEM is in red.

SPECIES	MODULE	ACCESSORIES	TYPE	FUNCTION	REFERENCES
Bacillus licheniformis	YxdJKLM	YxeA	YxeA		[60]
Bacillus subtilis	ApeABRS	**YxeA**	YxeA	transcribed with transporter, likely secreted	[61,62]
Enterococcus faecalis	SapABRS-RapAB	EF1533	YxeA		[148,149]
Lactococcus lactis	YsaABCD-KinG-LlrG	**YsaA**	VanZ-like		[57]
		YsaD	YxeA		[57,64]
Listeria monocytogenes	VirABRS-AnrA	lmo1744	GraX	Predicted NAD-dependent epimerase/dehydratase	[35]
		lmo1743			[35]
		AdeC		Adenine deaminase	[35]
		lmo2156	YxeA		[35]
		lmo2439	YxeA		[35]
		lmo1696	VanZ-like		[35]
Staphylococcus aureus	VraFG-GraRSX	**GraX**	GraX	Predicted NAD-dependent epimerase/dehydratase	[25,33,53,56]
	BraDERS-VraDEH	**VraH**	SHP		[59]
Staphylococcus epidermidis	VraFG-GraRSX	**GraX**	GraX	Predicted NAD-dependent epimerase/dehydratase	[90]
Streptococcus agalactiae	*Sa*NsrFPRK-Nsr	**Nsr**	Nsr	Nisin protease	[65–69,210,214]
Streptococcus pneumoniae	BceAB-SirRH	spr0811	SHP		[37]

Table 1.2: Accessory proteins of Bce modules. Proteins that have been shown to express with Bce modules and contribute to module function are shaded in grey. Potential accessory proteins encoded in Bce operons or homologs of known accessories are not shaded. Some of these potential accessory genes are upregulated by Bce modules, but their exact relationships to the modules are not known. The family or type of accessory is indicated: YxeA homologs, ABC (ABC transporters), VanZ-like, GraX homologs, SHP (small helical peptides).

What do Bce Modules Resist?

Individual Bce modules can recognize multiple AMPs, often of diverse structure and mechanism of action (Table 1.3). Many of these AMPs target the lipid II cycle intermediates lipid II, undecaprenyl pyrophosphate (UP) and undecaprenyl phosphate (UP), but Bce modules also respond to peptides that target membrane integrity as well as dual-function AMPs that both block cell wall synthesis and damage the membrane directly via pore formation (16,70). In addition, Bce modules in *L. monocytogenes* and *S. aureus* appear to respond to β-lactam antibiotics, albeit more weakly than they do to AMPs (71-75). Modules appear to show higher specificity for the AMPs than for the targets that AMPs bind. Individual modules can respond to various AMPs that each target different moieties on lipid intermediates through distinct binding modes, while also distinguishing between AMPs of similar structure and mechanism. For example, the *B. subtilis* PsdABRS module distinguishes between the structurally similar lipid II-binding actagardine and mersacidin, and between UP-binding laspartomycin and friulimicin (76,77). While almost all tested Bce modules respond to UPP-binding bacitracin, other UPP-binders such as tripropeptin C may not be recognized, as is the case of *B. subtilis* BceABRS (78). Currently there are no structures of AMP-bound Bce transporters or detailed mutational data to give insight into how Bce specificity is maintained, and whether there are key motifs for recognition of different classes of AMPs. Systematic studies of AMP recognition in Bce modules to reveal specificity determinants could help predict which compounds evade detection by these critical resistance systems.

While Bce modules were initially identified for their role in resistance against antimicrobial peptides produced by other bacteria (Bce stands for "bacitracin efflux"), it is important to emphasize that these complexes also respond to host-derived peptides such as LL-37, human β-defensin-3 (hBD3), and human neutrophil peptide HNP-1 (79). Recognition of these peptides may aid Bce-expressing pathogens in evading immune defenses. For example, in *E. faecalis, the* SapABRS-RapAB module contributes to cell survival in a *C. elegans* infection model through protection against AMPs of the innate immune system (80).

The degree to which cells can resist AMPs and the degree of upregulation of Bce-controlled genes are not perfectly linked. For example, both mersacidin and bacitracin induce *B. subtilis* BceABRS signaling to the same level, but resistance to bacitracin is much higher than to mersacidin (76). One implication of these findings is that sensing and resistance are at least

partially separable functions. This underscores a need for systematic studies comparing both degree of resistance and induction of Bce module signaling in response to diverse AMPs.

Module	Friulimicin B	Laspartomycin C	Bacitracin	Tripropeptin C	Nisin	Subtilin	Gallidermin	Nukacin-ISK1	Plectasin	Telavancin	TC84 (Thrombocidin-1 derivative)
BceABRS *(B. subtilis)*	71	71	12,45,70,73, 78, 136	72	70	70	70		156		146
PsdABRS (*B. subtilis*)	71	71	70		70	70	70		70		146
ApeABRS (*B. subtilis*)			70		70	70	70		70		146
YvcPQRS (*B. thuringiensis*)			147								
SapABRS-RapAB (*E. faecalis*)			92,150,151		92		92				
SapABRS-RapAB *(E. faecium*)			154								
ApsABRS-DerAB (*L. casei*)			156		155,156	156			156		
PsdABRS (*L. casei*)			118,156		156	156			156		
AnrAB-VirABRS (*L. monocytogenes*)			65,66		65,66,129		65				
VraFG-GraRSX (*S. epidermidis*)					47						
VraFG-GraRSX (*S. aureus*)			23,91,101,193		23,169,193,201		193	201			
VraDEH-BraDERS (*S. aureus*)			37,68,76,90, 101, 116		37,67,76,90,106		37	201		172	
MbrABCD (*S. mutans*)			82,96,124,134, 208, 210		96						
NsrFPRK (*S. agalactiae*)			80,126		57,80,204,205		80,95				
BceAB-SirRH (*S. pneumoniae*)			31,81,212		81,212						
BceABRS (*S. thermophilus*)			93								
YsaBC-KinG-LlrG (*L. lactis*)			34,50		34,50,56						
BceABRS *(S. suis*)			20								
YxdJKLM (*B. licheniformis*)			52								
YtsABCD (*B. licheniformis*)			52								

Table 1.3: Bce module response to antimicrobials. Shaded squares indicate peptides that induce Bce signaling and/or are resisted by Bce modules. Unshaded squares with references indicate compounds which do not induce Bce module activity. AMPs are colored by primary target (Green = undecaprenyl phosphate, light blue = undecaprenyl pyrophosphate, pink = membrane+lipid II intermediates, yellow = lipid II, purple = cell synthesis enzymes, red = membrane, and dark blue = cytoplasmic target)

Table 1.3 (cont'd)

Module	TC19 (Thrombocidin-1 derivative)	Daptomycin	Insect Defensins	Human Defensins	Enduracidin	Vancomycin	Mersacidin	Actagardine	Teicoplanin
BceABRS (*B. subtilis*)	146				70	70	70	70	
PsdABRS (*B. subtilis*)	146				70	70	70	70	
ApeABRS (*B. subtilis*)	146				70	70	70	70	
YvcPQRS (*B. thuringiensis*)									
SapABRS-RapAB (*E. faecalis*)		151				92,151	92		92
SapABRS-RapAB (*E. faecium*)		102,103							
ApsABRS-DerAB (*L. casei*)			155	155		118,156	156		156
PsdABRS (*L. casei*)									
AnrAB-VirABRS (*L. monocytogenes*)						65			
VraFG-GraRSX (*S. epidermidis*)				47					
VraFG-GraRSX (*S. aureus*)		32,88,114,173, 182,191,193, 198,202,203		89,114, 184		26,27,29,69, 84,114,181, 182,191,193	169		29
VraDEH-BraDERS (*S. aureus*)		37,173	179	169	172	37	168		
MbrABCD (*S. mutans*)				82,124					
NsrFPRK (*S. agalactiae*)						80,126			
BceAB-SirRH (*S. pneumoniae*)		216				81		81	
BceABRS (*S. thermophilus*)									
YsaBC-KinG-LlrG (*L. lactis*)						34,50			
BceABRS (*S. suis*)									
YxdJKLM (*B. licheniformis*)						52			
YtsABCD (*B. licheniformis*)						52			

Table 1.3 (cont'd)

Module	Ramoplanin	Lysobactin	Planosporicin	Microbisporicin	Lcn972	Fosfomycin	Beta lactams	BP2 (BPI derivative)	Duramycin	Briaciidin	Indolicidin
BceABRS (*B. subtilis*)	70							146	70		
PsdABRS (*B. subtilis*)	70							146	70		
ApeABRS (*B. subtilis*)	70							146			
YvcPQRS (*B. thuringiensis*)											
SapABRS-RapAB (*E. faecalis*)							92,153				
SapABRS-RapAB (*E. faecium*)											
ApsABRS-DerAB (*L. casei*)											
PsdABRS (*L. casei*)											
AnrAB-VirABRS (*L. monocytogenes*)							65,66				
VraFG-GraRSX (*S. epidermidis*)											
VraFG-GraRSX (*S. aureus*)							69			173	23
VraDEH-BraDERS (*S. aureus*)						67	67,68			173	
MbrABCD (*S. mutans*)							96				
NsrFPRK (*S. agalactiae*)	80	80					126				
BceAB-SirRH (*S. pneumoniae*)	81		81	81							
BceABRS (*S. thermophilus*)											
YsaBC-KinG-LlrG (*L. lactis*)					34,50						
BceABRS (*S. suis*)											
YxdJKLM (*B. licheniformis*)											
YtsABCD (*B. licheniformis*)											

Table 1.3 (cont'd)

Module	Vancoresmycin	LL-37	Gramicidin	Enterocin L50	Colistin	Polymyxin B	Aureocin A53	Tachyplesin	Brevinin	Histatin	Magainin
BceABRS (*B. subtilis*)		54									
PsdABRS (*B. subtilis*)		54									
ApeABRS (*B. subtilis*)		54									
YvcPQRS (*B. thuringiensis*)											
SapABRS-RapAB (*E. faecalis*)						153					
SapABRS-RapAB (*E. faecium*)											
ApsABRS-DerAB (*L. casei*)		155									
PsdABRS (*L. casei*)											
AnrAB-VirABRS (*L. monocytogenes*)											
VraFG-GraRSX (*S. epidermidis*)		47,217				77		47	47	47	47
VraFG-GraRSX (*S. aureus*)		22–24, 85,86,173,188, 193,196,198			48,76,193	22,88,114,188,193					
VraDEH-BraDERS (*S. aureus*)		173	37,67		76	37					
MbrABCD (*S. mutans*)		124								124	
NsrFPRK (*S. agalactiae*)		126				126					
BceAB-SirRH (*S. pneumoniae*)	31	212	212		81						
BceABRS (*S. thermophilus*)											
YsaBC-KinG-LlrG (*L. lactis*)				33,158			33,158				
BceABRS (*S. suis*)											
YxdJKLM (*B. licheniformis*)											
YtsABCD (*B. licheniformis*)											

Table 1.3 (cont'd)

Module	Pediocin	Glabridin	Lincomycin	Sublancin	Gentamicin	Arylomycin G0775	FL9	LP5
BceABRS (*B. subtilis*)				70				
PsdABRS (*B. subtilis*)								
ApeABRS (*B. subtilis*)								
YvcPQRS (*B. thuringiensis*)								
SapABRS-RapAB (*E. faecalis*)								
SapABRS-RapAB (*E. faecium*)								
ApsABRS-DerAB (*L. casei*)								
PsdABRS (*L. casei*)								
AnrAB-VirABRS (*L. monocytogenes*)	218	165						
VraFG-GraRSX (*S. epidermidis*)								
VraFG-GraRSX (*S. aureus*)					69,84,191,193	219	220	189
VraDEH-BraDERS (*S. aureus*)					184			
MbrABCD (*S. mutans*)								
NsrFPRK (*S. agalactiae*)								
BceAB-SirRH (*S. pneumoniae*)			212					
BceABRS (*S. thermophilus*)								
YsaBC-KinG-LlrG (*L. lactis*)								
BceABRS (*S. suis*)								
YxdJKLM (*B. licheniformis*)								
YtsABCD (*B. licheniformis*)								

How do Bce Modules Work?

Bce modules appear to recognize antimicrobial peptides in complex with their target lipids (81). The transporter extracellular domain is responsible for recognizing target AMPs; domain swap experiments in *S. aureus* revealed that exchanging extracellular domains of related transporters alters their specificity (53,82). The extracellular domain is also the least conserved region in Bce transporters in both sequence and predicted structure, which may explain how individual Bce modules are tuned to a unique set of AMPs (43). While motifs related to recognition of specific antimicrobial peptides have not been identified, work in the *S. aureus* VraFG-GraRSX module suggests that a small "guard loop" within the extracellular domain is required for resistance (83). The guard loop is present in most but not all predicted structures of Bce transporters.

The Bce kinase, rather than binding a ligand directly, senses the detoxifying activity of the transporter in a mechanism described as "flux sensing" (84). Kinase activation requires interaction with a functional Bce transporter, as mutation of conserved residues involved in transporter ATP hydrolysis abolishes signaling (85,86). Once activated by transporter interaction with substrate AMPs, the Bce kinase phosphorylates its OmpR family response regulator, which upregulates expression of the Bce transporter by binding a TNACA-N4-TGTAA consensus sequence in the promoter (Fig. 1.4A) (21,43,87-89). As the number of Bce transporters on the membrane increases, the AMP burden per transporter decreases, slowing activity of individual transporters and reducing kinase activation. This highly regulated negative-feedback system allows for rapid adaptation to AMP concentrations spanning multiple orders of magnitude by tuning resistance system expression to match current levels of stress (21,84).

Sensing of transporter activity appears to require the short (~10 residue) extracellular "loop" connecting the two kinase transmembrane helices. Work in the *S. aureus* VraFG-GraRSX module has determined specific residues within this short sequence, particularly D35 near the end of the loop, critical for kinase function, and species-specific differences in the extracellular loop that alter downstream gene expression (33,90-95). Activation of the Bce kinase may involve a piston-like downward shift of TM2, which is transduced to the catalytic domains through an intervening linker (51). In most Bce kinases, this linker region contains a HAMP-like domain as observed in the cryo-EM structures of *B. subtilis* BceS that will be described in Chapter 3, however a few Bce kinases such as *S. aureus* BraS possess a shorter linker predicted to adopt a

marginally stable coiled-coil conformation without a HAMP domain (51,55,96). In either case, transmembrane helix movement induced by conformational changes in the transporter likely shifts the conformational state of the linker region to favor kinase activation, which may occur through rotation and charge stabilization in the DHp domain (51). No structures of an activated Bce kinase in complex with its transporter yet exist to clarify this process, but signaling assays in *B. subtilis* expressing either ATP-binding or ATP-hydrolysis deficient BceAB suggest that the nucleotide binding state of the transporter alone appears to not be enough to shift the kinase into an on state (49.85). AMP binding and/or the process of ATP hydrolysis may induce additional conformational changes that drive kinase activation.

Bce modules appear work through a "target protection" mechanism in which lipid II cycle intermediates are freed from the grasp of AMPs by the Bce transporter (81). Studies on *B. subtilis* BceABRS, *S. agalactiae Sa*NsrFPRK, and *S. mutans* MbrABCD suggest that the modules neither import AMPs into the cell nor inactivate them. Experimental evidence for removal of AMPs from the membrane into the surrounding media is mixed, though a mechanism in which AMPs are completely detached from the membrane would make sense for protecting cell wall synthesis and membrane integrity (81,97,98). This process of AMP removal has led to Bce modules being described as "hydrophobic vacuum cleaners" that pump AMPs off the membrane and away from the cell, similarly to the bacitracin self-immunity transporter BcrABC in *B. licheniformis* (79,99). Bce module transporters are structurally dissimilar to the exporters BcrABC and the eukaryotic Pgp for which the model was first proposed, and likely mediate peptide release through a distinct mechanism.

AMPs such as bacitracin and nisin undergo significant conformational changes during binding to form a cage around the target lipid (100-105). Freeing lipids bound by such AMPs would require breaking of multiple bonds and induction of conformational change in the AMP. How this may be mediated by Bce transporters for structurally distinct target AMPs remains to be determined. Bce modules resistance of AMPs that directly target the membrane rather than bind lipid II cycle intermediates is even more poorly understood. Recent work in *E. faecalis* and *S. aureus* suggest that Bce module expression and/or activity may be sensitive to changes in the lipid environment, but more work is needed to determine exactly how membrane composition affects Bce module function and how this may translate to resistance of membrane targeting AMPs (80,106).

Intriguingly, some Bce modules have two transporters which appear to split the tasks of resistance and signaling. These include the VraDEH-BraDERS module of *S. aureus* and *S. epidermidis,* the AnrAB-VirABRS module of *L. monocytogenes*, and the RapAB-SapABRS module of *Enterococcus faecalis* and *Enterococcus faecium* (Table 1.1) (52,72,82,107,108). Both transporters are required for full functionality of the module, but BACTH analysis suggests that only one of the transporters associates with the signaling kinase (52). Signaling assays with deletion mutants suggest that the transporter associated with the kinase is required for expression of Bce-regulated genes, while the second transporter may be primarily involved in resistance (Fig. 1.4A, middle) (108). This model would suggest that both transporters interact with the same set of AMPs, first to detect and then to detoxify, however the extracellular domains of transporter pairs vary in predicted structure and show very low sequence and even structural similarity (Fig. 1.4B). It is unclear what advantages there might be to a two-transporter module, and how effective signaling and resistance can be maintained over time between very divergent transporters.

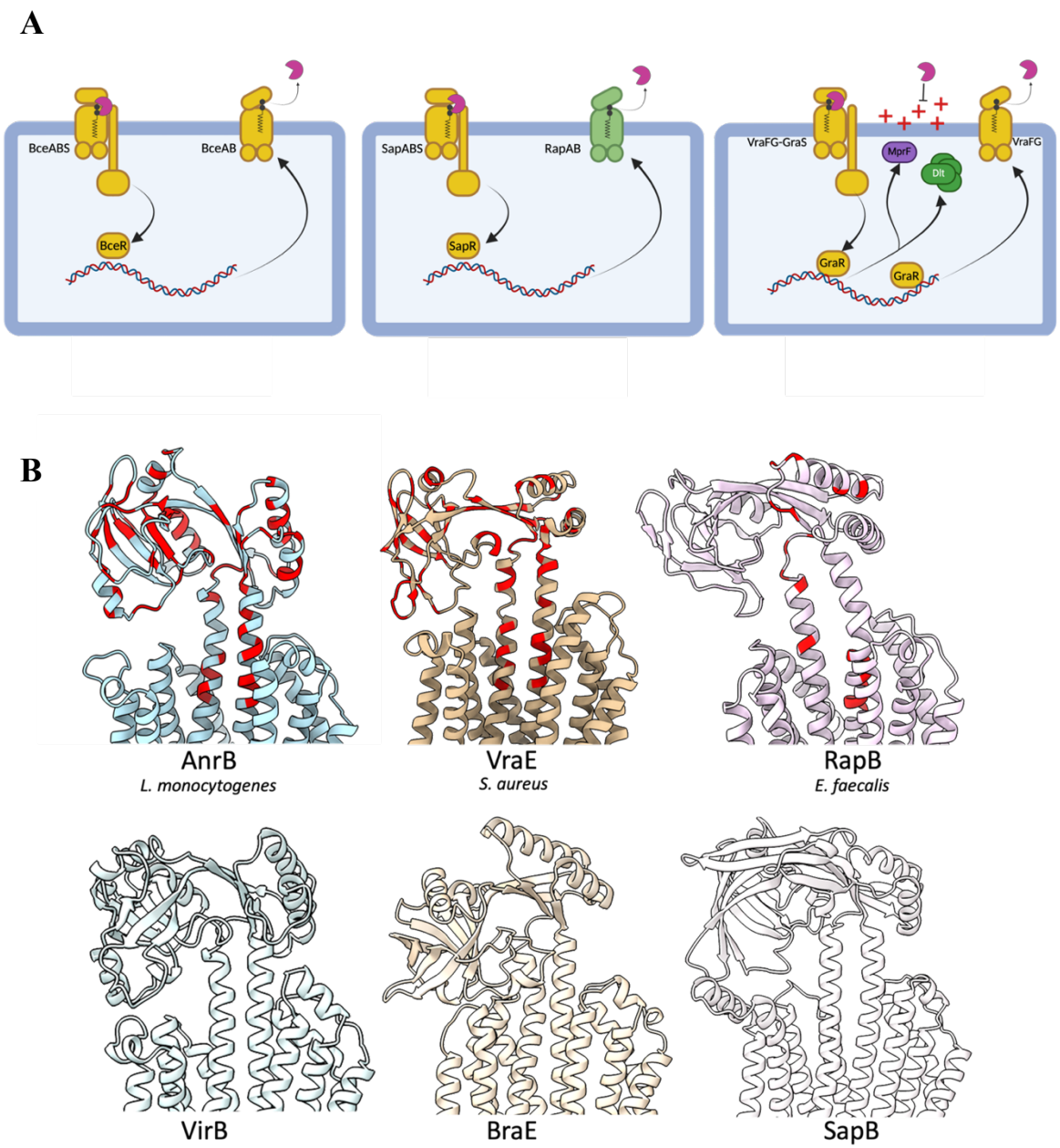

Figure 1.4: Bce transporter-kinase pairs can mediate resistance through three routes (A): by upregulating their own transporter (left); by upregulating a different Bce transporter dedicated to detoxification (middle); by upregulating Bce transporters and other resistance-related genes such as those involved in modifying the cell envelope to repel cationic AMPs (right). Comparison between transporters in two-transporter modules (B). Top: AlphaFold models of resistance transporters AnrB, VraE, and RapB. Bottom: AlphaFold models of signaling transporters below their paired resistance transporter. Positions in resistance transporters that have the same or similar residue as that of their signaling transporter, as determined by sequence alignments, colored in red.

Bce Modules and the Cell Envelope Stress Response

As a critical front-line defense system against antimicrobial peptides, Bce modules are embedded in broader cell envelope stress response (CESR) networks that allow for comprehensive protection of the cell's outer layers. Many of the major components of CESR networks are shared across species. Bce modules typically function as a highly targeted defense against specific stressors, while UPP phosphatases adjust the rates of cell wall synthesis (109). General stress-sensing systems such as LiaFSR family proteins, extracytoplasmic sigma factors and other regulators, and cell envelope-modifying enzymes provide additional support by reducing the ability of AMPs to bind to the cell surface and changing cell physiology to adapt to stressful conditions.

Despite common components, the architecture of CESR networks varies from species to species, and as a result, the role of Bce modules in the broader cell wall stress response varies. In *B. subtilis,* the Bce modules BceABRS and PsdABRS appear to function as self-contained, highly targeted systems that form a first and most important line of defense against specific AMPs, while additional layers of defense come from the UPP phosphatases UppC and BcrC, Lia family envelope stress regulators, and extracytoplasmic sigma factors (20,21,110). Other Bce modules play broader regulatory roles in coordinating expression of a diverse regulon of stress-related genes. These genes often include cell-wall modifying enzymes that contribute to AMP defense; Bce modules in *B. subtilis, E. faecalis, E. faecium, L. monocytogenes, S. aureus,* and *L. lactis* have been found to regulate the *dlt* operon and/or *mprF,* which increase cell surface charge by modifying teichoic acids and phosphatidylglycerol respectively (23,25,34,35,61,111-115). In species such as *S. aureus* and *S. epidermidis,* Bce modules coordinate widespread gene expression alongside general stress response regulators such as LiaFSR homolog VraTSR (116,117). In some cases, LiaFSR homologs do not act in parallel to Bce modules; in *E. faecalis,* LiaFSR itself regulates expression of the Bce kinase SapRS (23,108,118). In addition, Bce modules and other regulatory systems can be cross-regulated, not only between Bce modules but also between other sensory systems. For example, in *S. aureus,* the Stk1 kinase, implicated in cell-wall metabolism and virulence, can phosphorylate the GraR response regulator to increase its DNA binding affinity (119). Further complicating CESR systems, CESR components often have negative feedback relationships, resulting in changes in expression of one component driving compensating expression in others to maintain cell wall homeostasis (21,81,85). An

example of this is seen in *E. faecalis,* where deletion of the resistance-mediating transporter RapAB results in increased expression of the *dlt* operon (23). Importantly, since Bce kinase signaling is influenced by the AMP burden on Bce transporters, changes in the rate of lipid II cycling, such as due to CESR-induced increase in UPP phosphatase expression, also alter Bce transporter expression (20).

In addition to conserved CESR proteins, some Bce modules also regulate other non-Bce ABC transporters that work alongside Bce transporters to mediate antimicrobial peptide resistance. In *Streptococcus suis,* an ABC transporter SstFEG is encoded upstream of and is regulated by the Bce module BceABRS (30). Both SstFEG and BceAB contribute to bacitracin resistance. Another Bce-associated transporter, MadEFG, is regulated by the *Enterococcus faecalis* module SapABRS-RapAB (80). This transporter contributes to resistance to some but not all peptides recognized by the Bce module. In both species, the Bce module and the additional transporter independently contribute to resistance, with maximum resistance occurring when both transporters are expressed together.

The complexity of CESR networks challenge interpretation of the wide substrate range of Bce modules. AMPs may be resisted directly by the detoxifying action of Bce transporters, or indirectly through upregulation of alternative resistance factors (Fig. 1.4A, right). The direct involvement of Bce transporters in resistance has several examples: *S. agalactiae Sa*NsrFP in *L. lactis* confers nisin resistance even in absence of the module-associated nisin protease Nsr, and *E. faecalis* RapAB heterologously-expressed in *B. subtilis* in absence of its two-component system provides protection against bacitracin (97,108). On the other hand, in some cases Bce transporters fail to provide resistance when expressed alone; for example, the VraFG-GraRSX module mediates colistin resistance, but not when the VraFG transporter is overexpressed alone (53). Detangling the relative importance of Bce modules vs Bce-regulated genes or other CESR factors in resistance to different classes of AMPs will be critical for a complete understanding of AMP resistance strategies and for development of effective antimicrobials or resistance inhibitors.

Bce Modules Beyond Antimicrobial Peptide Resistance

Beyond mediating antimicrobial peptide resistance, Bce modules help regulate a variety of cell physiological processes including transport, metabolism, biofilm formation, motility, and virulence (Table 1.1). These broad regulatory roles make Bce modules essential for adaptation to environmental stressors and for virulence in some pathogenic species.

Bce modules contribute to acid, temperature, and oxidative stress tolerance in *S. pneumoniae*, *S. agalactiae, S. aureus, L. lactis* and *Lactobacillus casei,* often through regulation of cell envelope modifying enzymes. In *L. casei,* cells lacking Bce response regulator ApsR have an altered membrane lipid composition and experience delayed induction of the acid tolerance response, growth defects in 0.5% bile and at 42°C, and enter stationary phase earlier than wildtype cells (24,120). Similarly, cell wall modification by Bce-regulated MprF and the *dlt* operon contribute to environmental stress tolerance in *S. aureus* and *L. lactis* (25,32,121-123). Interestingly, under acid stress GraS signaling is equally active with and without the extracellular loop aspartates critical for AMP-induced signaling (27). This suggests that Bce kinases can be activated through a different mechanism by environmental stressors that may impact the membrane than by AMP stress.

Bce modules also influence population-level behaviors such as biofilm formation and quorum sensing. Altered biofilm formation with Bce module deletions has been observed in species such as *Staphylococcus aureus, Streptococcus agalactiae, Streptococcus mutans*, and *Listeria monocytogenes* (73,124-130). Impairment of either the BraDERS-VraDE or VraFG-GraRSX Bce modules in *S. aureus* results in decreased expression of biofilm-promoting genes, increased autolysis, and upregulation of biofilm-inhibiting proteases (73,124,125). Some of these effects on biofilm formation may be mediated by Bce-modulated biofilm regulators, such as the LytSR two-component system and the Agr quorum sensing system (25). Regulation of quorum sensing systems also has other effects; expression of the VraFG-GraRSX regulon appears to be growth-dependent, likely mediated by a negative feedback loop between the Agr quorum sensing system and its regulator, GraRSX (25,35). As a result, *S. aureus* has a greater ability to sense and resist AMPs in exponential phase growth than in stationary phase. The opposite effect is observed in *L. monocytogenes,* where VirR-mediated *dlt* operon induction significantly increases after twelve hours of growth (131).

A diversity of other genes related to transport, metabolism, redox processes, and motility

indicate general remodeling of cell processes upon stress mediated through Bce modules. In *L. monocytogenes*, deletions in the VirABRS module result in decreased expression of motility genes *flaA, motA* and *motB* (129). BraS kinase deletion strains of *S. aureus* show impaired ability to import metal cations (73). In some species, Bce module activation leads to increased expression of metabolic genes including those for terminal oxidases (*qoxABCD* in *S. aureus)*, carbon utilization (*glpQ* in *S. aureus, adhP* in *S. agalactiae, adeC* in *L. monocytogenes*), amino acid metabolism (*aroC,* and *glyA* in *S. pneumoniae*), and even ribosome synthesis (*rplE* and *rimP* in *S. aureus*) (25,26,35,112,115,128). These results show that Bce module activation can have far-reaching effects on cell physiology in times of stress beyond merely protecting the lipid II cycle.

By inducing environmental stress responses, coordinating cell behavior, and regulating diverse stress-related genes, Bce modules contribute significantly to virulence of pathogenic species. In some cases, Bce modules regulate key virulence factors. For example, in *S. aureus,* the GraRSX regulon includes hemolysins, virulence regulators, and attachment proteins (25). *In vitro* experiments have shown that *S. aureus* GraRSX, and its extensive regulon, is required for growth in acidic conditions in macrophage phagolysosomes, and in acidic antimicrobial uFFA-rich environments as would be encountered on skin (27,32). These virulence factors can give Bce-expressing bacteria an advantage in mixed infections; *S. pneumoniae* SirRH-related gene expression is responsible for increased cell survival in pneumocytes co-infected with influenza virus (26). The *in vitro* evidence for Bce-mediated virulence has been validated in numerous *in vivo* infection models, in which Bce modules contribute to increased survival in a variety of clinically relevant host environments (28,30,31,112,128,132). As a result, targeting Bce modules may be a useful strategy for combating infection by simultaneously increasing susceptibility to AMPs and decreasing fitness in the host.

Summary

Despite years of research on Bce modules in multiple species, progress toward understanding Bce modules has been impeded by lack of clarity around the relationship between Bce two component systems and Bce transporters, limited and sometimes contradictory biochemical data, and species-to-species differences in how Bce modules integrate into broader stress response systems. In the following chapters, I will describe our work to capture structures of the *B. subtilis* BceABRS module by cryo-electron microscopy. This work provides a first glimpse into how Bce module components come together into all-in-one AMP sensing, detoxification, and signaling machines, and how Bce module components regulate each others' dynamics to mediate effective antimicrobial resistance.

REFERENCES

1. Kumar, S., Mollo, A., Kahne, D. & Ruiz, N. The Bacterial Cell Wall: From Lipid II Flipping to Polymerization. *Chem. Rev.* 122, 8884–8910 (2022).

2. Piepenbreier, H., Diehl, A. & Fritz, G. Minimal exposure of lipid II cycle intermediates triggers cell wall antibiotic resistance. *Nat Commun* 10, 2733 (2019).
3. Koo, H. B. & Seo, J. Antimicrobial peptides under clinical investigation. *Pept. Sci.* 111, (2019).

4. Dijksteel, G. S., Ulrich, M. M. W., Middelkoop, E. & Boekema, B. K. H. L. Review: Lessons Learned From Clinical Trials Using Antimicrobial Peptides (AMPs). *Front. Microbiol.* 12, 616979 (2021).

5. Shukla, R., *et al.* Teixobactin kills bacteria by a two-pronged attack on the cell envelope. *Nature* 1–7 (2022). doi:10.1038/s41586-022-05019-y

6. Shukla, R., *et al*. An antibiotic from an uncultured bacterium binds to an immutable target. *Cell* (2023). doi:10.1016/j.cell.2023.07.038

7. Ling, L. L., *et al*. A new antibiotic kills pathogens without detectable resistance. *Nature* 517, 455–459 (2015).

8. Hover, B. M., *et al.* Culture-independent discovery of the malacidins as calcium-dependent antibiotics with activity against multidrug-resistant Gram-positive pathogens. *Nat. Microbiol.* 3, 415–422 (2018).

9. Ganesan, N., Mishra, B., Felix, L. & Mylonakis, E. Antimicrobial Peptides and Small Molecules Targeting the Cell Membrane of Staphylococcus aureus. *Microbiol. Mol. Biol. Rev.* 87, e00037-22 (2023).

10. Butler, M. S., *et al*. Glycopeptide antibiotics: Back to the future. *J. Antibiot.* 67, 631–644 (2014).

11. Atkinson, D. J., Naysmith, B. J., Furkert, D. P. & Brimble, M. A. Enduracididine, a rare amino acid component of peptide antibiotics: Natural products and synthesis. *Beilstein J. Org. Chem.* 12, 2325–2342 (2016).

12. Knerr, P. J. & Donk, W. A. van der. Discovery, Biosynthesis, and Engineering of Lantipeptides. *Annu. Rev. Biochem.* 81, 479–505 (2012).

13. Sahl, H.-G. & Bierbaum, G. Lantibiotics: Biosynthesis and Biological Activities of Uniquely Modified Peptides from Gram-Positive Bacteria. *Microbiology* 52, 41–79 (1998).

14. Zanetti, M. Cathelicidins, multifunctional peptides of the innate immunity. *J. Leukoc. Biol.* 75, 39–48 (2004).

15. Fu, J., *et al*. Mechanisms and regulation of defensins in host defense. *Signal Transduct. Target. Ther.* 8, 300 (2023).

16. Wiedemann, I., *et al*. Specific Binding of Nisin to the Peptidoglycan Precursor Lipid II Combines Pore Formation and Inhibition of Cell Wall Biosynthesis for Potent Antibiotic Activity. *J. Biol. Chem.* 276, 1772–1779 (2001).

17. Shariati, A., *et al*. Global prevalence and distribution of vancomycin resistant, vancomycin intermediate and heterogeneously vancomycin intermediate Staphylococcus aureus clinical isolates: a systematic review and meta-analysis. *Sci. Rep.* 10, 12689 (2020).

18. Reinseth, I. S., *et al*. The Increasing Issue of Vancomycin-Resistant Enterococci and the Bacteriocin Solution. *Probiotics Antimicrob. Proteins* 12, 1203–1217 (2020).

19. Revilla-Guarinos, A., Gebhard, S., Mascher, T. & Zúñiga, M. Defence against antimicrobial peptides: different strategies in Firmicutes: Antimicrobial peptide resistance in Firmicutes. *Environ Microbiol* 16, 1225–1237 (2014).

20. Piepenbreier, H., *et al*. From Modules to Networks: a Systems-Level Analysis of the Bacitracin Stress Response in Bacillus subtilis. *Msystems*, (2020).

21. Radeck, J., *et al*. Anatomy of the bacitracin resistance network in Bacillus subtilis: Anatomy of the bacitracin resistance network. *Mol Microbiol* 100, 607–620 (2016).

22. Revilla-Guarinos, A., *et al*. Characterization of a regulatory network of peptide antibiotic detoxification modules in Lactobacillus casei BL23. *Appl Environ Microb* 79, 3160–70 (2013).

23. Morris, S. M., Fritz, G., Rogers, T. & Gebhard, S. Novel regulatory logic in the antibiotic resistance response of Enterococcus faecalis against cell envelope targeting antibiotics. *Biorxiv* 2022.11.16.516778 (2022). doi:10.1101/2022.11.16.516778

24. Alcántara, C. & Zúñiga, M. Proteomic and transcriptomic analysis of the response to bile stress of Lactobacillus casei BL23. *Microbiology* 158, 1206–1218 (2012).

25. Falord, M., *et al*. Investigation of the Staphylococcus aureus GraSR Regulon Reveals Novel Links to Virulence, Stress Response and Cell Wall Signal Transduction Pathways. *Plos One* 6, e21323 (2011).

26. Reinoso-Vizcaíno, N. M., *et al*. The pneumococcal two-component system SirRH is linked to enhanced intracellular survival of Streptococcus pneumoniae in influenza-infected pulmonary cells. *Plos Pathog* 16, e1008761 (2020).

27. Kuiack, R. C., Veldhuizen, R. A. W. & McGavin, M. J. Novel Functions and Signaling Specificity for the GraS Sensor Kinase of Staphylococcus aureus in Response to Acidic pH. *J Bacteriol* 202, (2020).

28. Hava, D. L. & Camilli, A. Large-scale identification of serotype 4 Streptococcus pneumoniae virulence factors - PMC. *Mol Microbiol* 45, 1389–1406 (2002).

29. Paterson, G. K., Blue, C. E. & Mitchell, T. J. Role of two-component systems in the virulence of Streptococcus pneumoniae. *J. Méd. Microbiol.* 55, 355–363 (2006).

30. Ma, J., *et al*. Bacitracin resistance and enhanced virulence of Streptococcus suis via a novel efflux pump. *Bmc Vet Res* 15, 377 (2019).

31. Trihn, M., *et al.* Two-Component System Response Regulators Involved in Virulence of Streptococcus pneumoniae TIGR4 in Infective Endocarditis. *Plos One* 8, e54320 (2013).

32. Flannagan, R. S., Kuiack, R. C., McGavin, M. J. & Heinrichs, D. E. Staphylococcus aureus Uses the GraXRS Regulatory System To Sense and Adapt to the Acidified Phagolysosome in Macrophages. *Mbio* 9, e01143-18 (2018).

33. Li, M., *et al*. The antimicrobial peptide-sensing system aps of Staphylococcus aureus. *Mol Microbiol* 66, 1136–1147 (2007).

34. Kraus, D., *et al*. The GraRS regulatory system controls Staphylococcus aureus susceptibility to antimicrobial host defenses. *Bmc Microbiol* 8, 85 (2008).

35. Mandin, P., *et al*. VirR, a response regulator critical for Listeria monocytogenes virulence. *Mol Microbiol* 57, 1367–1380 (2005).

36. Doddangoudar, V. C., Boost, M. V., Tsang, D. N. C. & O'Donoghue, M. M. Tracking changes in the vraSR and graSR two component regulatory systems during the development and loss of vancomycin non-susceptibility in a clinical isolate. *Clin Microbiol Infec* 17, 1268–1272 (2011).

37. Becker, P., Hakenbeck, R. & Henrich, B. An ABC Transporter of Streptococcus pneumoniae Involved in Susceptibility to Vancoresmycin and Bacitracin. *Antimicrob Agents Ch* 53, 2034–2041 (2009).

38. Berscheid, A., *et al*. Generation of a vancomycin-intermediate Staphylococcus aureus (VISA) strain by two amino acid exchanges in VraS. *J Antimicrob Chemoth* 69, 3190–3198 (2014).

39. Tymoszewska, A., *et al*. Lactococcus lactis Resistance to Aureocin A53- and Enterocin L50-Like Bacteriocins and Membrane-Targeting Peptide Antibiotics Relies on the YsaCB-KinG-LlrG Four-Component System. *Antimicrob Agents Ch* 65, e00921-21 (2021).

40. López-González, M. J., *et al*. Adaptive Evolution of Industrial Lactococcus lactis Under Cell Envelope Stress Provides Phenotypic Diversity. *Front Microbiol* 9, 2654 (2018).

41. Miller, W. R., *et al*. LiaR-independent pathways to daptomycin resistance in Enterococcus faecalis reveal a multilayer defense against cell envelope antibiotics. *Mol. Microbiol.* 111, 811–824 (2019).

42. Bjørkeng, E. K, *et al*. ICESluvan, a 94-Kilobase Mosaic Integrative Conjugative Element Conferring Interspecies Transfer of VanB-Type Glycopeptide Resistance, a Novel Bacitracin Resistance Locus, and a Toxin-Antitoxin Stabilization System. *J. Bacteriol.* 195, 5381–5390 (2013).

43. Dintner, S., *et al*. Coevolution of ABC Transporters and Two-Component Regulatory Systems as Resistance Modules against Antimicrobial Peptides in Firmicutes Bacteria. *J Bacteriol* 193, 3851–3862 (2011).

44. Coumes-Florens, S., *et al.* A new highly conserved antibiotic sensing/resistance pathway in firmicutes involves an ABC transporter interplaying with a signal transduction system. *Plos One* 6, e15951 (2011).

45. Greene, N. P., Kaplan, E., Crow, A. & Koronakis, V. Antibiotic Resistance Mediated by the MacB ABC Transporter Family: A Structural and Functional Perspective. *Front Microbiol* 9, 950 (2018).

46. Thomas, C. & Tampé, R. Structural and Mechanistic Principles of ABC Transporters. *Annu Rev Biochem* 89, 605–636 (2020).

47. Mascher, T., Helmann, J. D. & Unden, G. Stimulus Perception in Bacterial Signal-Transducing Histidine Kinases. *Microbiol Mol Biol R* 70, 910–938 (2006).

48. Mascher, T. Bacterial (intramembrane-sensing) histidine kinases: signal transfer rather than stimulus perception. *Trends Microbiol* 22, 559–565 (2014).

49. Rietkötter, E., Hoyer, D. & Mascher, T. Bacitracin sensing in Bacillus subtilis. *Mol Microbiol* 68, 768–85 (2008).

50. Dintner, S., *et al*. A Sensory Complex Consisting of an ATP-binding Cassette Transporter and a Two-component Regulatory System Controls Bacitracin Resistance in Bacillus subtilis. *J Biol Chem* 289, 27899–27910 (2014).

51. Koh, A., *et al*. Conformation control of the histidine kinase BceS of Bacillus subtilis by its cognate ABC-transporter facilitates need-based activation of antibiotic resistance. *Mol Microbiol* 115, 157–174 (2021).

52. Randall, C. P., *et al*. Acquired Nisin Resistance in Staphylococcus aureus Involves Constitutive Activation of an Intrinsic Peptide Antibiotic Detoxification Module. *Msphere* 3, e00633-18 (2018).

53. Falord, M., Karimova, G., Hiron, A. & Msadek, T. GraXSR Proteins Interact with the VraFG ABC Transporter To Form a Five-Component System Required for Cationic Antimicrobial Peptide Sensing and Resistance in Staphylococcus aureus. *Antimicrob Agents Ch* 56, 1047–1058 (2012).

54. Kallenberg, F., Dintner, S., Schmitz, R. & Gebhard, S. Identification of Regions Important for Resistance and Signalling within the Antimicrobial Peptide Transporter BceAB of Bacillus subtilis. *J Bacteriol* 195, 3287–3297 (2013).

55. George, N. L. & Orlando, B. J. Architecture of a complete Bce-type antimicrobial peptide resistance module. *Nat. Commun.* 14, 3896 (2023).

56. Muzamal, U., Gomez, D., Kapadia, F. & Golemi-Kotra, D. Diversity of two-component systems: insights into the signal transduction mechanism by the Staphylococcus aureus two-component system GraSR. *F1000research* 3, 252 (2014).

57. Campelo, A. B., *et al*. Mutations Selected After Exposure to Bacteriocin Lcn972 Activate a Bce-Like Bacitracin Resistance Module in Lactococcus lactis. *Front Microbiol* 11, 1805 (2020).

58. Stogios, P. J. & Savchenko, A. Molecular mechanisms of vancomycin resistance. *Protein Sci.* 29, 654–669 (2020).

59. Popella, P., *et al*. VraH Is the Third Component of the Staphylococcus aureus VraDEH System Involved in Gallidermin and Daptomycin Resistance and Pathogenicity. *Antimicrob. Agents Chemother.* 60, 2391–2401 (2016).

60. Wecke, T., Veith, B., Ehrenreich, A. & Mascher, T. Cell Envelope Stress Response in Bacillus licheniformis : Integrating Comparative Genomics, Transcriptional Profiling, and Regulon Mining To Decipher a Complex Regulatory Network. *J. Bacteriol.* 188, 7500–7511 (2006).

61. Joseph, P., Guiseppi, A., Sorokin, A. & Denizot, F. Characterization of the Bacillus subtilis YxdJ response regulator as the inducer of expression for the cognate ABC transporter YxdLM. *Microbiology* 150, 2609–2617 (2004).

62. Pietiäinen, M., *et al*. Cationic antimicrobial peptides elicit a complex stress response in Bacillus subtilis that involves ECF-type sigma factors and two-component signal transduction systems. *Microbiology* 151, 1577–1592 (2005).

63. Krawczyk-Balska, A. & Markiewicz, Z. The intrinsic cephalosporin resistome of Listeria monocytogenes in the context of stress response, gene regulation, pathogenesis and therapeutics. *J. Appl. Microbiol.* 120, 251–265 (2016).

64. Kramer, N. E., Hijum, S. A. F. T. van, Knol, J., Kok, J. & Kuipers, O. P. Transcriptome analysis reveals mechanisms by which Lactococcus lactis acquires nisin resistance. *Antimicrob Agents Ch* 50, 1753–61 (2006).

65. Khosa, S., AlKhatib, Z. & Smits, S. H. J. NSR from Streptococcus agalactiae confers resistance against nisin and is encoded by a conserved nsr operon. *Bchm* 394, 1543–1549 (2013).

66. Sun, Z., *et al*. Novel Mechanism for Nisin Resistance via Proteolytic Degradation of Nisin by the Nisin Resistance Protein NSR. *Antimicrob. Agents Chemother.* 53, 1964–1973 (2009).

67. Zaschke-Kriesche, J., *et al*. Bypassing lantibiotic resistance by an effective nisin derivative. *Bioorgan Med Chem* 27, 3454–3462 (2019).

68. Desmond, A., *et al*. Bioengineered Nisin A Derivatives Display Enhanced Activity against Clinical Neonatal Pathogens. *Antibiotics* 11, 1516 (2022).

69. Porta, N., *et al*. Small-molecule inhibitors of nisin resistance protein NSR from the human pathogen Streptococcus agalactiae. *Bioorg. Med. Chem.* 27, 115079 (2019).

70. Sancho-Vaello, E., *et al*. The structure of the antimicrobial human cathelicidin LL-37 shows oligomerization and channel formation in the presence of membrane mimics. *Sci. Rep.* 10, 17356 (2020).

71. Collins, B., *et al*. The ABC Transporter AnrAB Contributes to the Innate Resistance of Listeria monocytogenes to Nisin, Bacitracin, and Various β-Lactam Antibiotics. *Antimicrob Agents Ch* 54, 4416–4423 (2010).

72. Jiang, X., *et al*. The VirAB-VirSR-AnrAB Multicomponent System Is Involved in Resistance of Listeria monocytogenes EGD-e to Cephalosporins, Bacitracin, Nisin, Benzalkonium Chloride, and Ethidium Bromide. *Appl Environ Microb* 85, (2019).

73. Kolar, S. L., *et al*. NsaRS is a cell-envelope-stress-sensing two-component system of Staphylococcus aureus. *Microbiology* 157, 2206–2219 (2011).

74. Yoshida, Y., *et al*. Bacitracin sensing and resistance in Staphylococcus aureus. *Fems Microbiol Lett* 320, 33–39 (2011).

75. Chen, L., *et al.* The Role of graRS in Regulating Virulence and Antimicrobial Resistance in Methicillin-Resistant Staphylococcus aureus. *Front. Microbiol.* 12, 727104 (2021).

76. Staroń, A., Finkeisen, D. E. & Mascher, T. Peptide Antibiotic Sensing and Detoxification Modules of Bacillus subtilis. *Antimicrob Agents Ch* 55, 515–525 (2011).

77. Diehl, A., *et al*. The Cell Envelope Stress Response of Bacillus subtilis towards Laspartomycin C. *Antibiotics* 9, 729 (2020).

78. Hashizume, H., *et al*. Tripropeptin C Blocks the Lipid Cycle of Cell Wall Biosynthesis by Complex Formation with Undecaprenyl Pyrophosphate. *Antimicrob. Agents Chemother.* 55, 3821–3828 (2011).

79. Ohki, R., *et al*. The BceRS two-component regulatory system induces expression of the bacitracin transporter, BceAB, in Bacillus subtilis. *Mol Microbiol* 49, 1135–44 (2003).

80. Miller, W. R., *et al*. Membrane Lipids Augment Cell Envelope Stress Signaling and Resistance to Antibiotics and Antimicrobial Peptides in Enterococcus faecalis. *bioRxiv* (2023). doi:10.1101/2023.10.17.562839

81. Kobras, C. M., *et al*. BceAB-Type Antibiotic Resistance Transporters Appear To Act by Target Protection of Cell Wall Synthesis. *Antimicrob Agents Ch* 64, (2020).

82. Hiron, A., *et al*. Bacitracin and nisin resistance in Staphylococcus aureus: a novel pathway involving the BraS/BraR two-component system (SA2417/SA2418) and both the BraD/BraE and VraD/VraE ABC transporters. *Mol Microbiol* 81, 602–622 (2011).

83. Costa, S. K., Cho, J. & Cheung, A. L. GraS Sensory Activity in Staphylococcus epidermidis Is Modulated by the "Guard Loop" of VraG and the ATPase Activity of VraF. *J Bacteriol* 203, e00178-21 (2021).

84. Fritz, G., *et al*. A New Way of Sensing: Need-Based Activation of Antibiotic Resistance by a Flux-Sensing Mechanism. *Mbio* 6, e00975-15 (2015).

85. Bernard, R., *et al*. Resistance to Bacitracin in Bacillus subtilis: Unexpected Requirement of the BceAB ABC Transporter in the Control of Expression of Its Own Structural Genes. *J Bacteriol* 189, 8636–8642 (2007).

86. Gottstein, J., *et al*. New insights into the resistance mechanism for the BceAB-type transporter SaNsrFP. *Sci Rep-uk* 12, 4232 (2022).

87. Diagne, A. M., *et al*. Identification of a two-component regulatory system involved in antimicrobial peptide resistance in Streptococcus pneumoniae. *Plos Pathog* 18, e1010458 (2022).

88. Ouyang, J., Tian, X.-L., Versey, J., Wishart, A. & Li, Y.-H. The BceABRS Four-Component System Regulates the Bacitracin-Induced Cell Envelope Stress Response in Streptococcus mutans. *Antimicrob Agents Ch* 54, 3895–3906 (2010).

89. Meehl, M., Herbert, S., Götz, F. & Cheung, A. Interaction of the GraRS Two-Component System with the VraFG ABC Transporter To Support Vancomycin-Intermediate Resistance in Staphylococcus aureus. *Antimicrob Agents Ch* 51, 2679–2689 (2007).

90. Li, M., *et al*. Gram-positive three-component antimicrobial peptide-sensing system. *Proc National Acad Sci* 104, 9469–9474 (2007).

91. Cho, J., *et al*. L. The extracellular loop of the membrane permease VraG interacts with GraS to sense cationic antimicrobial peptides in Staphylococcus aureus. *Plos Pathog* 17, e1009338 (2021).

92. Cho, J., Manna, A. C., Snelling, H. S. & Cheung, A. L. GraS signaling in Staphylococcus aureus is regulated by a single D35 residue in the extracellular loop. *Microbiol. Spectr.* e01982-23 (2023). doi:10.1128/spectrum.01982-23

93. Cheung, A. L., Cho, J., Bayer, A. S., Yeaman, M. R., *et al*. Role of the Staphylococcus aureus Extracellular Loop of GraS in Resistance to Distinct Human Defense Peptides in PMN and Invasive Cardiovascular infections. *Infect Immun* 89, e00347-21 (2021).

94. Cheung, A. L., *et al*. Site-Specific Mutation of the Sensor Kinase GraS in Staphylococcus aureus Alters the Adaptive Response to Distinct Cationic Antimicrobial Peptides. *Infect Immun* 82, 5336–5345 (2014).

95. Chaili, S., *et al*. The GraS Sensor in Staphylococcus aureus Mediates Resistance to Host Defense Peptides Differing in Mechanisms of Action. *Infect Immun* 84, 459–466 (2016).

96. Bhate, M. P., *et al*. Structure and Function of the Transmembrane Domain of NsaS, an Antibiotic Sensing Histidine Kinase in Staphylococcus aureus. *J Am Chem Soc* 140, 7471–7485 (2018).

97. Reiners, J., *et al*. The N-terminal Region of Nisin Is Important for the BceAB-Type ABC Transporter NsrFP from Streptococcus agalactiae COH1. *Front Microbiol* 8, 1643 (2017).

98. Tsuda, H., *et al*. Genes Involved in Bacitracin Resistance in Streptococcus mutans. *Antimicrob Agents Ch* 46, 3756–3764 (2002).

99. Podlesek, Z., *et al*. Bacillus licheniformis bacitracin-resistance ABC transporter: relationship to mammalian multidrug resistance. *Mol Microbiol* 16, 969–76 (1995).

100. Economou, N. J., Cocklin, S. & Loll, P. J. High-resolution crystal structure reveals molecular details of target recognition by bacitracin. *Proc National Acad Sci* 110, 14207–14212 (2013).

101. Hsu, S.-T. D., *et al*. The nisin–lipid II complex reveals a pyrophosphate cage that provides a blueprint for novel antibiotics. *Nat Struct Mol Biol* 11, 963–967 (2004).

102. Hsu, S.-T. D., *et al*. NMR Study of Mersacidin and Lipid II Interaction in Dodecylphosphocholine Micelles Conformational Changes are a Key to Antimicrobial Activity. *J. Biol. Chem.* 278, 13110–13117 (2003).

103. Fujinami, D., *et al*. The lantibiotic nukacin ISK-1 exists in an equilibrium between active and inactive lipid-II binding states. *Commun. Biol.* 1, 150 (2018).

104. Medeiros-Silva, J., *et al*. High-resolution NMR studies of antibiotics in cellular membranes. *Nat. Commun.* 9, 3963 (2018).

105. Breukink, E. & Kruijff, B. de. Lipid II as a target for antibiotics. *Nat Rev Drug Discov* 5, 321–32 (2006).

106. Yeo, W.-S., *et al*. Regulation of Bacterial Two-Component Systems by Cardiolipin. *Infect. Immun.* 91, e00046-23 (2023).

107. Kawada-Matsuo, M., Yoshida, Y., Nakamura, N. & Komatsuzawa, H. Role of two-component systems in the resistance of Staphylococcus aureus to antibacterial agents. *Virulence* 2, 427–430 (2011).

108. Gebhard, S., *et al.* Identification and Characterization of a Bacitracin Resistance Network in Enterococcus faecalis. *Antimicrob Agents Ch* 58, 1425–1433 (2014).

109. Radeck, J., Lautenschläger, N. & Mascher, T. The Essential UPP Phosphatase Pair BcrC and UppP Connects Cell Wall Homeostasis during Growth and Sporulation with Cell Envelope Stress Response in Bacillus subtilis. *Front Microbiol* 8, 2403 (2017).

110. Zhang, Q., *et al.* Comprehensive and Comparative Transcriptional Profiling of the Cell Wall Stress Response in Bacillus subtilis. *bioRxiv* (2023). doi:10.1101/2023.02.03.526509

111. Prater, A. G., *et al*. Environment Shapes the Accessible Daptomycin Resistance Mechanisms in Enterococcus faecium. *Antimicrob. Agents Chemother.* 63, (2019).

112. Camejo, A., *et al*. In Vivo Transcriptional Profiling of Listeria monocytogenes and Mutagenesis Identify New Virulence Factors Involved in Infection. *PLoS Pathog.* 5, e1000449 (2009).

113. Grubaugh, D., *et al*. The VirAB ABC Transporter Is Required for VirR Regulation of Listeria monocytogenes Virulence and Resistance to Nisin. *Infect. Immun.* 86, (2018).

114. Yang, S.-J., *et al*. The Staphylococcus aureus Two-Component Regulatory System, GraRS, Senses and Confers Resistance to Selected Cationic Antimicrobial Peptides. *Infect Immun* 80, 74–81 (2012).

115. Herbert, S., *et al*. Molecular Basis of Resistance to Muramidase and Cationic Antimicrobial Peptide Activity of Lysozyme in Staphylococci. *Plos Pathog* 3, e102 (2007).

116. Pietiäinen, M., *et al*. Transcriptome analysis of the responses of Staphylococcus aureus to antimicrobial peptides and characterization of the roles of vraDE and vraSR in antimicrobial resistance. *Bmc Genomics* 10, 429 (2009).

117. Kawada-Matsuo, M., *et al*. Three Distinct Two-Component Systems Are Involved in Resistance to the Class I Bacteriocins, Nukacin ISK-1 and Nisin A, in Staphylococcus aureus. *Plos One* 8, e69455 (2013).

118. Prater, A. G., *et al.* Daptomycin Resistance in Enterococcus faecium Can Be Delayed by Disruption of the LiaFSR Stress Response Pathway. *Antimicrob. Agents Chemother.* 65, (2021).

119. Fridman, M., *et al*. Two Unique Phosphorylation-Driven Signaling Pathways Crosstalk in Staphylococcus aureus to Modulate the Cell-Wall Charge: Stk1/Stp1 Meets GraSR. *Biochemistry* 52, 7975–7986 (2013).

120. Revilla-Guarinos, A., *et al*. Characterization of the response to low pH of Lactobacillus casei ΔRR12, a mutant strain with low D-alanylation activity and sensitivity to low pH. *J Appl Microbiol* 116, 1250–1261 (2014).

121. Beetham, C. M., Schuster, C. F., Santiago, M., Walker, S. & Gründling, A. Histidine and its uptake are essential for the growth of Staphylococcus aureus at low pH. *bioRxiv* 2023.07.25.550546 (2023). doi:10.1101/2023.07.25.550546

122. Villanueva, M., García, B., *et al*. Sensory deprivation in Staphylococcus aureus. *Nat Commun* 9, 523 (2018).

123. Wu, C., He, G. & Zhang, J. Physiological and proteomic analysis of Lactobacillus casei in response to acid adaptation. *J. Ind. Microbiol. Biotechnol.* 41, 1533–1540 (2014).

124. Boles, B. R., Thoendel, M., Roth, A. J. & Horswill, A. R. Identification of Genes Involved in Polysaccharide-Independent Staphylococcus aureus Biofilm Formation. *Plos One* 5, e10146 (2010).

125. Shanks, R. M. Q., *et al*. Genetic Evidence for an Alternative Citrate-Dependent Biofilm Formation Pathway in Staphylococcus aureus That Is Dependent on Fibronectin Binding Proteins and the GraRS Two-Component Regulatory System. *Infect Immun* 76, 2469–2477 (2008).

126. Tian, X.-L., *et al*. The BceABRS four-component system that is essential for cell envelope stress response is involved in sensing and response to host defence peptides and is required for the biofilm formation and fitness of Streptococcus mutans. *J Med Microbiol* 67, 874–883 (2018).

127. Nagasawa, R., *et al*. Potential Risk of Spreading Resistance Genes within Extracellular-DNA-Dependent Biofilms of Streptococcus mutans in Response to Cell Envelope Stress Induced by Sub-MICs of Bacitracin. *Appl. Environ. Microbiol.* 86, (2020).

128. Yang, Y., *et al*. Role of Two-Component System Response Regulator bceR in the Antimicrobial Resistance, Virulence, Biofilm Formation, and Stress Response of Group B Streptococcus. *Front Microbiol* 10, 10 (2019).

129. Jiang, X., *et al*. Role of the VirSR-VirAB system in biofilm formation of Listeria monocytogenes EGD-e. *Food Res. Int.* 145, 110394 (2021).

130. Zhu, X., *et al*. A Putative ABC Transporter Is Involved in Negative Regulation of Biofilm Formation by Listeria monocytogenes. *Appl. Environ. Microbiol.* 74, 7675–7683 (2008).

131. Kang, J., Wiedmann, M., Boor, K. J. & Bergholz, T. M. VirR-Mediated Resistance of Listeria monocytogenes against Food Antimicrobials and Cross-Protection Induced by Exposure to Organic Acid Salts. *Appl. Environ. Microbiol.* 81, 4553–4562 (2015).

132. Watson, D. W., Iglesias, S. L., Vasarhelyi, E. M. & Heinrichs, D. E. GraXRS-Dependent Resistance of Staphylococcus aureus to Human Osteoarthritic Synovial Fluid. *mSphere* 6, e00143-21 (2021).

133. George, N. L., Schilmiller, A. L. & Orlando, B. J. Conformational snapshots of the bacitracin sensing and resistance transporter BceAB. *Proc National Acad Sci* 119, e2123268119 (2022).

134. Omardien, S., *et al*. Synthetic antimicrobial peptides delocalize membrane bound proteins thereby inducing a cell envelope stress response. *Biochim. Biophys. Acta (BBA) - Biomembr.* 1860, 2416–2427 (2018).

135. Rismondo, J. & Schulz, L. M. Not Just Transporters: Alternative Functions of ABC Transporters in Bacillus subtilis and Listeria monocytogenes. *Microorg* 9, 163 (2021).

136. Ahmad, A., Majaz, S. & Nouroz, F. Two-component systems regulate ABC transporters in antimicrobial peptide production, immunity and resistance. *Microbiology* 166, 4–20 (2020).

137. Clemens, R., Zaschke-Kriesche, J., Khosa, S. & Smits, S. H. J. Insight into Two ABC Transporter Families Involved in Lantibiotic Resistance. *Frontiers Mol Biosci* 4, 91 (2018).

138. Kingston, A. W., Zhao, H., Cook, G. M. & Helmann, J. D. Accumulation of heptaprenyl diphosphate sensitizes Bacillus subtilis to bacitracin: implications for the mechanism of resistance mediated by the BceAB transporter. *Mol Microbiol* 93, 37–49 (2014).

139. Wolf, D., Domínguez-Cuevas, P., Daniel, R. A. & Mascher, T. Cell Envelope Stress Response in Cell Wall-Deficient L-Forms of Bacillus subtilis. *Antimicrob Agents Ch* 56, 5907–5915 (2012).

140. Fang, C., *et al*. Insulation and wiring specificity of BceR-like response regulators and their target promoters in Bacillus subtilis. *Mol Microbiol* 104, 16–31 (2016).

141. Höfler, C., *et al*. Cannibalism stress response in Bacillus subtilis. *Microbiology* 162, 164–176 (2016).

142. Bernard, R., *et al*. YtsCD and YwoA, two independent systems that confer bacitracin resistance to Bacillus subtilis. *Fems Microbiol Lett* 228, 93–97 (2003).

143. Mascher, T. Intramembrane-sensing histidine kinases: a new family of cell envelope stress sensors in Firmicutes bacteria. *Fems Microbiol Lett* 264, 133–144 (2006).

144. Joseph, P., Fichant, G., Quentin, Y. & Denizot, F. Regulatory relationship of two-component and ABC transport systems and clustering of their genes in the Bacillus/Clostridium group, suggest a functional link between them. *J. Mol. Microbiol. Biotechnol.* 4, 503–13 (2002).

145. Been, M. de, *et al*. Comparative analysis of two-component signal transduction systems of Bacillus cereus, Bacillus thuringiensis and Bacillus anthracis. *Microbiology* 152, 3035–3048 (2006).

146. Been, M. de, *et al* The identification of response regulator-specific binding sites reveals new roles of two-component systems in Bacillus cereus and closely related low-GC Gram-positives. *Environ Microbiol* 10, 2796–809 (2008).

147. Zhang, S., *et al*. The two-component signal transduction system YvcPQ regulates the bacterial resistance to bacitracin in Bacillus thuringiensis. *Arch Microbiol* 198, 773–84 (2016).

148. Abranches, J., *et al*. The Cell Wall-Targeting Antibiotic Stimulon of Enterococcus faecalis. *PLoS ONE* 8, e64875 (2013).

149. Darnell, R. L., *et al*. M. Genomewide Profiling of the Enterococcus faecalis Transcriptional Response to Teixobactin Reveals CroRS as an Essential Regulator of Antimicrobial Tolerance. *mSphere* 4, e00228-19 (2019).

150. Prieto, A. M. G., *et al*. The Two-Component System ChtRS Contributes to Chlorhexidine Tolerance in Enterococcus faecium. *Antimicrob. Agents Chemother.* 61, (2017).

151. Zhang, Q., *et al*, A. Cross-regulation of Aps-promoters in Lacticaseibacillus paracasei by the PsdR response regulator in response to lantibiotics. *Sci. Rep.* 14, 3319 (2024).

152. Revilla-Guarinos, A., *et al*. ABC Transporter DerAB of Lactobacillus casei Mediates Resistance against Insect-Derived Defensins. *Appl. Environ. Microbiol.* 86, (2020).

153. Tymoszewska, A. & Aleksandrzak-Piekarczyk, T. The Lactococcal dgkB (yecE) and dxsA Genes for Lipid Metabolism Are Involved in the Resistance to Cell Envelope-Acting Antimicrobials. *Int J Mol Sci* 22, 1014 (2021).

154. Wu, H., *et al*, J. Positive regulation of the DLT operon by TCSR7 enhances acid tolerance of Lactococcus lactis F44. *J. Dairy Sci.* 105, 7940–7950 (2022).

155. Veiga, P., *et al*. SpxB Regulates O-Acetylation-dependent Resistance of Lactococcus lactis Peptidoglycan to Hydrolysis. *J. Biol. Chem.* 282, 19342–19354 (2007).

156. Nguyen, T. V. A. & Hong, S. H. Construction and comparative analysis of two-component system and metabolic network profile based phylogenetic trees. *Biotechnol. Bioprocess Eng.* 14, 129–133 (2009).

157. Recio, M. V., *et al*. Chitin Attenuates Expression of Listeria monocytogenes Virulence Genes in vitro. *Front. Microbiol.* 11, 588906 (2020).

158. Wambui, J., *et al.* The Analysis of Field Strains Isolated From Food, Animal and Clinical Sources Uncovers Natural Mutations in Listeria monocytogenes Nisin Resistance Genes. *Front. Microbiol.* 11, 549531 (2020).

159. Pang, X., *et al*. The Lipoteichoic Acid-Related Proteins YqgS and LafA Contribute to the Resistance of Listeria monocytogenes to Nisin. *Microbiol. Spectr.* 10, e02095-21 (2022).

160. Zhu, X., *et al*. Phenotypic, Proteomic, and Genomic Characterization of a Putative ABC-Transporter Permease Involved in Listeria monocytogenes Biofilm Formation. *Foodborne Pathog. Dis.* 8, 495–501 (2011).

161. Bombelli, A., *et al*. Effects of the antimicrobial glabridin on membrane integrity and stress response activation in Listeria monocytogenes. *Food Res. Int.* 175, 113687 (2024).

162. Muchaamba, F., Wambui, J., Stephan, R. & Tasara, T. Cold Shock Proteins Promote Nisin Tolerance in Listeria monocytogenes Through Modulation of Cell Envelope Modification Responses. *Front. Microbiol.* 12, 811939 (2021).

163. Guo, Q., *et al*. Two-component system virS/virR regulated biofilm formation of Listeria monocytogenes 10403S. *Food Biosci.* 55, 102973 (2023).

164. Sass, P., *et al*. The lantibiotic mersacidin is a strong inducer of the cell wall stress response of Staphylococcus aureus. *Bmc Microbiol* 8, 186–186 (2008).

165. Sass, P. & Bierbaum, G. Native graS mutation supports the susceptibility of Staphylococcus aureus strain SG511 to antimicrobial peptides. *Int J Med Microbiol* 299, 313–322 (2009).

166. Blake, K. L., Randall, C. P. & O'Neill, A. J. In Vitro Studies Indicate a High Resistance Potential for the Lantibiotic Nisin in Staphylococcus aureus and Define a Genetic Basis for Nisin Resistance. *Antimicrob Agents Ch* 55, 2362–2368 (2011).

167. Gebhard, S. & Mascher, T. Antimicrobial peptide sensing and detoxification modules: unravelling the regulatory circuitry of Staphylococcus aureus. *Mol Microbiol* 81, 581–7 (2011).

168. Makarova, O., *et al.* Genomics of experimental adaptation of Staphylococcus aureus to a natural combination of insect antimicrobial peptides. *Sci. Rep.* 8, 15359 (2018).

169. Kawada-Matsuo, M., *et al*. Involvement of the Novel Two-Component NsrRS and LcrRS Systems in Distinct Resistance Pathways against Nisin A and Nukacin ISK-1 in Streptococcus mutans. *Appl Environ Microb* 79, 4751–4755 (2013).

170. Kawada-Matsuo, M., Le, M. N.-T. & Komatsuzawa, H. Antibacterial Peptides Resistance in Staphylococcus aureus: Various Mechanisms and the Association with Pathogenicity. *Genes* 12, 1527 (2021).

171. Arii, K., *et al* Single mutations in BraRS confer high resistance against nisin A in Staphylococcus aureus. *MicrobiologyOpen* 8, e791 (2019).

172. Song, Y., Lunde, C. S., Benton, B. M. & Wilkinson, B. J. Further insights into the mode of action of the lipoglycopeptide telavancin through global gene expression studies. *Antimicrob. agents Chemother.* 56, 3157–64 (2012).

173. Mensa, B., Howell, G. L., Scott, R. & DeGrado, W. F. Comparative Mechanistic Studies of Brilacidin, Daptomycin, and the Antimicrobial Peptide LL16. *Antimicrob Agents Ch* 58, 5136–5145 (2014).

174. Joo, H.-S. & Otto, M. Mechanisms of resistance to antimicrobial peptides in staphylococci. *Biochimica Et Biophysica Acta Bba - Biomembr* 1848, 3055–3061 (2015).

175. Carniello, V., Harapanahalli, A. K., Busscher, H. J. & Mei, H. C. van der. Adhesion force sensing and activation of a membrane-bound sensor to activate nisin efflux pumps in Staphylococcus aureus under mechanical and chemical stresses. *J. Colloid Interface Sci.* 512, 14–20 (2018).

176. Pag, U., *et al.* Analysis of in vitro activities and modes of action of synthetic antimicrobial peptides derived from an α-helical 'sequence template.' *J. Antimicrob. Chemother.* 61, 341–352 (2008).

177. Blake, K. L. & O'Neill, A. J. Transposon library screening for identification of genetic loci participating in intrinsic susceptibility and acquired resistance to antistaphylococcal agents. *J. Antimicrob. Chemother.* 68, 12–16 (2013).

178. Shazely, B. E., Urbański, A., Johnston, P. R. & Rolff, J. In vivo exposure of insect AMP resistant Staphylococcus aureus to an insect immune system. *Insect Biochem. Mol. Biol.* 110, 60–68 (2019).

179. Côté-Gravel, J., *et al*. Characterization of a vraG Mutant in a Genetically Stable Staphylococcus aureus Small-Colony Variant and Preliminary Assessment for Use as a Live-Attenuated Vaccine against Intrammamary Infections. *PLOS ONE* 11, e0166621 (2016).

180. Cui, L., *et al*. DNA Microarray-Based Identification of Genes Associated with Glycopeptide Resistance in Staphylococcus aureus. *Antimicrob Agents Ch* 49, 3404–3413 (2005).

181. Cui, L., Neoh, H., Shoji, M. & Hiramatsu, K. Contribution of vraSR and graSR point mutations to vancomycin resistance in vancomycin-intermediate Staphylococcus aureus. *Antimicrob Agents Ch* 53, 1231–4 (2009).

182. Neoh, H., *et al*. Mutated Response Regulator graR Is Responsible for Phenotypic Conversion of Staphylococcus aureus from Heterogeneous Vancomycin-Intermediate Resistance to Vancomycin-Intermediate Resistance. *Antimicrob. Agents Chemother.* 52, 45–53 (2008).

183. Howden, B. P., *et al*. Genomic Analysis Reveals a Point Mutation in the Two-Component Sensor Gene graS That Leads to Intermediate Vancomycin Resistance in Clinical Staphylococcus aureus. *Antimicrob. Agents Chemother.* 52, 3755–3762 (2008).

184. Belcheva, A. & Golemi-Kotra, D. A Close-up View of the VraSR Two-component System a Mediator of Staphylococcus aureus Response To Cell Wall Damage. *J Biol Chem* 283, 12354–12364 (2008).

185. Matsuo, M., *et al*. Distinct two-component systems in methicillin-resistant Staphylococcus aureus can change the susceptibility to antimicrobial agents. *J. Antimicrob. Chemother.* 65, 1536–1537 (2010).

186. Matsuo, M., *et al*. Growth-phase dependence of susceptibility to antimicrobial peptides in Staphylococcus aureus. *Microbiol. (Read., Engl.)* 157, 1786–1797 (2011).

187. Cho, J., Rigby, W. F. C. & Cheung, A. L. The thematic role of extracellular loop of VraG in activation of the membrane sensor GraS in a cystic fibrosis MRSA strain differs in nuance from the CA-MRSA strain JE2. *Plos One* 17, e0270393 (2022).

188. Gardete, S., Kim, C., *et al*. Genetic pathway in acquisition and loss of vancomycin resistance in a methicillin resistant Staphylococcus aureus (MRSA) strain of clonal type USA300. *Plos Pathog* 8, e1002505 (2012).

189. Yoo, J. I., *et al*. Prevalence of amino acid changes in the yvqF, vraSR, graSR, and tcaRAB genes from vancomycin intermediate resistant Staphylococcus aureus. *J. Microbiol.* 51, 160–165 (2013).

190. Allard, M., *et al*. The expression of a putative exotoxin and an ABC transporter during bovine intramammary infection contributes to the virulence of Staphylococcus aureus. *Vet. Microbiol.* 162, 761–770 (2013).

191. Gottschalk, S., Ingmer, H. & Thomsen, L. E. The lysine-peptoid hybrid LP5 maintain activity under physiological conditions and affects virulence gene expression in Staphylococcus aureus. *Peptides* 78, 24–29 (2016).

192. Gottschalk, S., *et al*. Amphibian antimicrobial peptide fallaxin analogue FL9 affects virulence gene expression and DNA replication in Staphylococcus aureus. *J. Méd. Microbiol.* 64, 1504–1513 (2015).

193. Hu, Q., Peng, H. & Rao, X. Molecular Events for Promotion of Vancomycin Resistance in Vancomycin Intermediate Staphylococcus aureus. *Front. Microbiol.* 7, 1601 (2016).

194. Rajagopal, M., *et al*. Multidrug Intrinsic Resistance Factors in Staphylococcus aureus Identified by Profiling Fitness within High-Diversity Transposon Libraries. *mBio* 7, e00950-16 (2016).

195. Moran, J. C., Alorabi, J. A. & Horsburgh, M. J. Comparative Transcriptomics Reveals Discrete Survival Responses of S. aureus and S. epidermidis to Sapienic Acid. *Front. Microbiol.* 8, 33 (2017).

196. Vestergaard, M., *et al*. Inhibition of the ATP Synthase Eliminates the Intrinsic Resistance of Staphylococcus aureus towards Polymyxins. *mBio* 8, e01114-17 (2017).

197. Li, S., *et al*. Fitness Cost of Daptomycin-Resistant Staphylococcus aureus Obtained from in Vitro Daptomycin Selection Pressure. *Front. Microbiol.* 8, 2199 (2017).

198. El-Halfawy, O. M., *et al*. Discovery of an antivirulence compound that reverses β-lactam resistance in MRSA. *Nat Chem Biol* 16, 143–149 (2020).

199. Coe, K. A., *et al* Multi-strain Tn-Seq reveals common daptomycin resistance determinants in Staphylococcus aureus. *PLoS Pathog.* 15, e1007862 (2019).

200. Golla, R. M., *et al*. Resistome of Staphylococcus aureus in Response to Human Cathelicidin LL-37 and Its Engineered Antimicrobial Peptides. *ACS Infect. Dis.* 6, 1866–1881 (2020).

201. Dhankhar, P., Dalal, V., Kotra, D. G. & Kumar, P. In-silico approach to identify novel potent inhibitors against GraR of S. aureus. *Frontiers Biosci Landmark Ed* 25, 1337–1360 (2020).

202. Prieto, J. M., *et al* Inhibiting the two-component system GraXRS with verteporfin to combat Staphylococcus aureus infections. *Sci. Rep.* 10, 17939 (2020).

203. Shazely, B. E., Yu, G., Johnston, P. R. & Rolff, J. Resistance Evolution Against Antimicrobial Peptides in Staphylococcus aureus Alters Pharmacodynamics Beyond the MIC. *Front. Microbiol.* 11, 103 (2020).

204. Ledger, E. V. K., Mesnage, S. & Edwards, A. M. Human serum triggers antibiotic tolerance in Staphylococcus aureus. *Nat. Commun.* 13, 2041 (2022).

205. Zeden, M. S., *et al*. Metabolic reprogramming and flux to cell envelope precursors in a pentose phosphate pathway mutant increases MRSA resistance to β-lactam antibiotics. *bioRxiv* 2023.03.03.530734 (2023). doi:10.1101/2023.03.03.530734

206. Kang, Y. R., *et al*. Genetic alterations in methicillin-susceptible Staphylococcus aureus associated with high vancomycin minimum inhibitory concentration. *Int. J. Antimicrob. Agents* 62, 106971 (2023).

207. Camargo, I. L. B. da C., Neoh, H.-M., Cui, L. & Hiramatsu, K. Serial Daptomycin Selection Generates Daptomycin-Nonsusceptible Staphylococcus aureus Strains with a Heterogeneous Vancomycin-Intermediate Phenotype. *Antimicrob. Agents Chemother.* 52, 4289–4299 (2008).

208. Iwata, Y., *et al*. Down-regulation of the two-component system and cell-wall biosynthesis-related genes was associated with the reversion to daptomycin susceptibility in daptomycin non-susceptible methicillin-resistant Staphylococcus aureus. *Eur. J. Clin. Microbiol. Infect. Dis.* 36, 1839–1845 (2017).

209. Khosa, S., *et al*. Structure of the Response Regulator NsrR from Streptococcus agalactiae, Which Is Involved in Lantibiotic Resistance. *PLoS ONE* 11, e0149903 (2016).

210. Khosa, S., Lagedroste, M. & Smits, S. H. J. Protein Defense Systems against the Lantibiotic Nisin: Function of the Immunity Protein NisI and the Resistance Protein NSR. *Front Microbiol* 7, 504 (2016).

211. Khosa, S., *et al*. H. J. Structural basis of lantibiotic recognition by the nisin resistance protein from Streptococcus agalactiae. *Sci. Rep.* 6, 18679 (2016).

212. Reiners, J., *et al*. Insights in the Antimicrobial Potential of the Natural Nisin Variant Nisin H. *Front. Microbiol.* 11, 573614 (2020).

213. Furtmann, F., *et al*. Characterization of the nucleotide-binding domain NsrF from the BceAB-type ABC-transporter NsrFP from the human pathogen Streptococcus agalactiae. *Sci Rep-uk* 10, 15208 (2020).

214. Zaschke-Kriesche, J., Reiners, J., Lagedroste, M. & Smits, S. H. J. Influence of nisin hinge-region variants on lantibiotic immunity and resistance proteins. *Bioorganic Medicinal Chem.* 27, 3947–3953 (2019).

215. Hayes, K., *et al*. A novel bioengineered derivative of nisin displays enhanced antimicrobial activity against clinical Streptococcus agalactiae isolates. *J. Glob. Antimicrob. Resist.* 19, 14–21 (2019).

216. Pérez-Ibarreche, M., Field, D., Ross, R. P. & Hill, C. A Bioengineered Nisin Derivative To Control Streptococcus uberis Biofilms. *Appl. Environ. Microbiol.* 87, e00391-21 (2021).

217. Thomas, L. & Cook, L. Two-Component Signal Transduction Systems in the Human Pathogen Streptococcus agalactiae. *Infect. Immun.* 88, (2020).

218. Kitagawa, N., *et al*. Characterization of MbrC involved in bacitracin resistance in Streptococcus mutans. *Fems Microbiol Lett* 318, 61–67 (2011).

219. Sudhakar, P., *et al*. Construction and verification of the transcriptional regulatory response network of Streptococcus mutansupon treatment with the biofilm inhibitor carolacton. *BMC Genom.* 15, 362 (2014).

220. Saputo, S., Faustoferri, R. C. & Quivey, R. G. Vitamin D Compounds Are Bactericidal against Streptococcus mutans and Target the Bacitracin-Associated Efflux System. *Antimicrob. Agents Chemother.* 62, (2018).

221. Choi, A., *et al*. Human Saliva Modifies Growth, Biofilm Architecture and Competitive Behaviors of Oral Streptococci. *bioRxiv* 2023.08.21.554151 (2023). doi:10.1101/2023.08.21.554151

222. Mikami, Y., *et al*. Bacitracin Upregulates mbrAB Transcription via mbrCD to Confer Bacitracin Resistance in Streptococcus mutans. *J Pharmacol Sci* 117, 204–207 (2011).

223. Throup, J. P., *et al*. A genomic analysis of two-component signal transduction in Streptococcus pneumoniae. *Mol Microbiol* 35, 566–576 (2000).

224. Majchrzykiewicz, J. A., Kuipers, O. P. & Bijlsma, J. J. E. Generic and Specific Adaptive Responses of Streptococcus pneumoniae to Challenge with Three Distinct Antimicrobial Peptides, Bacitracin, LL-37, and Nisin. *Antimicrob Agents Ch* 54, 440–451 (2010).

225. Yu, W.-L., *et al*. TCS01 Two-Component System Influenced the Virulence of Streptococcus pneumoniae by Regulating PcpA. *Infect. Immun.* 91, e00100-23 (2023).

226. Hernandez-Morfa, *et al*. The oxidative stress response of Streptococcus pneumoniae: its contribution to both extracellular and intracellular survival. *Front. Microbiol.* 14, 1269843 (2023).

227. Thevenard, B., *et al*. Characterization of Streptococcus thermophilus two-component systems: In silico analysis, functional analysis and expression of response regulator genes in pure or mixed culture with its yogurt partner, Lactobacillus delbrueckii subsp. bulgaricus. *Int. J. Food Microbiol.* 151, 171–181 (2011).

228. Thevenard, B., *et al*. Response of S. thermophilus LMD-9 to bacitracin: Involvement of a BceRS/AB-like module and of the rhamnose–glucose polysaccharide synthesis pathway. *Int. J. Food Microbiol.* 177, 89–97 (2014).

229. Mascher, T., *et al*. Cell wall stress responses in Bacillus subtilis: the regulatory network of the bacitracin stimulon. *Mol Microbiol* 50, 1591–1604 (2003).

230. Faure, A., *et al*. Daptomycin avoids drug resistance mediated by the BceAB transporter in Streptococcus pneumoniae. *Microbiol. Spectr.* 12, e0363823 (2024).

231. Gilmore, M. S., *et al*. Genes Contributing to the Unique Biology and Intrinsic Antibiotic Resistance of Enterococcus faecalis. *mBio* 11, e02962-20 (2020).

232. Martínez-García, S., *et al*. Differential Expression of the apsXRS System by Antimicrobial Peptide LL-37 in Commensal and Clinical Staphylococcus epidermidis Isolates. *Indian J Microbiol* 59, 295–303 (2019).

233. Laursen, M. F., *et al*. A single exposure to a sublethal pediocin concentration initiates a resistance-associated temporal cell envelope and general stress response in Listeria monocytogenes. *Environ. Microbiol.* 17, 1134–51 (2013).

234. Stone, M. C., Mychack, A., Coe, K. A. & Walker, S. Combining Signal Peptidase and Lipoprotein Processing Inhibitors Overcomes Ayr Resistance in Staphylococcus aureus. *Antimicrob. Agents Chemother.* 67, e00115-23 (2023).

CHAPTER 2: CONFORMATIONAL SNAPSHOTS OF THE BACITRACIN SENSING AND RESISTANCE TRANSPORTER BCEAB

This chapter has been published as: **George, N. L**., Schilmiller, A. L. & Orlando, B. J. Conformational snapshots of the bacitracin sensing and resistance transporter BceAB. *Proc National Acad Sci* **119**, e2123268119 (2022).

Abstract

Antimicrobial peptides are diverse molecules that include powerful medications such as bacitracin and vancomycin, as well as potent bacterial signaling molecules. Several antimicrobial peptides elicit cell death in gram-positive species by binding to lipid II cycle intermediates and inhibiting the synthesis of peptidoglycan. Many gram-positive organisms have evolved an elegant mechanism to sense and resist such antimicrobial peptides. In these organisms, a "Bce-type" adenosine triphosphate–binding cassette (ABC) transporter forms a protein complex with a two-component system, and together these components sense and provide resistance to antimicrobial peptides present at the cell surface. Conformational switching of Bce-type transporters is proposed to be the stimulus that activates the associated two-component system through a novel flux-sensing mechanism. In this work, we determined the detergent-solubilized structure of the Bce-type ABC transporter BceAB from *Bacillus subtilis* in two distinct conformational states using cryo–electron microscopy. Together with mass spectrometry and enzymatic data, our structures reveal the overall architecture of the Bce-type transporter family, uncover a specialized lipid-binding pocket for lipid II cycle intermediates, and reveal the conformational changes that are proposed to initiate signaling through the associated two-component system.

Introduction

The cell wall of gram-positive bacteria is a formidable barrier against environmental stress and physical extremes. The outer layer of peptidoglycan surrounding the gram-positive bacterial cell is essential for survival and confers structural rigidity, mechanical strength, and protection against harsh and constantly changing environments (1). Not surprisingly, the pathway used for peptidoglycan biosynthesis (lipid II cycle) is an important target of antimicrobial compounds (2,3). Several antimicrobial peptides such as bacitracin or vancomycin bind to intermediates of the lipid II cycle, leading to inhibition of peptidoglycan synthesis and eventual cell death. Gram-positive organisms have evolved a variety of strategies to resist attack by these antimicrobial peptides, including modification of surface charge, biofilm formation, proteolytic degradation, and expression of efflux pumps (4). In Firmicute bacteria, a conserved antimicrobial peptide sensing and detoxification machinery has evolved that consists of an adenosine triphosphate (ATP)-binding cassette (ABC) transporter interfacing with a two-component system. These complexes have come to be known as "Bce modules" based on the initial discovery of the BceAB-RS system in *Bacillus subtilis* (5,6). In this system, BceA forms the ATPase domains and BceB is the membrane-spanning permease domain of the ABC transporter complex. BceS is a sensor histidine kinase that phosphorylates the response regulator BceR.

Elegant studies in *B. subtilis* suggest that the BceAB transporter mediates resistance to bacitracin through a target protection mechanism that involves freeing the lipid II cycle intermediate undecaprenyl-pyrophosphate (UPP) from the inhibitory grasp of bacitracin (7). However, the mechanism by which BceAB recognizes UPP–bacitracin complexes in the lipid membrane and subsequently dissociates the antimicrobial peptide from UPP remains unknown. BceAB also plays another critical role by providing the stimulus to initiate signaling through the BceRS two-component system (6). Gebhard and colleagues have demonstrated that the BceAB transporter forms a complex with the BceS histidine kinase (Fig. 2.1 *A* and *B*) (8). Protein coevolution analysis has revealed similar interactions between Bce-type ABC transporters and histidine kinases across Firmicute bacteria (9). The BceS sensor kinase belongs to the intramembrane sensing class of histidine kinases and lacks an extracellular ligand-binding domain. Rather than binding bacitracin directly, the BceS sensor kinase is proposed to sense the conformational cycling of the BceAB transporter through a "flux-sensing" mechanism (6, 10). Activation of BceS and subsequent phosphorylation of BceR leads to increased transcription of

the genes encoding the BceAB transporter, resulting in a positive feedback loop to fine-tune the levels of BceAB transporter required to detoxify bacitracin–UPP complexes at the cell membrane (Fig. 2.1 *A* and *B*) (11). This regulatory mechanism allows the cell to efficiently mitigate cell wall stress while minimizing the energetic cost of producing resistance machinery.

Although extensive biochemical studies have established the role of Bce modules in sensing and resisting diverse antimicrobial peptides in different organisms (12–15), relatively little is known about their structure and the conformational changes that underlie their function. Revealing how the components of Bce modules work together to sense and resist antimicrobial peptides is a critical step toward developing a comprehensive understanding of how gram-positive organisms adapt to envelope stress. In this work, we determined the cryo–electron microscopy (cryo-EM) structures of the BceAB transporter from *B. subtilis* in two different conformational states. Our studies demonstrate that BceAB adopts a distinct architecture among the ABC transporter superfamily, reveal a critical binding pocket in the transporter for undecaprenyl lipids of the lipid II cycle, and provide insight into conformational changes that mediate target protection and activate BceS for defense against antimicrobial peptides.

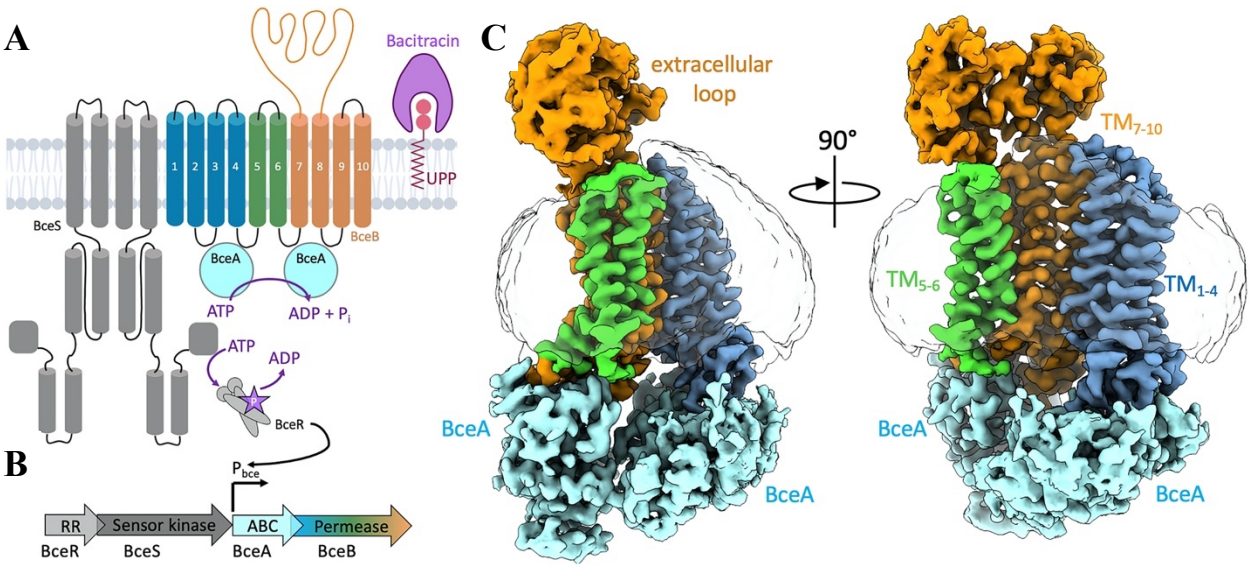

Figure 2.1: Overall structure of the BceAB complex. (*A*) Diagram depicting the organization and predicted membrane topology of a BceAB-RS bacitracin sensing and resistance module. BceA and BceB interact to form a complete ABC transporter complex. BceA subunits in the cytoplasm are colored cyan, and the TM helices and extracellular loop of BceB are colored blue, green, and orange. The BceAB transporter forms a complex with the BceS sensor kinase (dark gray). Conformational cycling of BceAB in response to recognition of bacitracin–UPP complexes initiates autophosphorylation of the BceS sensor kinase, which then phosphorylates (purple star with white P) the BceR response regulator (RR, light gray). Phosphorylated BceR binds to the P_{bce} promoter and up-regulates expression of the genes encoding the BceAB transporter. (*B*) Organization of BceRSAB genes in *B. subtilis*. BceR and BceS are constitutively expressed, whereas BceA and Bce B are controlled by the P_{bce} promoter that is up-regulated in response to phosphorylated BceR binding. (*C*) Cryo-EM structure of BceAB in a nucleotide-free conformation. BceA and BceB subunits are colored the same as depicted in (*A*). The detergent micelle is shown as a transparent gray outline.

Results

Overall Structure of the BceAB Transporter

In order to express and purify the BceAB transporter for structural studies, we cloned the *bceA* and *bceB* genes from *B. subtilis* behind separate promoters in a pETDuet-1 vector with the addition of a 6X-His tag on the N terminus of BceA. In our initial expression and purification optimization, we found that driving expression of *bceA* and *bceB* from separate promoters, rather than as a fused operon as natively exists in *B. subtilis*, consistently produced more intact purified BceAB complex. The transporter complex was expressed in *Escherichia coli* C41(DE3), solubilized from membranes in lauryl maltose neopentyl glycol (LMNG), and purified using sequential Co^{3+}-affinity and size-exclusion chromatography. This procedure generated highly pure and monodisperse samples amenable for structural studies (Fig. 2.2 *A* and B). The structure of BceAB from *B. subtilis* in a nucleotide-free conformation was determined at an overall resolution of 3.8 Å using single-particle cryo-EM (Fig. 2.1C, 2.3 and 2.4, and Table 2.1). Our cryo-EM structure confirms a previously predicted stoichiometry of the complex with two soluble BceA nucleotide-binding domains in complex with one BceB transmembrane (TM) subunit (8). Strikingly, the BceA subunits in the cytoplasmic region are arranged in a nonsymmetric fashion with one subunit significantly tilted toward the membrane plane (Figs. 2.1C and 2.5B). The asymmetric arrangement of BceA subunits is directly apparent in several side-view two-dimensional (2D) class averages of the BceAB complex (Fig. 2.3B). The overall structure of individual BceA subunits is similar to that observed for adenosine triphosphatase (ATPase) domains in other ABC transporters such as MacB (16) and LolCDE (17, 18) with the exception of an additional C-terminal helix that faces the interface between BceA subunits (Fig. 2.6A). In addition to other structural features described below, tilting of the BceA subunits in the cytoplasmic region makes the overall transporter complex asymmetrical in the nucleotide-free conformation.

One of the hallmarks of Bce-type transporters is a large ~200- to 250-residue loop region between TM helices 7 and 8 (designated TM_7 and TM_8). The sequence divergence of this loop region has been proposed to underlie specificity for different antimicrobial peptides between different Bce-type transporters (9, 12). In our cryo-EM structure of BceAB, the extracellular loop is positioned asymmetrically over one-half of the TM region (Figs. 2.1C and 2.5B). Three-dimensional (3D) variability analysis in CryoSPARC (19) revealed intrinsic flexibility of the

extracellular loop region with respect to the TM domain (Movie 2.1), which resulted in a lower overall resolution in this extracellular region compared to the TM and cytoplasmic regions (Fig. 2.4B). Despite low sequence similarity to other ABC transporters of known structure, the extracellular loop in BceB adopts a fold with Sabre and Porter subdomains (Fig. 2.6B) similar to those seen in gram-negative mechanotransmission ABC transporters MacB and LolCDE (Fig. 2.6C).

The TM region of BceB is composed of 10 TM helices that are arranged in a unique overall configuration (Fig. 2.5B and C). TM helices 1 to 4 and 7 to 10 form individual bundles that are related by two-fold pseudosymmetry, and each represents an FtsX-domain fold like that observed in type VII mechanotransmission ABC transporters (Fig. 2.6D) (20). TM_5 and TM_6 interact primarily with one another and are positioned closer to the $TM_{7–10}$ bundle than the $TM_{1–4}$ bundle, such that the overall TM arrangement of BceB is asymmetrical (Fig. 2.5C). TM_7 and TM_8 form long extended stalk helices that support the large extracellular domain at its base (Fig. 2.5B). When viewed from the extracellular space, the overall TM helix arrangement of BceB is curved, with TM_2, TM_4, TM_6, and TM_7 creating a large lipid-exposed cavity that faces the hydrophobic membrane environment (Figs. 2.1C and 2.5C). Several phospholipid-like densities filling this hydrophobic curved pocket were directly observed in our cryo-EM maps (Fig. 2.4G). Although certain features of the BceAB complex, such as FtsX-like TM folds and an extracellular domain with Sabre and Porter subdomains, are similar to those found in other transporter systems, the TM helix arrangement and highly asymmetrical arrangement of the BceAB complex are distinct among ABC transporters of known structure.

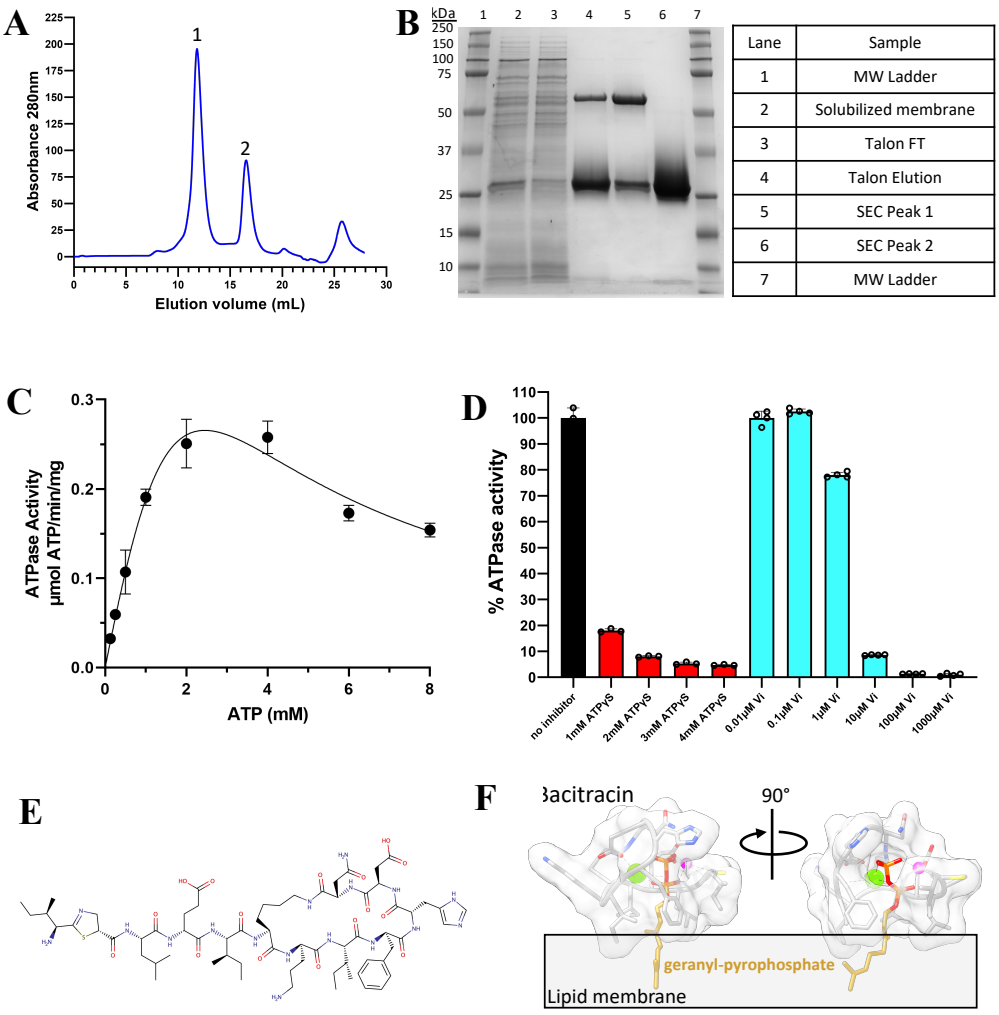

Lane	Sample
1	MW Ladder
2	Solubilized membrane
3	Talon FT
4	Talon Elution
5	SEC Peak 1
6	SEC Peak 2
7	MW Ladder

Figure 2.2: A) Gel filtration chromatogram of detergent-solubilized and Talon-purified BceAB. Peak one corresponds to the intact BceAB complex, and peak 2 corresponds to the free BceA nucleotide-binding domain. B) Reducing SDS- PAGE analysis of BceAB. The predicted molecular weight of BceA is 28 kDa, and the predicted molecular weight of BceB is 72 kDa. Molecular weight markers are denoted to the left and right of the gel. The table to the right indicates the sample run in each well of the gel. C) ATPase activity of detergent-solubilized BceAB measured using an NADH-coupled regenerating ATPase assay. Data were fit with a model of substrate-inhibition (solid line), demonstrating that the decrease in ATPase activity at high ATP concentrations is not a result of feedback inhibition by ADP. D) ATPase activity of detergent-solubilized BceAB in the presence of substrate analog ATPγS or the transition state analog ortho-vanadate. Both ATPγS (red bars, n = 3 independent measurements) and ortho-vanadate (cyan bars, n = 4 independent measurements) potently inhibited ATPase activity. E)

Figure 2.2 (cont'd)

Chemical representation of bacitracin. F) 3D view of the crystal structure (PDB: 4K7T) (21) of bacitracin (light grey sticks and surface) bound to the UPP analog geranyl-pyrophosphate (gold sticks with the pyrophosphate region colored red). The Zn2+ ion that helps coordinate bacitracin to the pyrophosphate moiety is shown as a green sphere. The lipid membrane is shown as a dark grey box to show the orientation of UPP and bacitracin relative to the lipid bilayer.

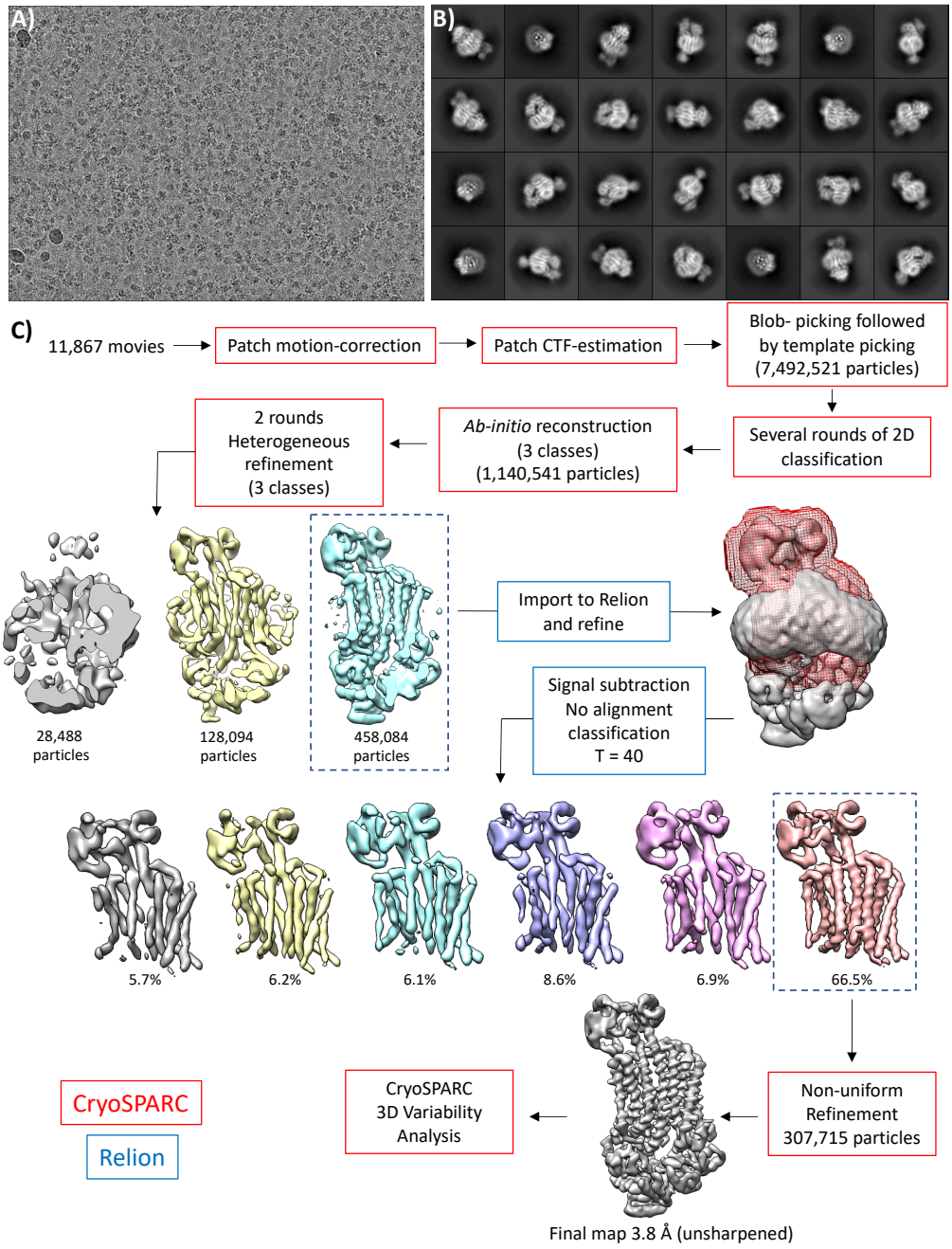

Figure 2.3: Cryo-EM Data Processing for Nucleotide-Free BceAB. A) Representative cryo-electron micrograph of detergent-solubilized BceAB showing well-distributed particles in thin ice. B) 2D-averages of detergent-solubilized and nucleotide-free BceAB. A variety of views of the transporter are readily discernable showing the asymmetric BceA nucleotide-binding domain subunits, TM helices, and extracellular domains. C) Data processing workflow to obtain the final 3D reconstruction of BceAB. Steps highlighted in red boxes were performed in CryoSPARC, and steps highlighted in blue boxes were performed in Relion 3.0.

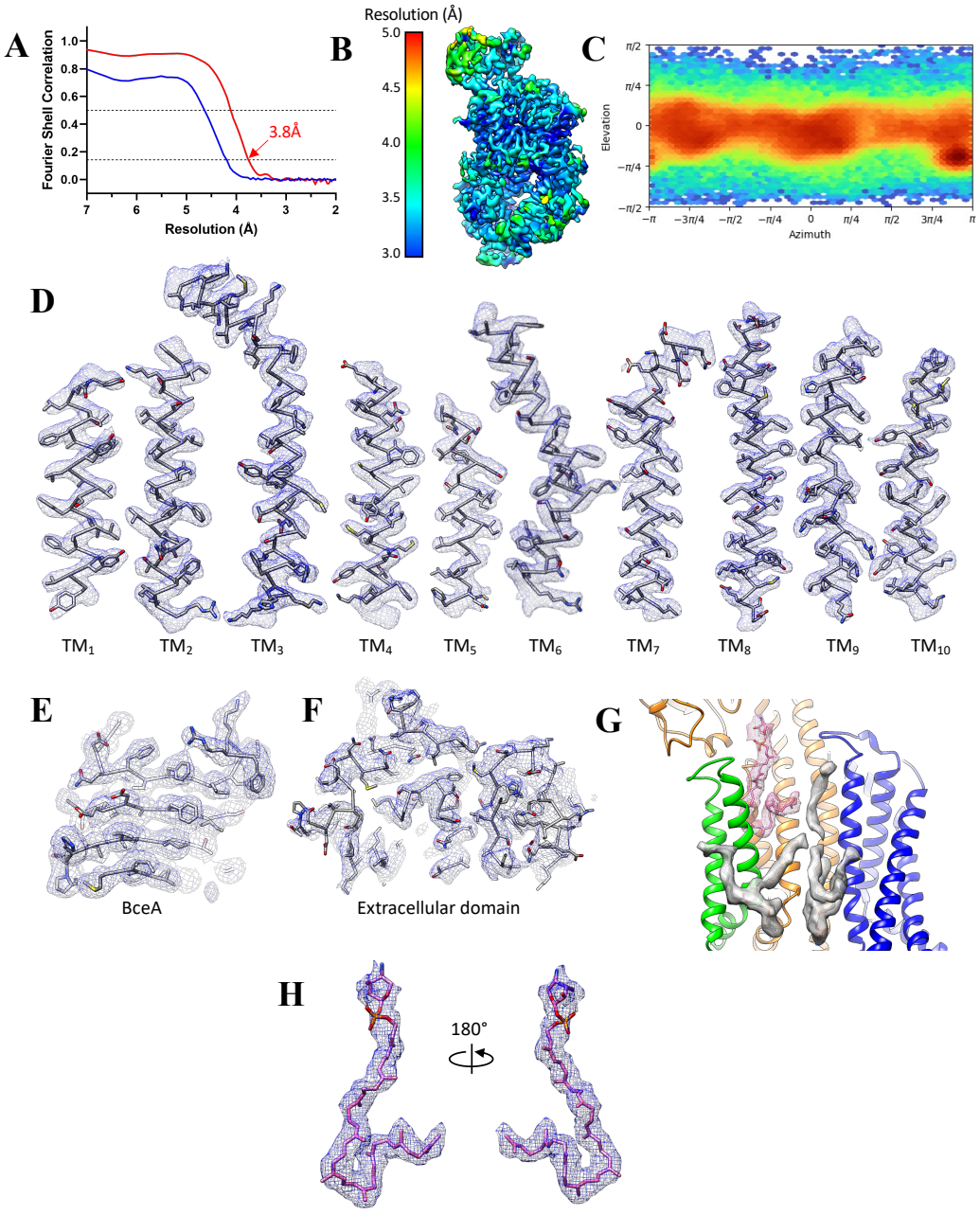

Figure 2.4: Cryo-EM Data Analysis for Nucleotide-Free BceAB. A) Fourier-shell correlation (FSC) curves for the final 3D reconstruction of BceAB in the nucleotide-free state. Both curves represent gold standard FSC calculated from half-maps of the final refinement. The blue curve is calculated without masking, and the red curve is calculated using a tight mask auto generated during non-uniform refinement in CryoSPARC. FSC values of 0.143 and 0.5 are indicated by dashed black lines. B) Local resolution of the final 3D reconstruction for nucleotide- free BceAB. Intrinsic flexibility results in lower resolution estimates for the extracellular domain.

Figure 2.4 (cont'd)

C) Angular distribution of all particles that resulted in the final 3D construction. D) Final cryo-EM map in the BceB TM helix region showing features suitable for de novo model building. E) Final cryo-EM map in the BceA nucleotide-binding domain region demonstrating clear definition of " sheets and side-chains. F) Final cryo-EM map in the extracellular domain region. G) View of the front hydrophobic region of BceB TM helices showing lipid density for several phospholipids (grey volume). H) Cryo-EM map for 4-amino-4-deoxy-α-L-arabinopyranosyl undecaprenyl phosphate in the lipid binding pocket.

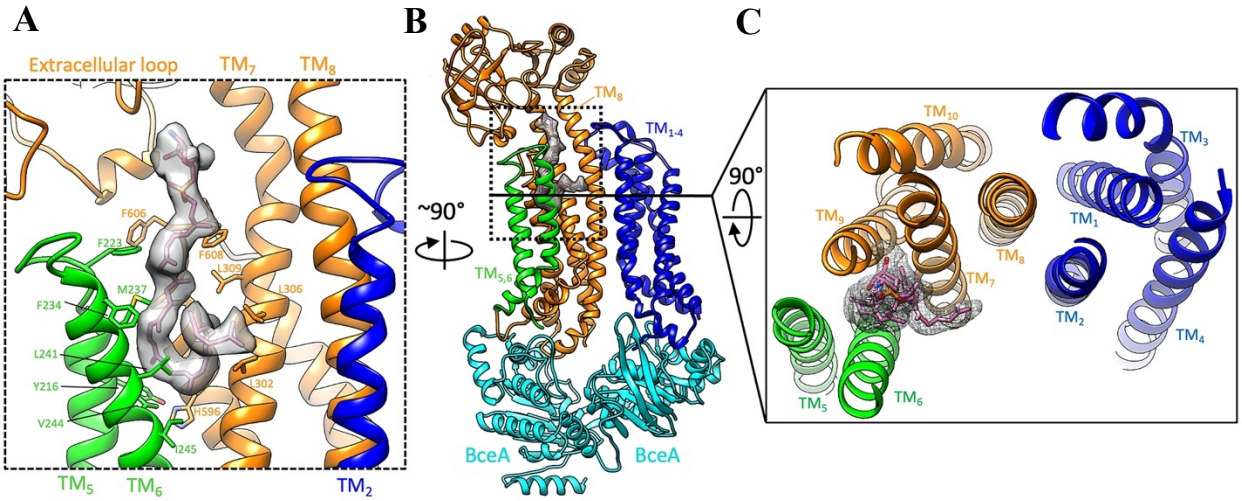

Figure 2.5: Lipid-binding pocket and TM arrangement in BceB. (*A*) Zoomed-in view of the lipid-binding pocket outlined with a dotted box in (*B*). Individual TM helices are labeled, along with specific residue side chains lining the lipid-binding pocket. The cryo-EM map encompassing AUP is shown as a transparent gray surface. The hydrophilic headgroup of the lipid is positioned directly beneath the extracellular domain. (*B*) Overall atomic model of BceAB in a nucleotide-free conformation, showing an asymmetric arrangement of BceA subunits and the protrusion of the large extracellular domain above $TM_{5–10}$. (*C*) Sliced view from the extracellular space of the TM helix arrangement observed in BceB. Binding of AUP (magenta sticks inside gray mesh) is clearly observed between $TM_{5,6}$ and $TM_{7,9}$.

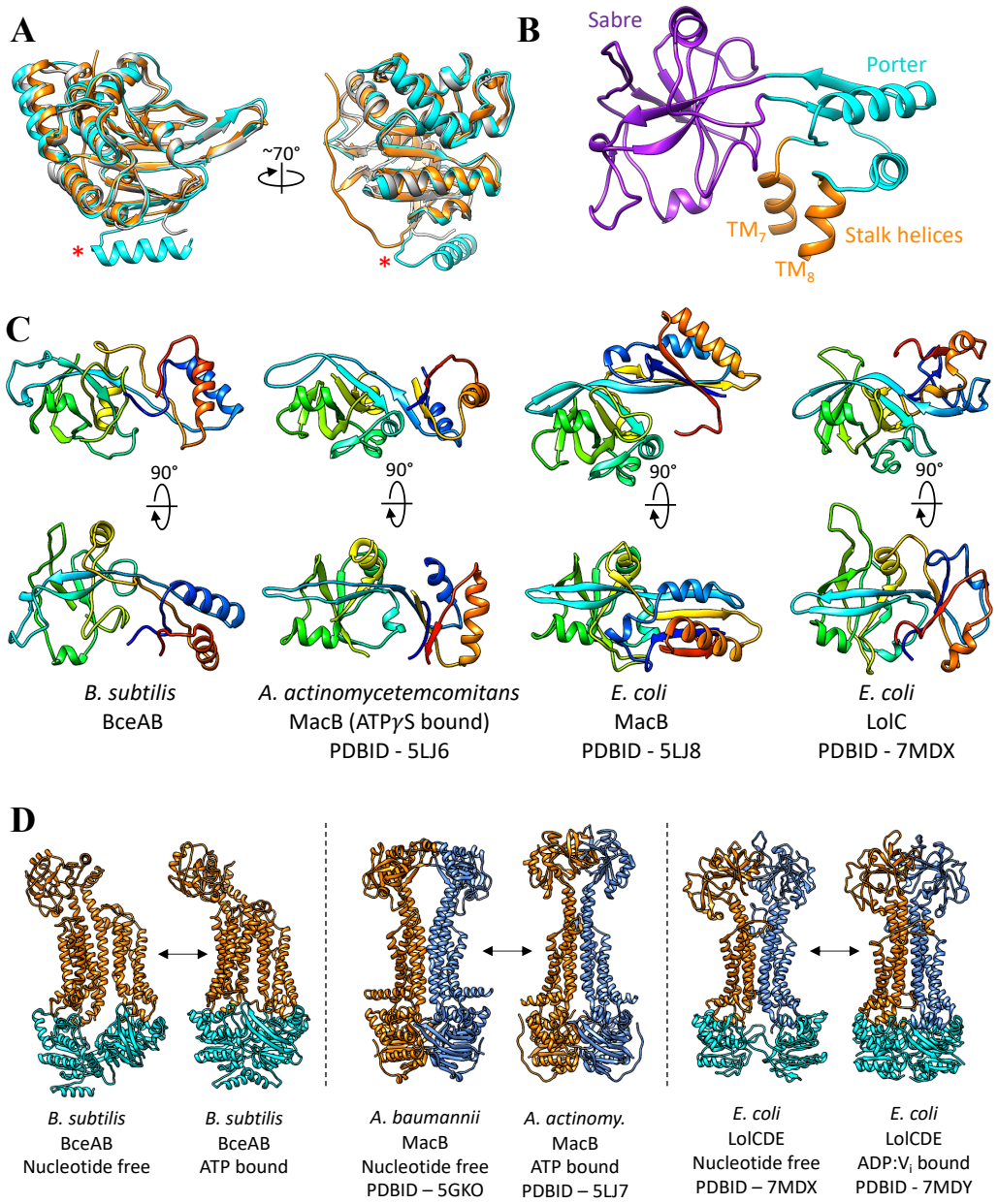

Figure 2.6: Comparison of BceAB to Gram-negative Mechanotransmission ABC Transporters. A) Comparison of BceA (cyan) to nucleotide-binding domains LolD (grey) and MacB (orange) from gram-negative transporters. BceA has an additional helix at the C-terminus (red asterisk) that is not seen in nucleotide-binding domains of other transporter complexes. B) Structure of the extracellular loop domain of BceB demonstrating Sabre and Porter domains similar to mechanotransmission type ABC transporters from gram-negative bacteria. C) Comparison of the extracellular loop domain observed in BceB versus mechanotransmission ABC transporters in gram-negative species. The top two rows of structures are colored in rainbow with the

Figure 2.6 (cont'd)

N-terminus of the extracellular domain blue, and transitioning to red at the C- terminus of the polypeptide chain. The bottom row of structures is in the same orientation as the middle row, but is colored with the Sabre and Porter domains as indicated in pane C. D) Comparison of the overall structure and conformational changes in BceAB compared to the ABC transporters MacB and LolCDE found in gram-negative bacteria. Individual protein chains are colored differently to highlight the different topology and assembly of individual transporters. In MacB the extracellular domain, TM helices, and nucleotide-binding domain are fused into one chain, whereas in BceAB and LolCDE the nucleotide- binding domains are individual polypeptides.

Data Collection and Processing	BceAB Nucleotide-free (EMDB-25811) (PDB 7TCG)	BceAB ATP-bound (EMDB-25812) (PDB 7TCH)
Magnification	105,000	105,00
Voltage (kV)	300	300
Electron exposure (e-/Å^2)	60.5	60.5
Defocus range (μm)	0.7-2.5	0.7-2.5
Pixel size (Å)	0.872	0.872
Symmetry imposed	C1	C1
Initial particle images (no.)	1,534,924	1,226,441
Final particle images (no.)	307,715	305,229
Map resolution (Å)	3.8	3.7
FSC threshold	0.143	0.143
Refinement		
Model resolution (Å)	3.9	3.8
FSC threshold	0.5	0.5
Map sharpening *B* factor (Å^2)	-180	-177
Model composition		
Non-hydrogen atoms	8891	9043
Protein residues	1123	1135
Ligands	1	3
B factors (Å^2)		
Protein	46.75	52.45
Ligand	25.95	38.71
R.m.s deviations		
Bond lengths (Å)	0.002	0.003
Bond angles (°)	0.536	0.575
Validation		
MolProbity score	1.78	1.79
Clashscore	5.54	5.67
Poor rotamers (%)	0	0
Ramachandran plot		
Favored (%)	92.11%	92.03%
Allowed (%)	7.89%	7.97%
Disallowed (%)	0	0

Table 2.1: Cryo-EM data collection and refinement statistics

Enzymatic Analysis of BceAB

Previous attempts to express and purify the BceAB transporter have resulted in enzyme preparations devoid of ATPase activity (8). We suspect that this lack of activity may stem from the use of dodecyl-maltopyranoside as the detergent used for solubilization and purification of the complex, as we found BceAB to be highly unstable in this detergent. However, when solubilized and purified in LMNG detergent, BceAB remained stable and retained a high level of specific ATPase activity (Fig. 2.7A). Interestingly, BceAB displayed an ATPase profile consistent with substrate and/or product inhibition, where increasing concentrations of ATP resulted in slightly reduced ATPase activity (Fig. 2.7A). This effect was consistently seen even when an ATP-regenerating assay system was used (Fig. 2.2C), suggesting that the slight inhibition at high ATP concentrations is not due to feedback inhibition by adenosine diphosphate (ADP) produced during the hydrolysis reaction. Ruling out the possibility of feedback ADP inhibition, the kinetics of ATP hydrolysis by detergent-solubilized BceAB suggest that ATP may bind to a lower affinity inhibitory site at high concentrations.

The ATPase activity of purified BceAB was potently inhibited by common ATPase inhibitors such as the substrate analog ATPγS or sodium ortho-vanadate (Fig. 2.2D). Furthermore, substitution of E169 to glutamine in the BceA nucleotide-binding domain completely abolished ATPase activity (Fig. 2.7A). Interestingly, the addition of Zn^{2+}-bacitracin also had a pronounced inhibitory effect on BceAB ATPase activity by decreasing the maximum velocity (V_{max}) and increasing the Michaelis constant (K_m) of the ATP hydrolysis reaction (Fig. 2.7B). In order to further probe the observed inhibition, we incubated BceAB with either Zn^{2+}-bacitracin, bacitracin alone, or Zn^{2+}-acetate. When bacitracin was supplied without the added Zn^{2+} ion, no inhibition of ATPase activity was observed, whereas Zn^{2+}-acetate produced an inhibition profile similar to that observed with Zn^{2+}-bacitracin (Fig. 2.7C). This result suggests that the inhibition observed upon addition of Zn^{2+}-bacitracin results from free Zn^{2+} interfering with the ATPase reaction (likely by mimicking Mg^{2+} in the ATP-binding site) rather than a direct effect of bacitracin on BceAB. Bacitracin is commonly sold as a Zn^{2+} salt, and divalent cations such as zinc mediate the interaction between bacitracin and the pyrophosphate moiety of UPP (Fig. 2.2E and F) (21). However, bacitracin can also utilize Mg^{2+} as a divalent cation to support interaction with UPP (22), and we were surprised to see that Zn^{2+}-free bacitracin had no effect on BceAB ATPase activity even when supplied in a reaction buffer that contained excess Mg^{2+} (Fig.

2.7C). The lack of an inhibitory or stimulatory effect of bacitracin on BceAB ATPase activity was highly unanticipated and provoked a closer inspection of the lipid-binding properties of purified BceAB.

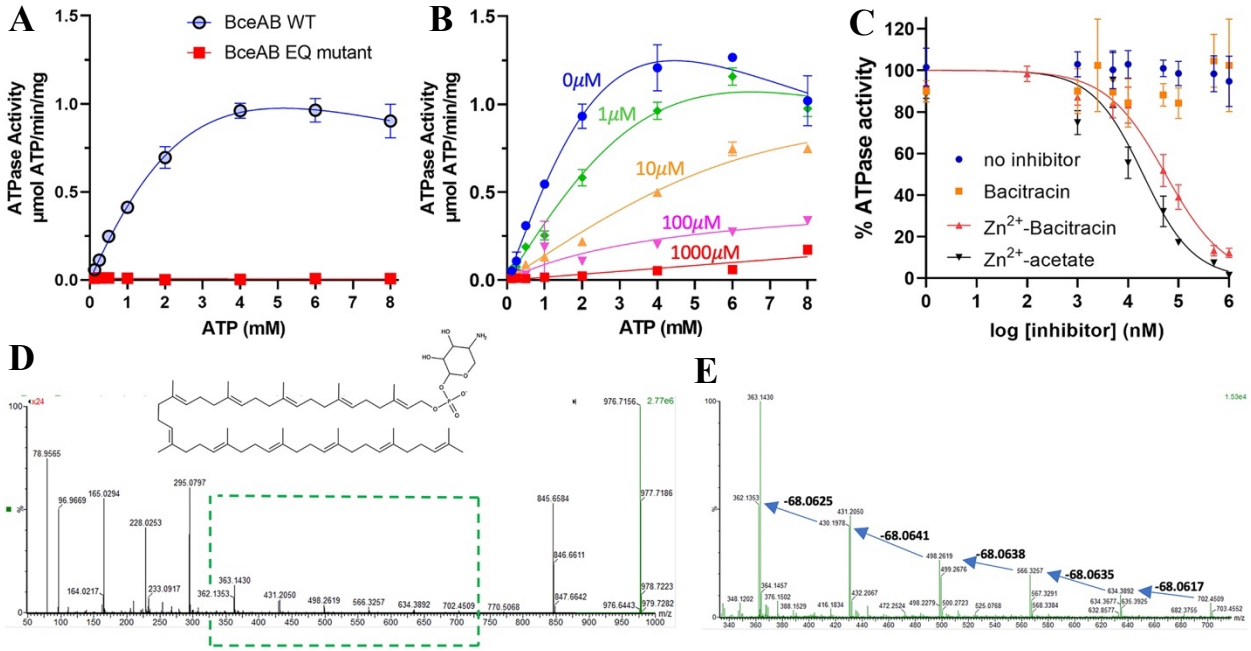

Figure 2.7: Biochemical characterization of BceAB. (*A*) ATPase activity of detergent-solubilized wild-type (WT) BceAB (open blue circles) compared to the E169Q variant (red squares). Data were fit with a model of substrate inhibition (solid lines). All data points were repeated in triplicate with the same batch of protein. Error bars represent SD from triplicate measurements. (*B*) ATPase activity of detergent-solubilized wild-type (WT) BceAB in the presence of increasing concentrations of Zn^{2+}-bacitracin. Concentrations of Zn^{2+}-bacitracin added in each reaction are indicated above each curve. Data were fit with a substrate inhibition model (solid lines). All data points were repeated in triplicate with the same batch of protein. Error bars represent SEM from triplicate measurements. (*C*) Inhibition of BceAB ATPase activity in the presence of Zn^{2+}-bacitracin, bacitracin, or Zn^{2+}-acetate. All data points were repeated in triplicate, and error bars represent SD from triplicate measurements. Inhibition by Zn^{2+}-bacitracin or Zn^{2+}-acetate was fit with a model of log[inhibitor] versus normalized response in GraphPad Prism. (*D*) Negative mode electrospray ionization (ESI(-)) MS/MS spectrum with *m/z* selection of 976 in the quadrupole and a 20- to 80-V ramp in the collision cell. *m/z* 976.7156 is consistent with a predicted formula of $C_{60}H_{99}NO_7P$ (expected *m/z* 976.7159, −0.7 ppm mass error). Fragment ions consistent with $C_{55}H_{90}O_4P^-$ (undecaprenyl phosphate *m/z* 845.6584) and $C_5H_{11}NO_7P^-$ (phospho-4-amino-4-deoxy-arabinose *m/z* 228.0253) are visible. The green dashed box represents the view in panel *E*. (*E*) Zoomed-in view of the 340 to 710 *m/z* region of the spectrum shown in *D* demonstrating successive neutral losses of C_5H_8 (68.06 Da) prenyl units.

Specialized Lipid-Binding Pocket

BceAB is proposed to recognize complexes between bacitracin and the lipid II cycle intermediate UPP. To recognize such peptide–lipid complexes, it is expected that the transporter should contain a binding site that allows for concomitant recognition of UPP in the membrane plane and bacitracin in the extracellular space. In the TM region of BceB, TM_5 and TM_6 are located adjacent to TM_7 and TM_9, where together these four helices form a V-shaped pocket facing the extracellular space (Fig. 2.5B and C). The extracellular domain of BceB is positioned directly above this pocket, where it is supported at the base by stalks from TM_7 and TM_8 (Fig. 2.5B). Contained within the pocket is a long lipid-like density displaying features consistent with repeating prenyl units (Fig. 2.5A and B and Fig. 2.4H). The headgroup of this lipid extends above the BceB TM helices into the aqueous region directly beneath the extracellular domain (Fig. 2.5B). The location and properties of this lipid-binding pocket match closely with that expected for a bona-fide UPP-binding pocket. However, the limited resolution of the cryo-EM map in the headgroup region of the bound lipid combined with the unanticipated results of Zn^{2+}-bacitracin inhibition in ATPase assays prompted a more thorough investigation of the lipid species bound within this pocket.

In order to help ascertain the potential identity of the lipid seen in the V-shaped pocket between $TM_{5,6}$ and $TM_{7,9}$, we performed liquid chromatography–tandem mass spectrometry (MS/MS) analysis on the lipids that copurified with BceAB. In addition to bacterial membrane phospholipids containing phosphoethanolamine and phosphoglycerol headgroups (Figs. 2.8A and 2.9), we identified a later eluting peak with *m/z* 978.7301 in positive ion mode and *m/z* 976.7136 in negative ion mode (Fig. 2.8A). Based on the accurate mass, MS/MS analysis (Fig. 2.7D and E and Fig. 2.8B-E), and similarity to spectra obtained for a related lipid from *Francisella novicida* (23), we annotated this lipid species as 4-amino-4-deoxy-α-L-arabinopyranosyl undecaprenyl phosphate (AUP). AUP is a modified undecaprenyl-phosphate lipid common in bacteria such as *E. coli*, where modification of lipid A with aminoarabinose is used to resist attack by polymyxin antimicrobials (24, 25).

Although copurification of BceAB with an undecaprenyl-phosphate lipid containing an alternate headgroup is likely the result of expressing a gram-positive transporter in a gram-negative host, several lines of evidence suggest that the lipid-binding pocket observed in our cryo-EM structure is the native binding location for UPP. First, several residues lining the

pocket, such as G215, S219, and A301, have previously been shown through random chemical mutagenesis studies to be involved in bacitracin sensing and/or resistance by BceAB (26). Moreover, the orientation of the lipid observed in our structure would orient the pyrophosphate moiety of UPP directly beneath the extracellular domain. As bacitracin is known to bind the pyrophosphate moiety of UPP (21), this would position the UPP-bound bacitracin complex in direct vicinity for interaction with the extracellular domain. Thus, our cryo-EM maps and mass spectrometry analysis in conjunction with previous biochemical experiments suggest that the V-shaped pocket formed between $TM_{5–7}$ and TM_9 is the preferred binding location for UPP and other undecaprenyl-phosphate–containing lipids of the lipid II cycle.

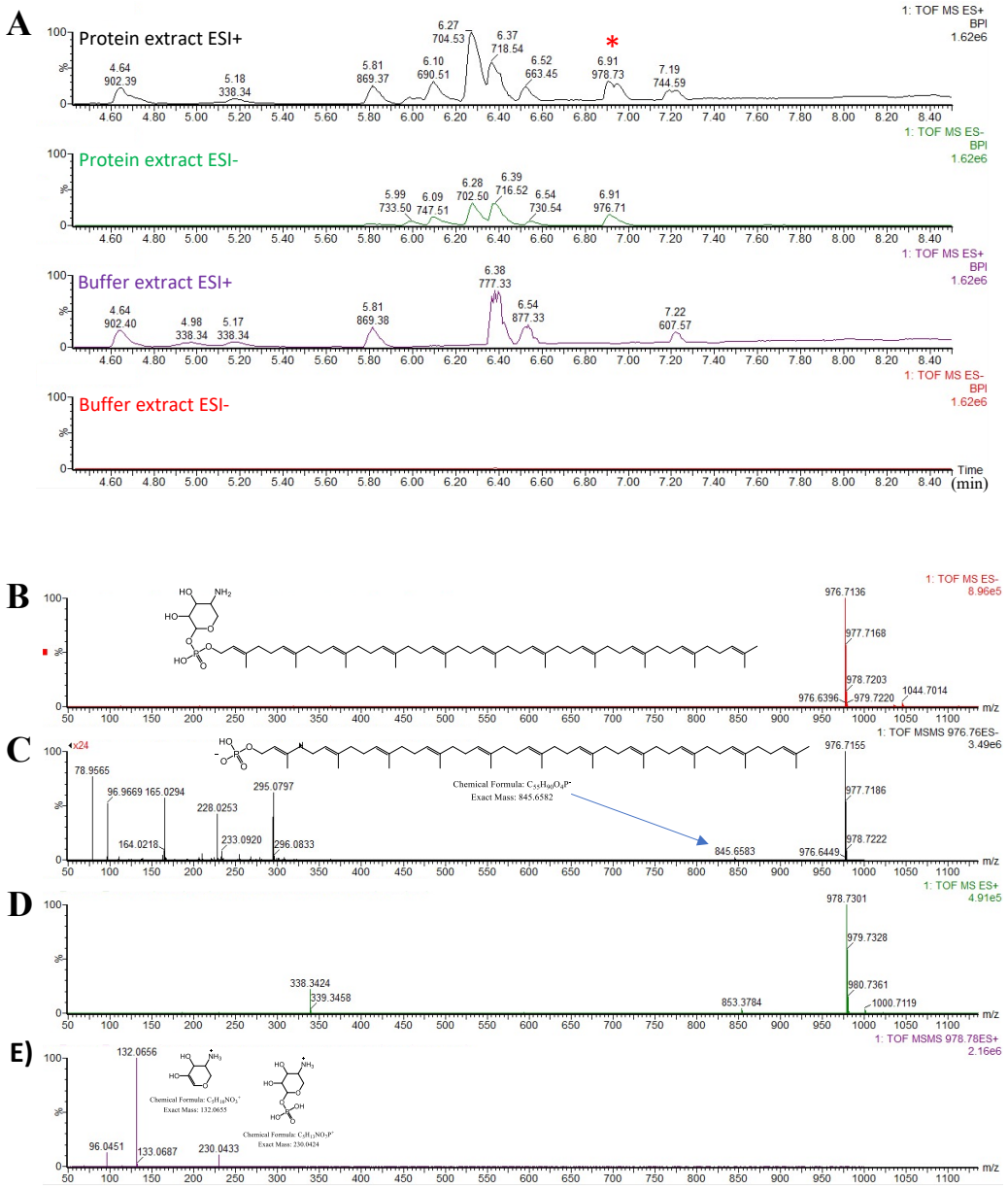

Figure 2.8: Mass spectrometry analysis of co-purified lipid. A) LCMS chromatograms of organic extracts from purified BceAB (black and green traces) or a buffer control (purple and red traces) showing distinct separation of lipid species on a C18 column. Extracts were analyzed in either positive (ESI+; black and purple traces) or negative (ESI-; green and red traces) electrospray ionization mode. The red asterisk indicates the peak with a neutral mass of 977.7 Da that was further analyzed by MS/MS. B) MS spectrum (with no collision energy) obtained using negative ion mode for the 977.7 neutral mass species marked with an asterisk in A. C) MS/MS spectrum of m/z 976 in negative ion mode. A neutral loss of the deoxy-amino- arabinose results

Figure 2.8 (cont'd)

in the m/z 845.6583 fragment which is consistent with the formula C55H90O4P- (undecaprenyl phosphate, expected mass 845.6577, 0.7 ppm mass error). The m/z 228.0253 fragment would be the deoxy-amino- arabinose anion with formula C5H11NO7P- (expected mass 228.0273, -8.8 ppm mass error). The m/z 96.96 and 78.95 ions are H2PO4- and PO3- fragments. D) MS spectrum (with no collision energy) obtained in positive ion mode for the 977.7 neutral mass species marked with an asterisk in A. E) MS/MS spectrum of m/z 978 in positive ion mode. The phospho-deoxy-amino-arabinose fragment is seen at m/z 230.0433 (C5H13NO7P+, expected mass 230.0430, 1.3 ppm mass error). A further loss of the phosphate group gives the m/z 132.0656 deoxy-amino-arabinose fragment (expected mass 132.0661, -3.8 ppm mass error).

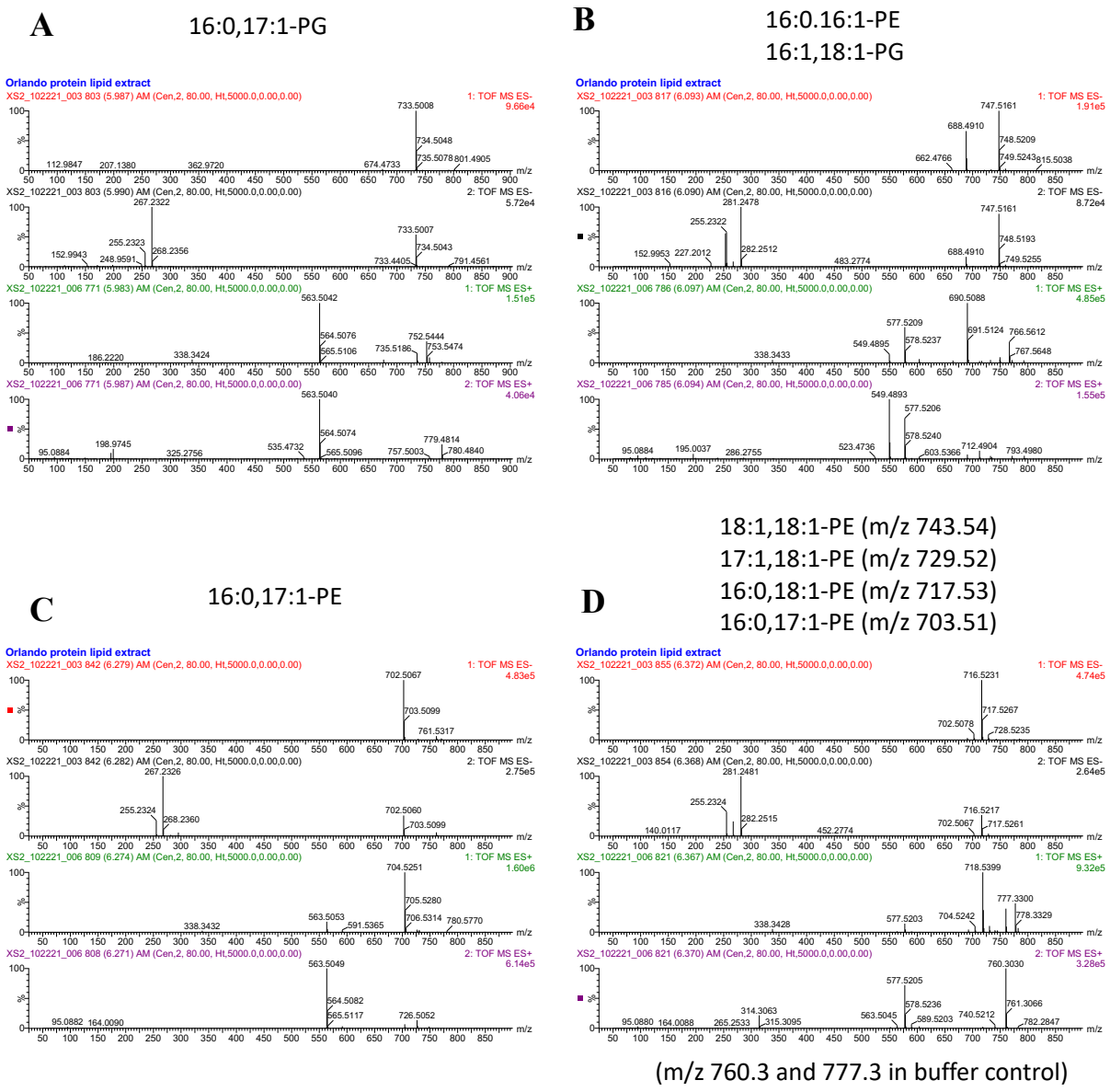

Figure 2.9: Mass spectrometry analysis of co-purified phospholipids. Shown are the MS spectra for several different lipid species identified at different elution times in the initial LC/MS run in Figure S5A. Data were acquired using a non-selective MSe method (described in Methods) with function 1 obtained without any collision energy and function 2 acquired using a collision energy ramp to induce fragmentation. The function number and ionization mode are listed in the upper right corner of each chromatogram (for example, 1: TOF MS ES- indicates function 1 data acquired by electrospray ionization in negative ion mode). Each panel (A-D) shows spectra for both functions 1 and 2 acquired in negative and positive ion modes and the lipid species identified based on the accurate mass and fragmentation patterns is listed

Figure 2.9 (cont'd)

(PG, phosphoglycerol; PE, phosphoethanolamine). Peaks at 6.09 min (B) and 6.37 min (D) contain multiple co-eluting lipids.

Structure of BceAB in an ATP-Bound Conformation

The conformational changes of BceAB elicited by ATP binding and hydrolysis are required to mediate resistance to bacitracin in *B. subtilis*, as well as to initiate signaling through the BceS sensor kinase (6). To understand the nature of these conformational changes, we utilized the ATPase-deficient E169Q variant of BceA to determine the cryo-EM structure of BceAB in an ATP-bound conformation at an overall resolution of ~3.7 Å (Figs. 2.10A, 2.11, and 2.12, Table 2.1). Binding of ATP induces the BceA subunits to transition into a symmetrical dimer arrangement (Fig. 2.10A), and clear density for ATP is observed between the signature and Walker A motifs in both potential ATP-binding sites between BceA monomers (Fig. 2.12G).

In the ATP-bound conformation, the cytosolic linker between TM_4 and TM_5 encompassing residues 178 to 196 of BceB becomes ordered and visible in the cryo-EM map (Fig. 2.10D and E). The linker spans across and interacts with the top of both BceA subunits and is in close proximity to one of the two ATP-binding sites. The linker position makes it such that the ATP-binding site in the front of the transporter is more buried and shielded from solvent than the opposite site in the rear (Fig. 2.10E). Thus, although the two ATP-binding sites in a BceA dimer are composed of identical binding interfaces, interaction of the $TM_{4–5}$ linker with the BceA subunits in the front of the transporter complex generates asymmetry between the two ATP-binding sites in the overall complex. Although from our cryo-EM structure alone we cannot distinguish if the two observed ATPase sites are equally functional, the different solvent accessibility and asymmetry induced by the cytosolic linker between TM_4 and TM_5 may underlie the substrate inhibition profiles observed in our ATPase assays (Fig. 2.7A and Fig. 2.2C). At high concentrations of ATP when both potential ATP-binding sites are saturated, interaction of the $TM_{4–5}$ linker with the top of the BceA monomers could potentially slow the dissociation of the BceA subunits after the ATP hydrolysis reaction is complete. This in turn could slow the dissociation of ADP and/or phosphate from the more obstructed site, resulting in the substrate inhibition profile we observed. However, further work is needed to dissect the potential role of each ATP-binding site in the overall function of the BceAB complex, particularly in an in vivo context.

Dimerization of BceA subunits in response to ATP binding also induced large-scale conformational shifts in the TM and extracellular regions of BceB. Most strikingly, in the ATP-bound conformation, the extracellular domain was rotated ~43° away from its position in the

nucleotide-free structure. This rotation was primarily a result of bending in the middle of the TM_8 at residue G525 (Fig. 2.10B). G525 was previously identified in a chemical mutagenesis screen as a residue involved in resistance to bacitracin and initiation of signaling through the BceS sensor kinase (26). Our cryo-EM structure confirmed that the flexibility and hinge-like properties of G525 allowed the extracellular domain to undergo large-scale conformational shifts in response to ATP binding. Although the G525 hinge allowed the extracellular domain to pivot atop the TM region, the internal structure of the extracellular domain itself remained stable, and the domain moved primarily as a rigid body between nucleotide-free and ATP-bound conformations.

Binding of ATP and dimerization of the BceA subunits also induced a conformational rearrangement of the TM helices in BceB (compare Figs. 2.5C and 3.10C). In the ATP-bound conformation, the $TM_{5–10}$ helical bundle rotated inward toward the opposite $TM_{1–4}$ bundle, closing off the large hydrophobic groove observed at the front of the complex in the nucleotide-free state (compare Figs. 2.1C and 3.10A). Although the $TM_{5–10}$ helical bundle underwent rotation largely as a rigid body, the rotation axis was centered more toward $TM_{7–10}$ than $TM_{5,6}$. For this reason, the rotation caused significant translation of $TM_{5,6}$ toward $TM_{1–4}$ in the opposite half of the transporter (Fig. 2.12E). In the ATP-bound conformation, TM_2 contacted TM_6 at the apex near the extracellular space (Fig. 2.10*C*), effectively sealing off the UPP-binding pocket from the lipid environment. Interestingly, clear lipid density corresponding to AUP was observed within the center of the TM helix bundle, where it was surrounded by several TM helices and shielded from the bulk lipid membrane (Fig. 2.10C and Fig. 2.12F and G). In this configuration, the aminoarabinosyl headgroup of AUP was pointed into the extracellular space, where it was almost completely solvent exposed and located far from the tilted extracellular domain (Fig. 2.12H). Thus, the overall conformational transition of BceAB induced by binding of ATP serves to sequester the bound AUP tightly within the TM helices and move the extracellular domain far from the headgroup of the lipid.

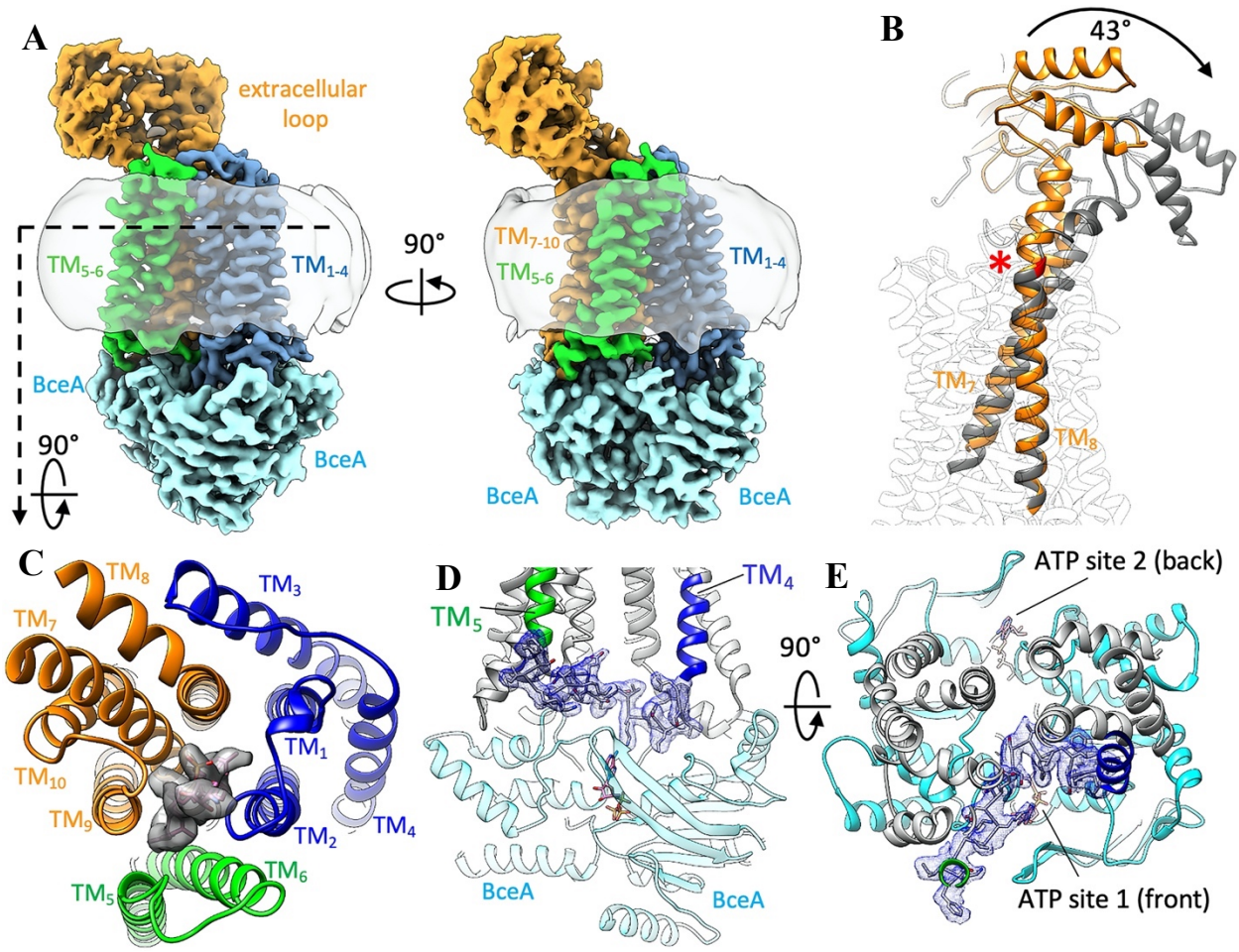

Figure 2.10: ATP binding induced conformational changes in BceAB. (*A*) Cryo-EM structure of ATP-bound BceAB (E169Q BceA variant). Subunits are colored the same in previous figures. The detergent micelle is shown as a transparent gray outline. (*B*) Structures of BceAB in the nucleotide-free (orange cartoon) and ATP-bound (gray cartoon) conformation were aligned at the intracellular region of $TM_{7,8}$. ATP binding induces helical bending at G525 (red cartoon and asterisk) and causes the extracellular domain to rotate ~40° away from the central *z* axis of the transporter. (*C*) View from the extracellular space of the TM helices of BceAB in an ATP-bound conformation. AUP is shown in magenta sticks and gray surface density, where it is captured on all sides by the inward collapse of the TM helices in the ATP-bound conformation. (*D*) The cytosolic linker between TM_4 and TM_5 becomes ordered in the ATP-bound conformation. The cryo-EM map for the linker is shown in blue mesh just above the bound ATP (magenta sticks). (*E*) View from the membrane of the two ATP-binding sites between the BceA monomers. The front ATP-binding site 1 is covered by the ordered TM_4-TM_5 linker, which substantially reduces solvent accessibility to the bound ATP compared to the back ATP-binding site 2.

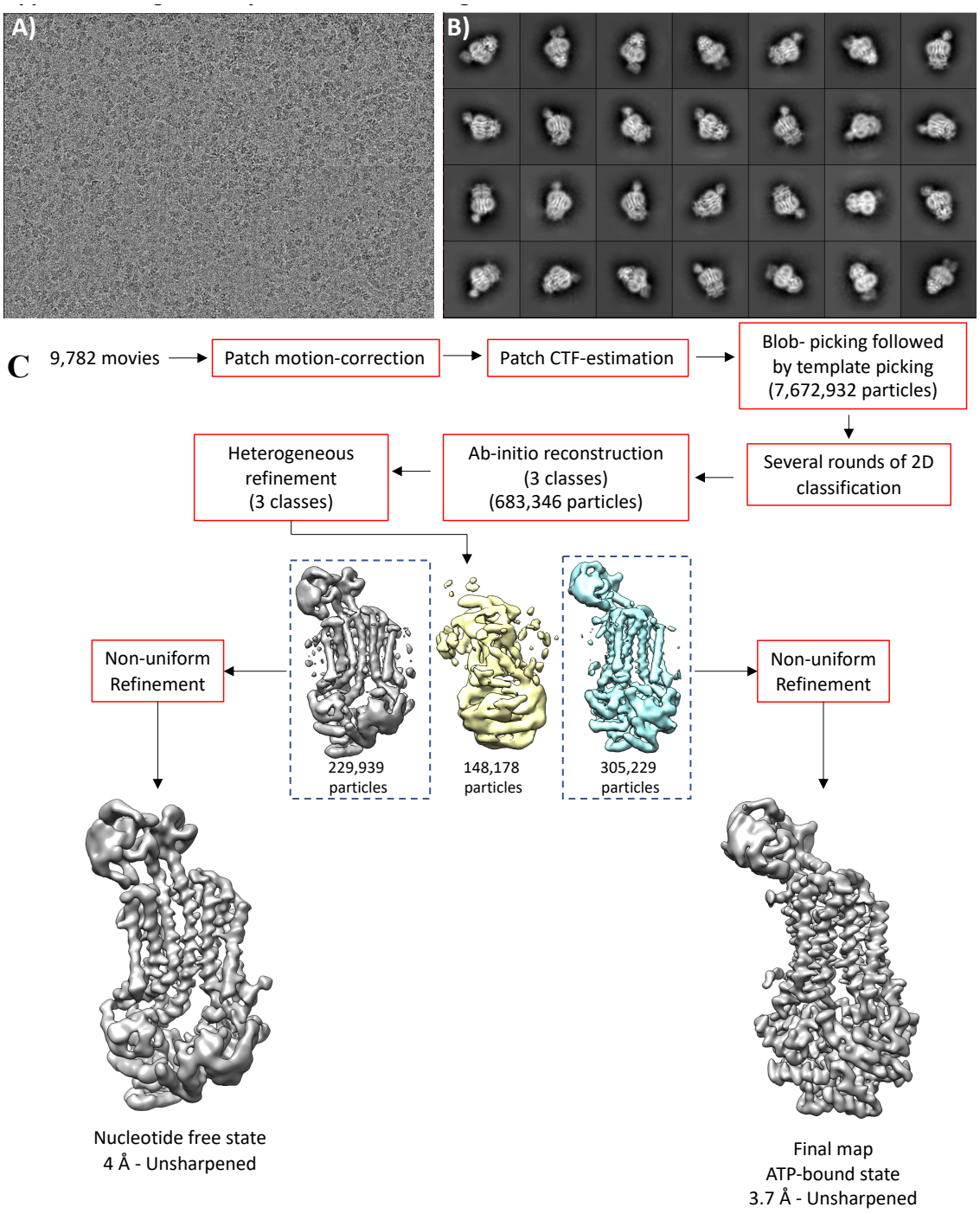

Figure 2.11: Cryo-EM Data Processing for ATP-bound BceAB E169Q. A) Cryo-electron micrograph of BceAB-E169Q mutant bound to ATP. B) 2D-averages of BceAB-E169Q mutant bound to ATP. 2D-averages clearly show the BceA subunits in a closed and dimerized configuration. C) Data processing workflow to obtain the final 3D reconstruction of BceAB-E169Q mutant bound to ATP. Heterogeneous refinement in CryoSPARC clearly separated a nucleotide-free conformation from the ATP bound conformation.

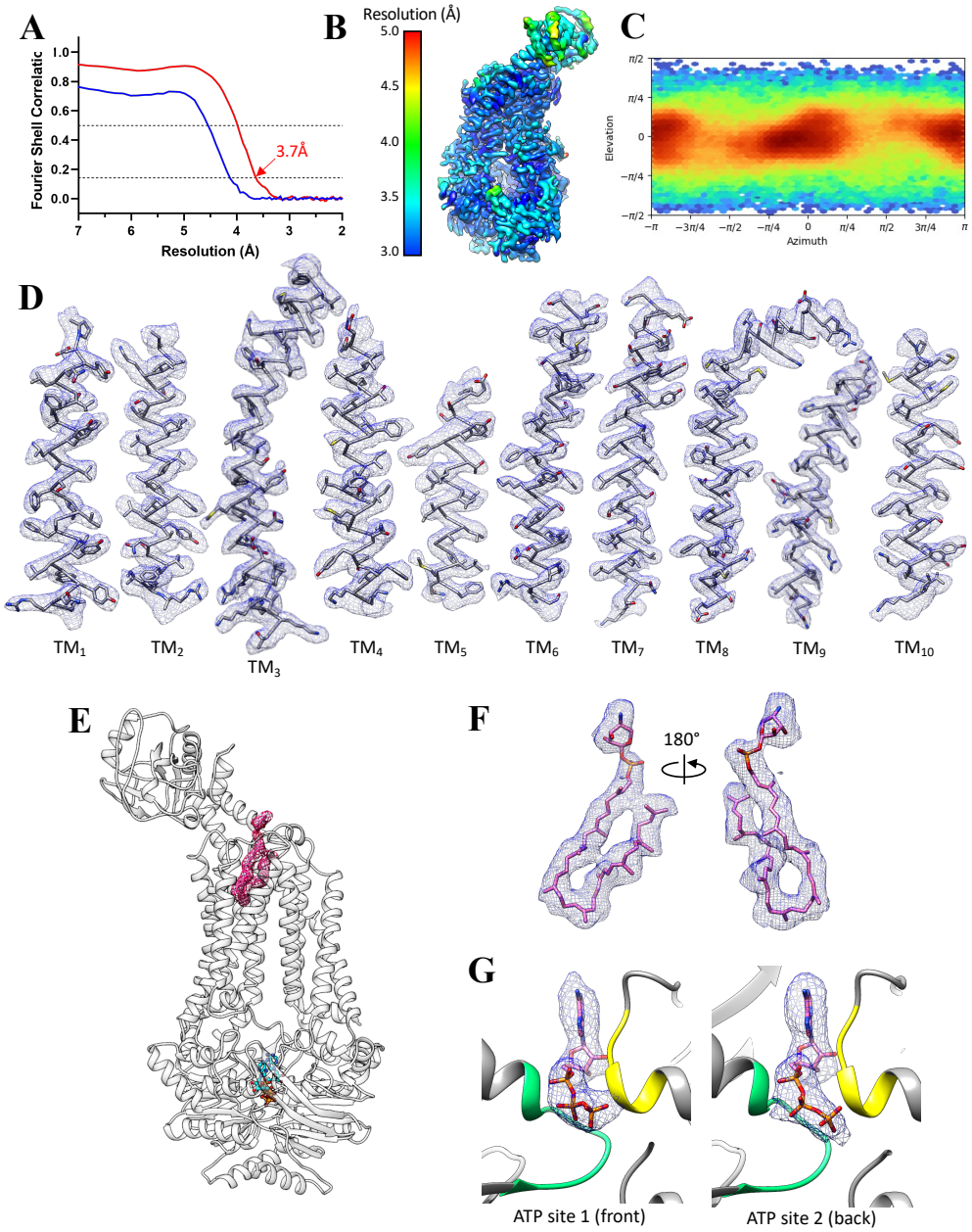

Figure 2.12: Cryo-EM Data Analysis for ATP-bound BceAB E169Q. A) Fourier-shell correlation (FSC) curves for the final 3D reconstruction of BceAB (containing E169Q BceA) bound to ATP. Both curves represent gold standard FSC calculated from half-maps of the final refinement. The blue curve is calculated without masking, and the red curve is calculated using a tight mask auto generated during non- uniform refinement in CryoSPARC. FSC values of 0.143 and 0.5 are indicated by dashed black lines. B) Local resolution of the final 3D reconstruction for BceAB (containing E169Q BceA) bound to ATP. C) Angular distribution of all particles that resulted in the final 3D construction. D) Final cryo-EM map in the BceB TM helix region

Figure 2.12 (cont'd)

showing features suitable for de novo model building. E) Overlay of the TM helices in the nucleotide-free conformation (clear white helices) versus the ATP-bound conformation (blue, orange and green). Directions of helical movements induced by ATP binding are shown as red arrows. F) Cryo-EM map for AUP in the lipid binding pocket. G) Cryo-EM map for ATP bound in both potential sites between the BceA dimer. The Walker A motif is colored green and the signature motif is colored yellow. H) Structural model of BceAB (formed using E169Q BceA) bound to ATP. ATP is shown as cyan balls and sticks. The cryo-EM map corresponding to AUP is shown as magenta mesh. The AUP phosphate headgroup protrudes into the extracellular space.

Discussion

Bce modules are widespread components of cell envelope stress response systems in gram-positive bacteria. Despite their importance to cell survival and resistance to a variety of medically relevant antibiotics, the precise mechanism by which Bce modules sense and respond to antimicrobial peptides has remained obscure. Our cryo-EM structures begin to shed light on the architecture and mechanism of these unusual membrane protein complexes. Compared to other ABC transporters, BceAB possesses a unique overall architecture with 10 TM helices and a single large extracellular domain. However, several structural features of the transporters are reminiscent of type VII mechanotransmission ABC transporters from gram-negative bacteria. The extracellular domain with Sabre and Porter subdomains, along with FtsX-like folds in the TM helix bundles, bear similarity to ABC transporters such as MacB and LolCDE (Fig. 2.6D) (16–18). Much like these transporters in gram-negative bacteria, our structural analysis suggests that Bce-type ABC transporters do not transport any molecules across lipid membranes. Rather, the structure and conformational changes of BceAB are consistent with a previously proposed mechanism of target protection (7) wherein the conformational cycling of the transporter frees lipid II cycle intermediates from the inhibitory grasp of antimicrobial peptides.

Our cryo-EM structures suggest a plausible overall mechanism for bacitracin recognition and resistance (Fig. 2.13). The structure of BceAB in a nucleotide-free conformation revealed a critical binding pocket for undecaprenyl lipid II intermediates such as UPP, with the headgroup of the bound lipid positioned directly beneath the large extracellular domain (Fig. 2.13, *State 1*). The bound lipid was located such that if bacitracin were to bind to the pyrophosphate moiety of UPP, it would be positioned to interact with the large extracellular domain of BceB (Fig. 2.13, *State 2*). While the precise points of interaction between bacitracin and BceAB have not yet been identified, the role of the extracellular domain in antimicrobial peptide recognition is supported by experiments in which the extracellular domain of *Staphylococcus aureus* Bce module transporter VraG was swapped with that of the closely related transporter VraE, resulting in altered ligand specificity (15). Subsequent binding of ATP between BceA subunits induces a conformational change of the entire complex such that the bound lipid is sandwiched tightly by the TM helices and remains in the plane of the membrane, while at the same time helical bending at G525 in TM_8 tilts the extracellular domain to facilitate removal of bacitracin from UPP (Fig. 2.13, *State 3*). The model presented in Fig. 2.13 is consistent with previous cell-based

biochemical studies that suggest BceAB releases bacitracin from UPP (7).

While our structural studies begin to paint a clear picture of the target protection mechanism mediated by BceAB, more in-depth structural and biochemical work will be required to understand some key aspects of the model proposed above. In particular, the precise molecular determinants that underlie interaction of bacitracin or other antimicrobial peptides with the extracellular domain of BceB remain unclear. In our ATPase assays, bacitracin failed to elicit an effect on BceAB activity, and free Zn^{2+} had a pronounced inhibitory effect. The fact that bacitracin lacked an effect on BceAB ATPase activity is seemingly at odds with the proposed detoxifying activity of the complex. However, this result is most readily explained by the unanticipated presence of an aminoarabinose-modified form of undecaprenyl-phosphate in the V-shaped pocket of BceB. Replacement of the pyrophosphate of UPP with the aminoarabinosyl headgroup of the copurified lipid likely prevents proper interaction between bacitracin and the lipid target and prevents BceAB from recognizing a proper ternary complex of Zn^{2+}–bacitracin–UPP. In order to obtain structural and functional insight into the interaction between antimicrobial peptides, lipid II cycle intermediates, and the extracellular domains of Bce-type transporters, future efforts will require altered protein expression and purification procedures to isolate complexes from more native host organisms with pools of unmodified lipid species.

Future emphasis should also be placed on understanding substrate specificity of Bce modules. Previous studies have shown that Bce modules within a single species each respond to a different suite of antimicrobial peptides. For instance, BceAB can interact with bacitracin–UPP complexes and also with similar complexes such as that formed between mersacidin and lipid II (27). How Bce-type transporters distinguish between apparently similar antimicrobial peptides is unclear. Our studies presented here provide the structural basis to begin untangling this complicated network of transporter–lipid–antimicrobial peptide interactions. Revealing the overall structure, specialized lipid-binding properties, and nucleotide-binding induced conformational changes of BceAB represents an important step forward in developing a comprehensive molecular understanding of antimicrobial peptide sensing and resistance mechanisms across gram-positive bacteria.

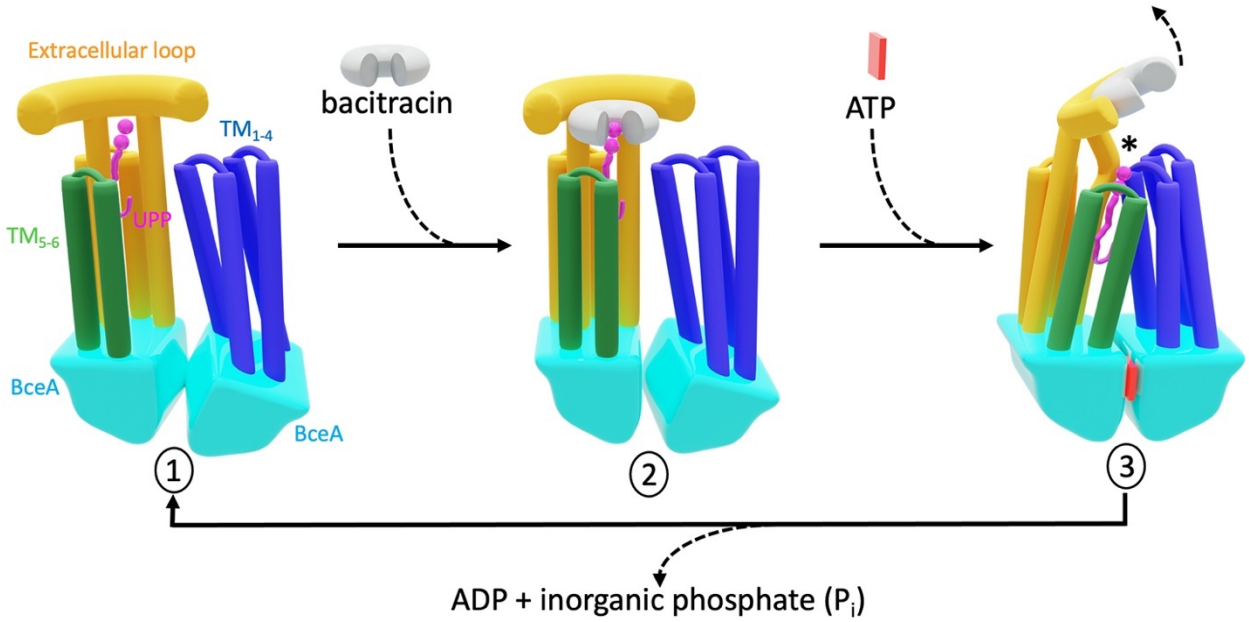

Figure 2.13: Model of bacitracin recognition and removal. Shown is a cartoon model of how BceAB recognizes bacitracin-bound UPP and removes the bacitracin from the lipid to mediate target protection. In the resting state (*State 1*), UPP (magenta) binds with the lipid tail between the $TM_{5,6}$ and $TM_{8–10}$ helical bundles and the pyrophosphate headgroup extending into the extracellular space just beneath the large extracellular loop domain. The BceA subunits are tilted in an asymmetric fashion. In *State 2*, bacitracin (white open donut) binds and wraps around the pyrophosphate moiety of UPP. The bound bacitracin is gripped by the extracellular domain. Subsequent binding of ATP (red square) binding induces dimerization of the BceA subunits, which collapses the TM helices around UPP in the membrane plane (*State 3*). Dimerization of BceA results in TM_8 helical bending (black asterisk), which tilts the extracellular domain and removes bacitracin from UPP. ATP hydrolysis causes the BceA subunits to dissociate from one another and relax the complex back to the resting state.

Methods

Protein Expression and Purification

The overlapped genes encoding BceA (28kDa; Uniprot ID: O34697) and BceB (72kDa; Uniprot ID: O34741) were initially PCR amplified from *B. subtilis* genomic DNA (primers 1 and 2, Table 2.2) and cloned between the Nde1 and Kpn1 sites of a pETDUET-1 vector. This procedure added a 6x-His tag to the N terminus of BceA. After initial expression and purification trials with this plasmid (or the same construct subcloned into a pET28a vector), we sought to separate the overlapped *bceA* and *bceB* genes and place each gene under the control of an individual promoter in petDUET-1. To construct this plasmid, the *bceA* gene with an N-terminal 6x-His tag (primers 3 and 4, Table 2.2) and the *bceB* gene (primers 5 and 6, Table 2.2) were separately PCR amplified from the initial pETDUET-1 expression plasmid. These two PCR fragments were then combined with a gBLOCK fragment encoding the second T7 promoter region of pETDUET-1 and assembled into a single DNA fragment (6x-His *bceA – T7 – bceB)* using NEB HiFi Assembly according to the manufacturer's protocol. Following assembly, the resulting DNA fragment was digested with Nco1 and Xho1 and cloned into a fresh pETDUET-1 vector that had been digested with the same enzymes. This procedure generated an expression plasmid containing DNA encoding N-terminally 6x-HIS tagged *bceA* with expression driven from one T7 promoter of petDUET-1 and DNA encoding *bceB* driven from the second T7 promoter. This plasmid with *bceA* and *bceB* behind separate T7 promoters in pETDUET-1 was used to produce BceAB for all structural and enzymatic studies.

The expression plasmid was transformed into C41(DE3) cells, and a starter culture from a single colony was grown at 37 °C in Luria Broth (LB) medium with 100 μg/mL ampicillin. The starter culture was used to inoculate 4 L of LB medium with 100 μg/mL ampicillin and Antifoam-204 in baffled Fernbach flasks. Cultures were grown at 37 °C to an optical density (OD_{600}) of ∼0.8 before reducing the temperature to 30 °C and inducing protein expression with 0.7 mM isopropyl-β-D-thiogalactoside. After 4 h of induction, the cultures were harvested by centrifugation, and the cell pellets were flash frozen in liquid nitrogen and stored at −80 °C.

Frozen cell pellets were thawed and resuspended in lysis buffer (25 mM Tris [pH 8], 150 mM NaCl, 10% glycerol, and 5 mM β-mercaptoethanol) supplemented with 1 μg/mL pepstatin A, 1 μg/mL leupeptin, 1 μg/mL aprotinin, 0.6 mM benzamidine, and 5,000 units of Dr. Nuclease (Syd Labs). Cells were lysed by sonication, and membranes were isolated by ultracentrifugation

at ∼100,000 × *g* for 1 h. Isolated membranes were resuspended in lysis buffer and solubilized with 1% LMNG by stirring for 1 h at 4 °C. Insoluble material was removed by ultracentrifugation at 100,000 × *g* for 1 h, and the resulting supernatant was applied to Co^{3+}-Talon resin. The resin was washed with ∼10 column volumes of buffer A (25 mM Tris [pH 8], 150 mM NaCl, 20 mM imidazole, 10% glycerol, and 0.005% LMNG) before eluting bound protein with buffer A containing 250 mM imidazole. The eluted protein was concentrated in a 100-kDa MWCO spin concentrator and injected onto a Superdex 200 Increase 10/300 GL column equilibrated in 25 mM Tris (pH 8), 150 mM NaCl, and 0.005% LMNG. Peak fractions corresponding to intact BceAB complex (peak 1, Fig. 2.2A, elution volume of ∼11 to 13 mL) were pooled, concentrated in a 100-kDa MWCO spin concentrator, and used immediately for cryo-EM studies or flash frozen in liquid nitrogen and stored at −80 °C for use in biochemical assays.

BceAB containing the E169Q variant of BceA was generated by site-directed mutagenesis using the Q5 Mutagenesis Kit (New England Biolabs) according to the manufacturer's protocol. The protein complex containing the BceA-E169Q variant was expressed and purified as described above. Before preparing grids for cryo-EM analysis, the protein complex was incubated with 5 mM ATP-Mg^{2+} for ∼30 min at room temperature.

Primer #	Primer sequence (5' → 3')
1	**ATATACATATGAGCGGACATCACCATCATCACCACGTGATTTTAGAAGCGAATAAA ATTC** amplify *bceA* from genomic DNA with an N-terminal 6x-His tag and Nde1 cut site (forward primer)
2	**TTATTGGTACCTCACAACGACGATTTAATG** amplify *bceA* from genomic DNA with a C-terminal Kpn1 cut site (reverse primer)
3	**TAAGAAGGAGATATACCATGAGCGGACATCACCAT** amplify *bceA* from genomic DNA and add Nco1 cut site (forward primer)
4	**TTAATGTTCATGCTGCACCC** amplify 6x-His *bceA* from pETDUET-1 (reverse primer)
5	**ATGAACATTAATCAGCTCATCC** amplify *bceB* from pETDUET-1 (forward primer)
6	**GTTTCTTTACCAGACTCGAGTCACAACGACGATTTAATGAC** amplify *bceB* from pETDUET-1 (reverse primer)
7	**TTTCGCTGATCAGCCGACCGGCG** BceA E129Q mutagenesis primer (forward primer)
8	**ATAATGCTCGGGTCATGATAAACG** BceA E129Q mutagenesis primer (reverse primer)
gBLOCK	**GGGTGCAGCATGAACATTAAGCGGCCGCATAATGCTTAAGTCGAACAGAAAGTAA TCGTATTGTACACGGCCGCATAATCGAAATTAATACGACTCACTATAGGGGAATTG TGAGCGGATAACAATTCCCCATCTTAGTATATTAGTTAAGTATAAGAAGGAGATAT ACATATGAACATTAATCAGCTCATCCT** gBlock fragment encoding the second T7 promoter region of pETDUET-1, with overlaps at the 5' end of the gBlock to 6xHis-*bceA* and the 3' end to *bceB*

Table 2.2: Primers used in this study.

ATPase Assay

Colorimetric ATPase assays were modified from a previously described protocol (28) and performed in 96-well plates. To each well 2 μg of purified BceAB was added, followed by buffer containing the indicated concentration of ATP, 4 mM $MgCl_2$ and, when appropriate, the indicated concentration of Zn^{2+}-bacitracin, Zn^{2+}-acetate, free bacitracin, ATPγS, or sodium-orthovanadate to a total reaction volume of 50 μL. Samples were incubated at 37 °C for 30 min before stopping the reaction by addition of 50 μL of a 12% (wt/vol) sodium dodecyl-sulfate solution. Then 100 μL of a 1:1 mixture of 12% ascorbic acid (wt/vol) and 2% ammonium molybdate (wt/vol) was added, followed by 150 μL of a solution containing 2% sodium citrate (wt/vol), 2% sodium (meta)arsenite (wt/vol), and 2% acetic acid (vol/vol). Absorbance at 850 nm was measured in a SpectraMax M5 plate reader and converted to total ATP consumed using a standard curve generated with K_2HPO_4 solutions. The rate of ATP consumption (μmol/min/mg) was plotted in GraphPad Prism, and curves were fit with a model of substrate inhibition {$Velocity = V_{max}*[ATP]/(K_m + [ATP]*(1+[ATP]/K_i))$}.

MS

To extract copurified lipids from BceAB, 200 μL of gel filtration–purified BceAB (0.7 mg/mL) was mixed with 600 μL of a 50:50 (vol/vol) mixture of isopropanol and methyl tertiary-butyl ether containing 0.01% butylated hydroxytoluene. A buffer control was run in parallel by replacing the BceAB protein solution with gel filtration buffer. Samples were vortexed and centrifuged to pellet the precipitated protein, and the supernatant was transferred to LC autosampler vials. Then, 5 μL of each sample was injected onto a Waters Acquity BEH-C18 column (2.1 × 100 mm) operated with a column temperature of 55 °C and a flow rate of 0.25 mL/min using a Waters Acquity UPLC. Compounds were separated using the following gradient: initial conditions were 50% mobile phase A (10 mM ammonium formate in water) and 50% mobile phase B (isopropanol/methanol, 90:10 vol/vol containing 5 mM ammonium formate), held at 50% B until an elapsed period of 0.5 min, ramped to 100% B at 7 min and held at 100% B until 8 min, returned to 50% B at 8.01 min, and held at 50% B until 10 min. Mass spectra were obtained on a Waters Xevo G2-XS quadrupole Time-of-Flight (TOF) mass spectrometer operated in both positive and negative electrospray ionization modes using a data-independent MS^e (Waters) method having alternating scans without collision energy or with a 20- to 80-V collision energy ramp. For follow-up MS/MS analyses, the *m/z* 978 (positive ion

mode) or *m/z* 976 (negative ion mode) species was selected in the quadrupole, followed by fragmentation in the collision cell with a 20- to 80-V energy ramp and subsequent scanning of daughter ions in the TOF analyzer. Data were processed using Waters Masslynx software.

Cryo-EM Imaging and Data Processing

Grids for cryo-EM imaging were prepared on a Vitrobot Mark IV by applying 2.5 μL of purified BceAB at ~7 mg/mL to Quantifoil R2/2 200-mesh grids that had been glow-discharged for 45 seconds at 15 mA in a Pelco EasyGlow. Grids were blotted for 5 s at 4 °C, 100% humidity, and a blot-force of 1 before being plunge frozen in liquid ethane cooled by liquid nitrogen. Frozen grids were screened for ice quality and particle distribution on a Talos Arctica equipped with a Falcon-3 detector. Final data collection was performed using Leginon (29) on a Titan Krios with a K3 direct electron detector and Gatan Quantum GIF energy filter set to a 20-eV slit width. Movies were collected in counting mode with a pixel size of 0.872 Å and a total dose of 60.5 electrons/Å^2.

Movies were corrected for beam-induced motion by performing patch motion correction in cryoSPARC (19), and contrast transfer function (CTF) parameters were determined by patch CTF estimation in cryoSPARC. Micrographs with fit CTF parameters worse than 6 Å were discarded, and further manual inspection was performed to remove obviously poor micrographs. Initial templates for particle picking were generated by performing blob picking followed by 2D classification in cryoSPARC, and several averages representing different views of BceAB were then used for template-based particle picking. Several rounds of 2D classification were performed to remove bad particles, and ab initio reconstruction in cryoSPARC was used to generate an initial 3D model for classification and refinement.

For the nucleotide-free conformation of wild-type BceAB, heterogeneous refinement in cryoSPARC was followed by classification with residual signal subtraction in Relion 3.0 (30) to isolate a particle population showing the highest resolution features in the TM and extracellular regions. Final nonuniform refinement and 3D variability analysis were performed in cryoSPARC. For the dataset containing the E169Q variant of BceA in BceAB bound to ATP, initial heterogeneous classification cryoSPARC revealed two distinct populations of particles corresponding to the nucleotide-free and ATP-bound conformations. Particles corresponding to the ATP-bound conformation were selected for final nonuniform refinement. Resolutions of all maps were calculated using the gold-standard Fourier shell correlation (FSC), and local

resolutions were calculated in cryoSPARC.

Model Building and Refinement

The quality of the cryo-EM map in the TM region was of sufficient quality to build all 10 TM helices of BceB de novo in COOT (31). All connecting loops between TM helices were also manually built, including the long linker between TM_4 and TM_5, which was disordered in the cryo-EM map of nucleotide-free BceAB but well-ordered in the ATP-bound conformation. An initial atomic model of BceA was generated using the SWISS-Model server (32) and the structure of the MacB nucleotide-binding domain (Protein Data Bank [PDB], accession No. 5LJ9) as a template. The BceA model was rigid body fit into the cryo-EM map and then manually adjusted in COOT. The C-terminal α-helix of BceA was not present in the homology model and was manually built in COOT.

To facilitate model building and refinement of the extracellular loop region of BceB (residues 325 to 513), we utilized the RoseTTAFold (33) algorithm available through the Robetta web server. The resulting model for the extracellular loop was docked into the cryo-EM map and manually adjusted in COOT. The ligand AUP was manually built using JLigand (34), and refinement restraints were generated with phenix.elbow (35). The final two prenyl units in the hydrophobic tail of AUP were disordered in the cryo-EM maps and were left unmodeled. The final complete atomic models of BceAB encompassing all residues of BceA and BceB were iteratively refined using phenix.real_space_refine (35) and manually adjusted in COOT. Model validation was performed with MolProbity (36).

Data Availability

Atomic models and cryo-EM maps data have been deposited in PDB, accession Nos. 7TCG and 7TCH and Electron Microscopy Data Bank accession Nos. 25811 and 25812). The protein sequences and links to genetic databases describing the genes encoding BceA (accession No. O34697) and BceB (accession No. O34741) are available in Uniprot.

Acknowledgements

We thank Dr. Sundharraman Subramanian and the Research Technology Support Facility (RTSF) Cryo-Electron Microscopy Facility at Michigan State University for assistance with cryo-EM screening and data collection. We are also grateful for the NIH Midwest Cryo-EM Consortium and Dr. Thomas Klose and Dr. Wen Jiang for providing microscope time and assistance with data collection at Purdue University. We thank members of the Michigan State University RTSF Mass Spectrometry and Metabolomics Core facility, in particular Dr. Dan Jones for assisting with MS data analysis. Finally, we are grateful to all members of the Orlando laboratory, Dr. Robert Hausinger, and Dr. Lee Kroos for careful reading of the manuscript and for providing constructive feedback.

REFERENCES

1. Egan, A. J. F., Errington, J. & Vollmer, W. Regulation of peptidoglycan synthesis and remodelling. *Nature Reviews Microbiology* vol. 18 446–460 (2020).

2. Malin, J. J. & de Leeuw, E. Therapeutic compounds targeting Lipid II for antibacterial purposes. *Infection and Drug Resistance* **12**, 2613–2625 (2019).

3. Breukink, E. & de Kruijff, B. Lipid II as a target for antibiotics. *Nature Reviews Drug Discovery* vol. 5 321–323 (2006).

4. Assoni, L. *et al.* Resistance Mechanisms to Antimicrobial Peptides in Gram-Positive Bacteria. *Frontiers in Microbiology* vol. 11 (2020).

5. Ohki, R. *et al.* The BceRS two-component regulatory system induces expression of the bacitracin transporter, BceAB, in Bacillus subtilis. *Molecular Microbiology* **49**, 1135–1144 (2003).

6. Rietkötter, E., Hoyer, D. & Mascher, T. Bacitracin sensing in Bacillus subtilis. *Molecular Microbiology* **68**, 768–785 (2008).

7. Kobras, C. M. *et al.* BceAB-Type Antibiotic Resistance Transporters Appear To Act by Target Protection of Cell Wall Synthesis. *Antimicrobial Agents and Chemotherapy* **64**, e02241-19 (2020).

8. Dintner, S., Heermann, R., Fang, C., Jung, K. & Gebhard, S. A sensory complex consisting of an ATP- binding cassette transporter and a two-component regulatory system controls bacitracin resistance in Bacillus subtilis. *Journal of Biological Chemistry* **289**, 27899–27910 (2014).

9. Dintner, S. *et al.* Coevolution of ABC transporters and two-component regulatory systems as resistance modules against antimicrobial peptides in Firmicutes bacteria. *Journal of Bacteriology* **193**, 3851–3862 (2011).

10. Bernard, R., Guiseppi, A., Chippaux, M., Foglino, M. & Denizot, F. Resistance to bacitracin in Bacillus subtilis: Unexpected requirement of the BceAB ABC transporter in the control of expression of its own structural genes. *Journal of Bacteriology* **189**, 8636–8642 (2007).

11. Fritz, G. *et al.* A new way of sensing: Need-based activation of antibiotic resistance by a flux-sensing mechanism. *mBio* **6**, e00975-15 (2015).

12. Clemens, R., Zaschke-Kriesche, J., Khosa, S. & Smits, S. H. J. Insight into two ABC transporter families involved in lantibiotic resistance. *Frontiers in Molecular Biosciences* vol. 4 (2018).

13. Gebhard, S. & Mascher, T. Antimicrobial peptide sensing and detoxification modules: Unravelling the regulatory circuitry of Staphylococcus aureus. *Molecular Microbiology* vol. 81 581–587 (2011).

14. Falord, M., Karimova, G., Hiron, A. & Msadeka, T. GraXSR proteins interact with the VraFG ABC transporter to form a five-component system required for cationic antimicrobial peptide sensing and resistance in Staphylococcus aureus. *Antimicrobial Agents and Chemotherapy* **56**, 1047–1058 (2012).

15. Hiron, A., Falord, M., Valle, J., Débarbouillé, M. & Msadek, T. Bacitracin and nisin resistance in Staphylococcus aureus: A novel pathway involving the BraS/BraR two-component system (SA2417/SA2418) and both the BraD/BraE and VraD/VraE ABC transporters. *Molecular Microbiology* **81**, 602–622 (2011).

16. Crow, A., Greene, N. P., Kaplan, E. & Koronakis, V. Structure and mechanotransmission mechanism of the MacB ABC transporter superfamily. *Proceedings of the National Academy of Sciences of the United States of America* **114**, 12572–12577 (2017).

17. Tang, X. *et al.* Structural basis for bacterial lipoprotein relocation by the transporter LolCDE. *Nature Structural and Molecular Biology* **28**, 347–355 (2021).

18. Sharma, S. *et al.* Mechanism of LolCDE as a molecular extruder of bacterial triacylated lipoproteins. *Nature Communications* **12**, (2021).

19. Punjani, A., Rubinstein, J. L., Fleet, D. J. & Brubaker, M. A. CryoSPARC: Algorithms for rapid unsupervised cryo-EM structure determination. *Nature Methods* **14**, 290–296 (2017).

20. Thomas, C. *et al.* Structural and functional diversity calls for a new classification of ABC transporters. *FEBS Letters* **594**, 3767–3775 (2020).

21. Economou, N. J., Cocklin, S. & Loll, P. J. High-resolution crystal structure reveals molecular details of target recognition by bacitracin. *Proceedings of the National Academy of Sciences of the United States of America* **110**, 14207–14212 (2013).

22. Stone, K. J. & Stromingert, J. L. Mechanism of Action of Bacitracin: Complexation with Metal Ion and C55-Isoprenyl Pyrophosphate. *Proceedings of the National Academy of Sciences of the United States of America* **68**, 3223–3227 (1971).

23. Wang, X., Ribeiro, A. A., Guan, Z. & Raetz, C. R. H. Identification of undecaprenyl phosphate-β-D- Galactosamine in francisella novicida and its function in lipid A modification. *Biochemistry* **48**, 1162– 1172 (2009).

24. Breazeale, S. D., Ribeiro, A. A. & Raetz, C. R. H. Oxidative decarboxylation of UDP-glucuronic acid in extracts of polymyxin-resistant Escherichia coli. Origin of lipid a species modified with 4-amino-4- deoxy-L-arabinose. *Journal of Biological Chemistry* **277**, 2886–2896 (2002).

25. Breazeale, S. D., Ribeiro, A. A., McClerren, A. L. & Raetz, C. R. H. A formyltransferase required for polymyxin resistance in Escherichia coli and the modification of lipid A with 4-amino-4-deoxy-L- arabinose: Identification and function of UDP-4-deoxy-4-formamido-L-arabinose. *Journal of Biological Chemistry* **280**, 14154–14167 (2005).

26. Kallenberg, F., Dintner, S., Schmitz, R. & Gebhard, S. Identification of regions important for resistance and signalling within the antimicrobial peptide transporter BceAB of Bacillus subtilis. *Journal of Bacteriology* **195**, 3287–3297 (2013).

27. Staroń, A., Finkeisen, D. E. & Mascher, T. Peptide antibiotic sensing and detoxification modules of Bacillus subtilis. *Antimicrobial Agents and Chemotherapy* **55**, 515–525 (2011).

28. Doerrler, W. T. & Raetz, C. R. H. ATPase activity of the MsbA lipid flippase of Escherichia coli. *Journal of Biological Chemistry* **277**, 36697–36705 (2002).

29. Suloway, C. *et al.* Automated molecular microscopy: The new Leginon system. *Journal of Structural Biology* **151**, 41–60 (2005).

30. Scheres, S. H. W. RELION: Implementation of a Bayesian approach to cryo-EM structure determination. *Journal of Structural Biology* **180**, 519–530 (2012).

31. Emsley, P. & Cowtan, K. Coot: Model-building tools for molecular graphics. *Acta Crystallographica Section D: Biological Crystallography* **60**, 2126–2132 (2004).

32. Waterhouse, A. *et al.* SWISS-MODEL: Homology modelling of protein structures and complexes. *Nucleic Acids Research* **46**, W296–W303 (2018).

33. Baek, M. *et al.* Accurate prediction of protein structures and interactions using a three-track neural network. *Science* **373**, 871–876 (2021).

34. Lebedev, A. A. *et al.* JLigand: A graphical tool for the CCP4 template-restraint library. *Acta Crystallographica Section D: Biological Crystallography* **68**, 431–440 (2012).

35. Liebschner, D. *et al.* Macromolecular structure determination using X-rays, neutrons and electrons: Recent developments in Phenix. *Acta Crystallographica Section D: Structural Biology* **75**, 861–877 (2019).

36. Davis, I. W. *et al.* MolProbity: All-atom contacts and structure validation for proteins and nucleic acids. *Nucleic Acids Research* **35**, (2007).

CHAPTER 3: ARCHITECTURE OF A COMPLETE BCE-TYPE ANTIMICROBIAL PEPTIDE RESISTANCE MODULE

This chapter has been published as: **George, N. L**. & Orlando, B. J. Architecture of a complete Bce-type antimicrobial peptide resistance module. *Nat. Commun.* **14**, 3896 (2023).

Abstract

Gram-positive bacteria synthesize and secrete antimicrobial peptides that target the essential process of peptidoglycan synthesis. These antimicrobial peptides not only regulate the dynamics of microbial communities but are also of clinical importance as exemplified by peptides such as bacitracin, vancomycin, and daptomycin. Many gram-positive species have evolved specialized antimicrobial peptide sensing and resistance machinery known as Bce modules. These modules are membrane protein complexes formed by an unusual Bce-type ABC transporter interacting with a two-component system sensor histidine kinase. In this work, we provide the first structural insight into how the membrane protein components of these modules assemble into a functional complex. A cryo-EM structure of an entire Bce module revealed an unexpected mechanism of complex assembly, and extensive structural flexibility in the sensor histidine kinase. Structures of the complex in the presence of a non-hydrolysable ATP analog reveal how nucleotide binding primes the complex for subsequent activation. Accompanying biochemical data demonstrate how the individual membrane protein components of the complex exert functional control over one another to create a tightly regulated enzymatic system.

Introduction

Antimicrobial peptides are chemically diverse molecules produced by a variety of organisms that not only play an important role in regulating microbial community dynamics, but are also harnessed as clinical tools to treat bacterial infections (1,2). Many antimicrobial peptides that are active against gram-positive species share a common mechanism of action involving binding to lipid intermediates of the cell-wall synthesis pathway (lipid II cycle), which leads to inhibition of cell-wall synthesis and cell death (Fig. 3.1) (3,4). Examples of such peptides in clinical use include bacitracin, which is found in common over-the-counter antibacterial ointments for minor cuts and abrasions, and vancomycin, which is used to treat serious infections of the skin, blood, and bone.

In addition to producing diverse antimicrobial peptides, gram-positive organisms have also evolved mechanisms to evade attack from these agents (5). One such mechanism widely found across Firmicute bacteria involves antimicrobial peptide sensing and resistance membrane protein complexes collectively known as Bce modules. These modules are composed minimally of an ATP-binding cassette (ABC) transporter which defends against antimicrobial peptides without transport across the membrane, and an interacting two-component system containing a sensor histidine kinase and response regulator (6,7). Of all such modules, the BceAB-RS system from *Bacillus subtilis*, after which the modules have been named, has been most extensively characterized (8-10). In this module *bceA* encodes the ATPase domains, *bceB* encodes the membrane-spanning permease domain of the ABC transporter BceAB, and *bceS* encodes the histidine kinase that phosphorylates the response regulator encoded by *bceR* (Fig. 3.2A) (11). Previous studies have established that BceAB mediates resistance against bacitracin, likely by freeing bacitracin from the lipid target undecaprenyl-pyrophosphate (UPP) (12,130). Functional BceAB is required to activate the sensor kinase BceS through a proposed flux-sensing mechanism in which BceS senses the conformational cycling of BceAB, leading to BceS autophosphorylation and subsequent recruitment and phosphorylation of BceR (14,15). Phosphorylated BceR then upregulates expression *bceA* and *bceB*, leading to a positive feedback loop that tunes the level of BceAB to meet the demand for bacitracin detoxification (15).

In recent work we used cryo-electron microscopy (cryo-EM) to provide the first two structural snapshots of a Bce-type ABC transporter, BceAB from *B. subtilis* (12). While these studies revealed the structure and conformational changes of Bce-type ABC transporters, the

architecture of a complete Bce module describing the stoichiometry and mode of interaction between the BceS kinase and BceAB transporter remained enigmatic. To understand this critical membrane protein interaction and the molecular details underpinning the Bce module flux-sensing mechanism, we have determined the cryo-EM structure of the complete BceAB-S complex from *B. subtilis* in nucleotide-free and ATPγS-bound states. Our analysis uncovers lipid mediated protein interaction between membrane components of a Bce module, a large degree of conformational heterogeneity within the sensor kinase, key conformational shifts that prime the complex for activation, and an unforeseen layer of reciprocal enzymatic regulation between membrane components of the complex.

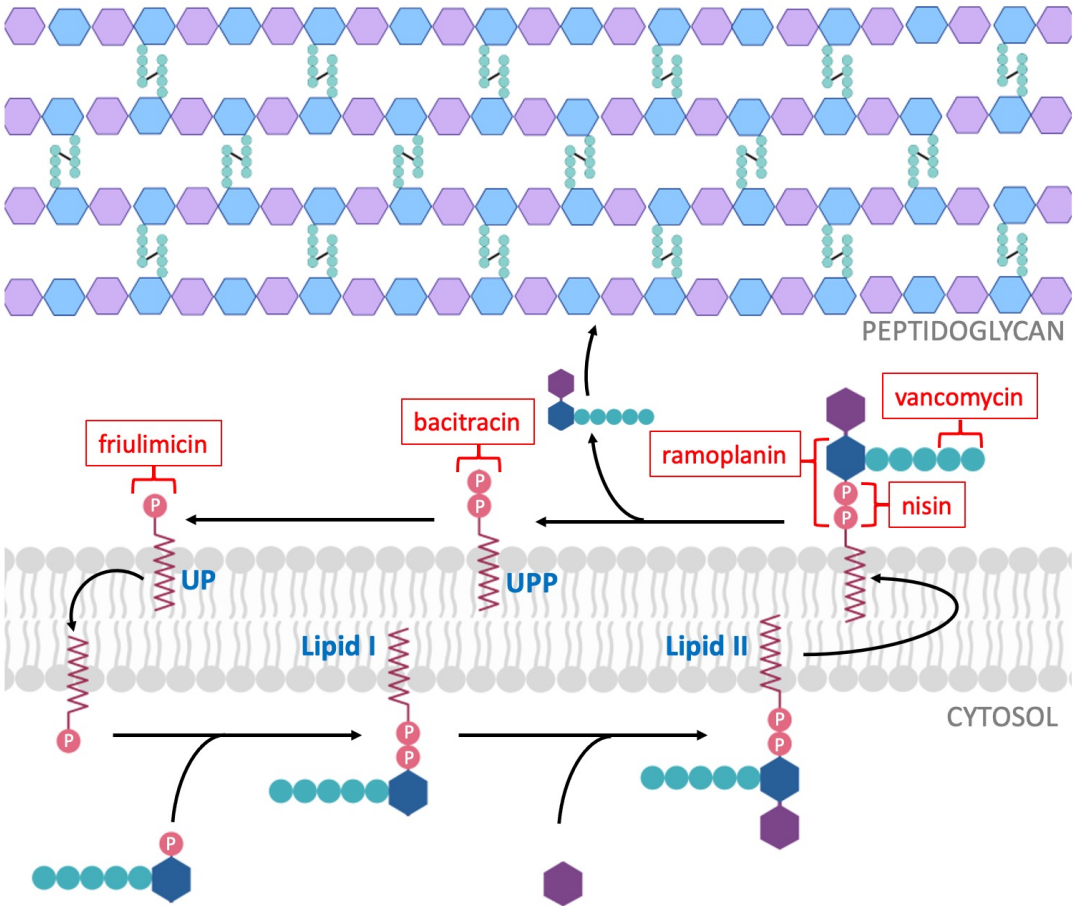

Figure 3.1: Schematic showing the lipid II cycle of peptidoglycan synthesis. Lipid intermediates are indicated in blue letters. (UPP: undecaprenyl pyrophosphate, UP: undecaprenyl phosphate). Antimicrobial peptides are indicated in red boxes, with brackets indicating the motifs they recognize on individual lipid intermediates.

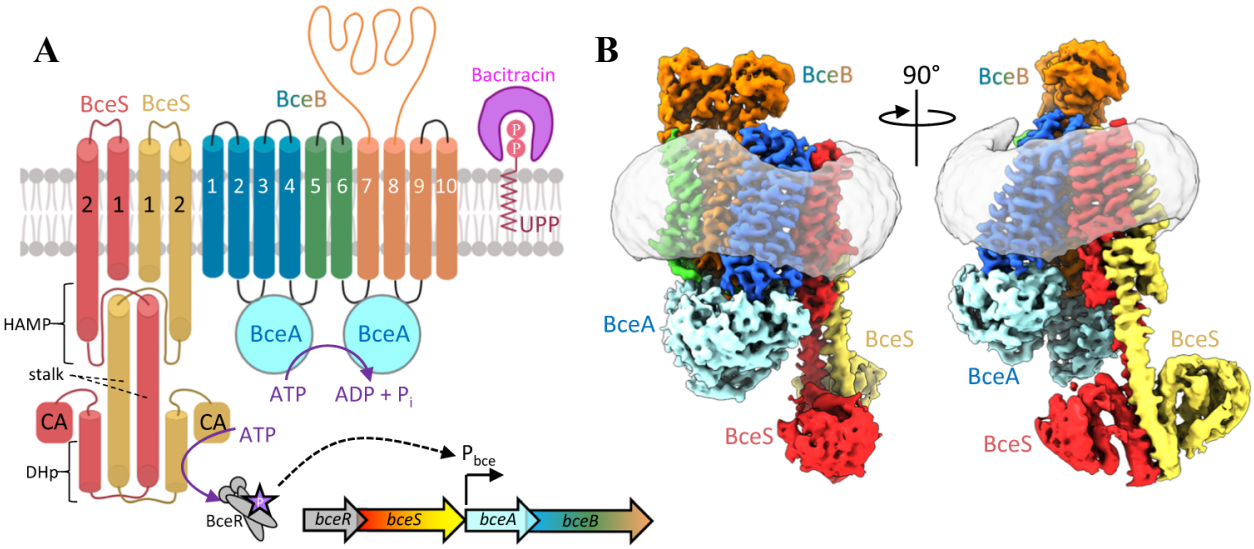

Figure 3.2: Diagram showing the topology and stoichiometry of the BceAB-S membrane protein complex (A). The transmembrane (TM) helices of BceB are colored blue, green, and orange, and labeled with white numbers. BceS monomers are colored red and yellow with TM helices indicated with black numbers. Individual domains in the cytoplasmic region of BceS are labeled in black. Bacitracin binding to the lipid target UPP is shown as a pink crescent surrounding the phosphates of UPP. Cryo-EM map (B) of the BceAB-S membrane protein complex in a nucleotide-free state. Protein components are colored the same as in (A). The detergent micelle is shown in grey surrounding the TM helices.

Results

Cryo-EM structure of nucleotide-free BceAB-S

To investigate the assembly of protein components in a Bce module, we overexpressed the genes encoding BceAB and the BceS sensor kinase from *B. subtilis* in *Escherichia coli* from a single plasmid containing a histidine tag on BceA (see methods). Following solubilization of bacterial membranes with lauryl-maltose neopentylglycol (LMNG) detergent, the BceAB-S complex was isolated by Co^{3+}-TALON affinity and size-exclusion chromatography. Comparison of the size-exclusion chromatogram with that obtained for the isolated BceAB ABC transporter revealed that co-production of BceS with BceAB resulted in a shift towards higher molecular weight species (Fig. 3.3B). SDS-PAGE analysis of the peak fractions from the two chromatograms confirmed that the molecular weight shift was a result of co-purification of BceS with BceAB (Fig. 3.3C). These results demonstrate that BceS forms a stable complex with BceAB, and that the entire membrane protein complex is stable in a detergent solubilized state.

To understand the molecular details of interaction between the BceS sensor kinase and BceAB, we pursued a cryo-EM structure of the detergent solubilized BceAB-S complex. Peak fractions from size-exclusion chromatography (Fig. 3.3B) were concentrated and applied to cryo-EM grids for high-resolution single-particle imaging. The resultant micrographs show a consistent particle distribution in thin ice (Fig. 3.3D), and 2D class-averages from this dataset show features consistent with those seen previously for isolated BceAB along with additional transmembrane helices (TM) and soluble domains that extend below the detergent belt corresponding to BceS (Fig. 3.4A). The cytoplasmic dimerization and histidine phosphotransfer (DHp) and catalytic (CA) domains of BceS are very fuzzy or almost completely absent in many of the 2D averages, indicating a high degree of conformational heterogeneity. Despite this heterogeneity we reconstructed 3D volumes of the entire BceAB-S complex at sub-nanometer resolutions in two TM helix conformations (Fig. 3.2B, Figs. 3.4-3.6, Table 3.1). These initial 3D reconstructions show that the BceAB transporter is complexed with the BceS dimer to form an overall complex with five individual protein chains in a BceA:B:S ratio of 2:1:2 (Fig. 3.2).

To gain more detailed insight into the interaction of BceS with BceAB, and a deeper understanding of the conformational heterogeneity present in the BceS cytoplasmic domains, we adopted segmented approaches to cryo-EM 3D classification and refinement focusing on specific regions of the complex. The results of these strategies are discussed below.

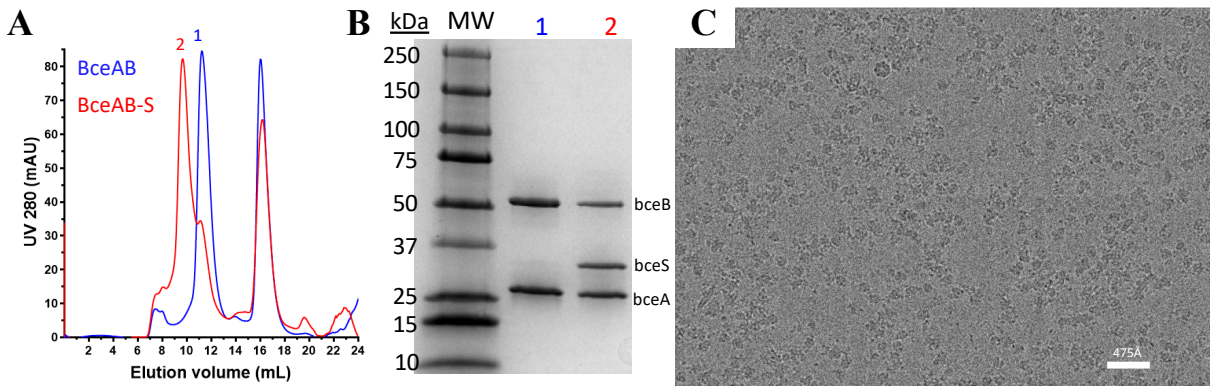

Figure 3.3: Biochemical characterization of BceAB-S. (A) Gel-filtration profiles of detergent solubilized BceAB (blue trace) and BceAB-S (red trace) complexes. Numbers indicate peaks from each gel-filtration run that were analyzed via SDS-PAGE. (B) SDS-PAGE analysis of gel-filtration peaks indicated in (A), demonstrating that the shift to higher molecular weight observed with BceAB-S is due to the presence of BceS. This experiment has been repeated twice with similar results. (C) Electron micrograph of detergent solubilized BceAB-S complexes showing a uniform particle distribution in thin ice. The white scale bar demonstrates a size of 475Å. Approximately ~9000 similar micrographs were obtained.

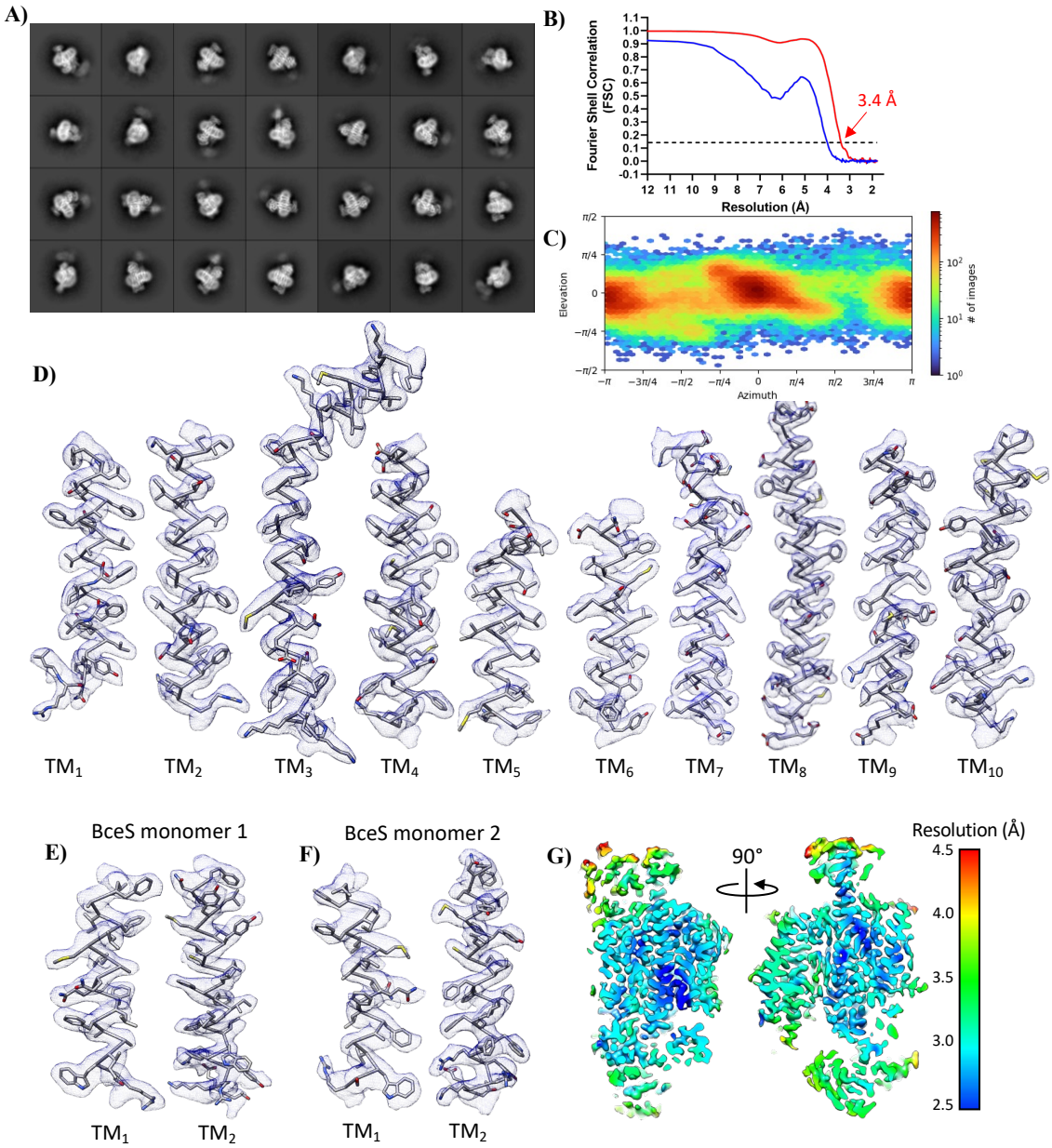

Figure 3.4: Cryo-EM data analysis of nucleotide-free BceAB-S TM state 1. (A) 2D class-averages of nucleotide-free BceAB-S particles. Flexibility of the BceS soluble domains is evident in most 2D averages. (B) Fourier shell correlation (FSC) curve for the final nucleotide-free BceAB-S TM state 1 reconstruction. Blue curve was generated without masking, and the red curve was generated with a tight auto-mask in CryoSPARC. Gold-standard FSC cutoff of 0.143 is indicated with a dashed black line. (C) Angle distribution of particles in the final reconstruction. (D-F) Exerimental cryo-EM map (transparent blue mesh) and fitted atomic model for TM helices throughout the BceAB-S complex. (G) Local resolution map indicating varying resolution throughout the cryo-EM map.

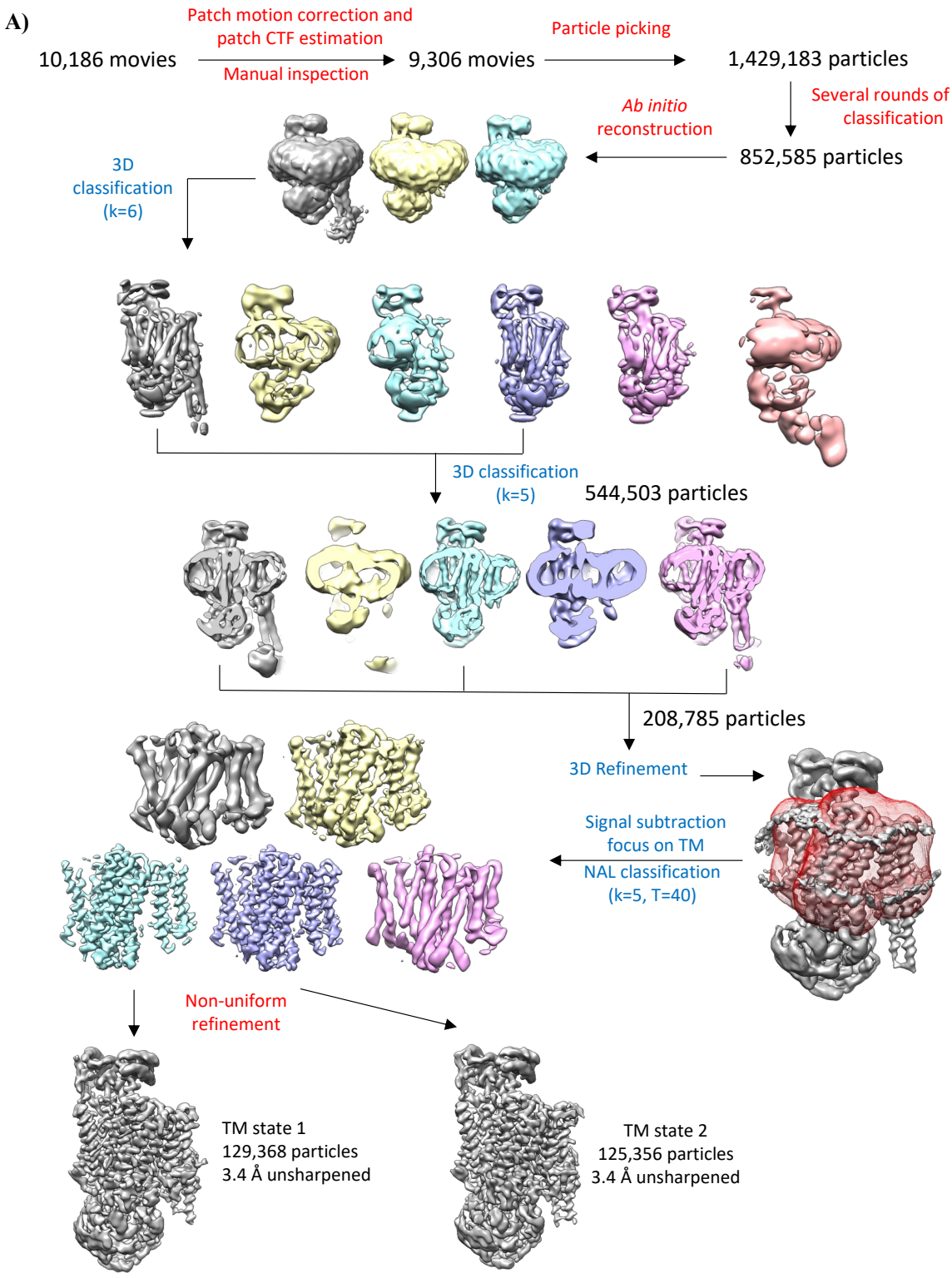

Figure 3.5: Cryo-EM data processing for nucleotide-free BceAB-S. Data processing to resolve high resolution features in the TM region of nucleotide-free BceAB-S. Steps indicated in red were performed in CryoSPARC, and steps in blue were performed in Relion.

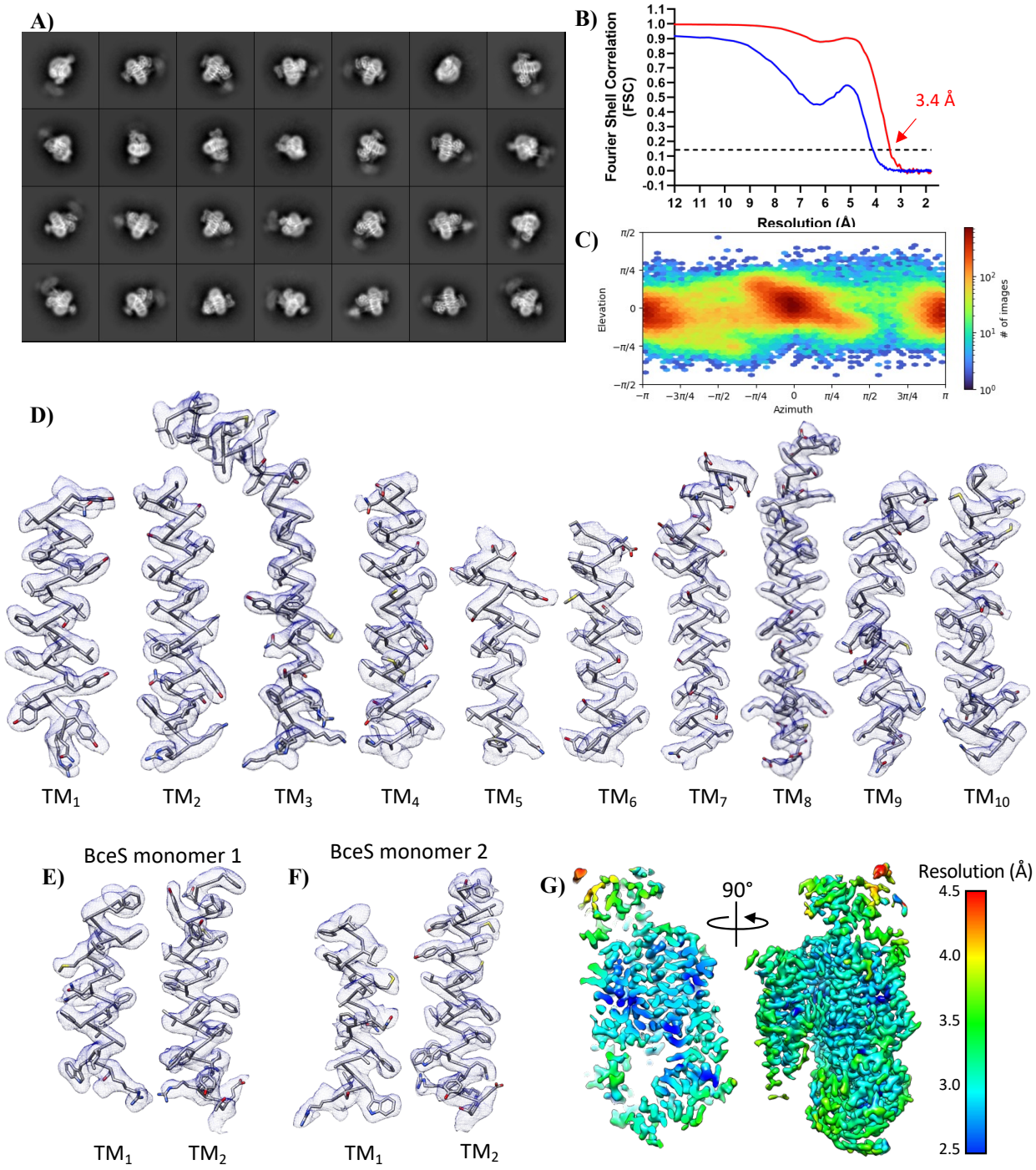

Figure 3.6: Cryo-EM data analysis of nucleotide-free BceAB-S TM state 2. (A) 2D class-averages of nucleotide-free BceAB-S particles. Flexibility of the BceS soluble domains is evident in most 2D averages. (B) FSC curve for the final nucleotide-free BceAB-S TM state 2 reconstruction. Blue curve was generated without masking, and the red curve was generated with a tight auto-mask in cryoSPARC. Gold-standard FSC cutoff of 0.143 is indicated with a dashed

Figure 3.6 (cont'd)

black line. (C) Angle distribution of particles in the final reconstruction. (D-F) Experimental cryo-EM map (transparent blue mesh) and fitted atomic model for TM helices throughout the BceAB-S complex. (G) Local resolution map indicating varying resolution throughout the cryo-EM map.

Data Collection and Processing	BceAB-S Nucleotide-free TM state-1 (EMDB-29690) (PDB 8G3A)	BceAB-S Nucleotide-free TM state-2 (EMDB-29691) (PDB3B)	BceAB-S Nucleotide-free BceS state-1 (EMDB-29694) (PDB 8G3F)	BceAB-S Nucleotide-free BceS state-2 (EMDB-29701) (PDB 8G3L)
Magnification	105,000	105,00	105,00	105,00
Voltage (kV)	300	300	300	300
Electron exposure (e-/Å^2)	60.5	60.5	60.5	60.5
Defocus range (μm)	0.7-2.5	0.7-2.5	0.7-2.5	0.7-2.5
Pixel size (Å)	0.872	0.872	0.872	0.872
Symmetry imposed	C1	C1	C1	C1
Initial particle images (no.)	852,585	852,585	1,392,136	1,392,136
Final particle images (no.)	129,368	125,346	120,730	186,936
Map resolution (Å)	3.4	3.5	3.7	3.5
FSC threshold	0.143	0.143	0.143	0.143
Refinement				
Model resolution (Å)	3.7	3.7	3.9	3.7
FSC threshold	0.5	0.5	0.5	0.5
Map sharpening *B* factor (Å^2)	-113	-110	-113	-110
Map-model CC				
CCmask	0.71	0.74	0.72	0.73
CCbox	0.60	0.63	0.68	0.67
CCvolume	0.66	0.69	0.68	0.68
CCpeaks	0.51	0.53	0.56	0.58
Model composition				
Non-hydrogen atoms	14441	14394	14441	14441
Protein residues	1791	1791	1791	1791
Ligands	4	3	4	4
B factors (Å^2)				
Protein	38.8	47.93	48.9	32.4
Ligand	17.6	18.64	15.9	6.5
R.m.s deviations				
Bond lengths (Å)	0.003	0.003	0.003	0.005
Bond angles (°)	0.544	0.538	0.611	0.655
Validation				
MolProbity score	1.75	1.69	1.84	1.80
Clashscore	6.37	5.82	8.08	7.67
Poor rotamers (%)	0.06	0.06	0.32	0.00
Ramachandran plot				
Favored (%)	94.04	94.55	94.04	94.49
Allowed (%)	5.85	5.45	5.96	5.51
Disallowed (%)	0.11	0	0	0

Table 3.1: Cryo-EM data collection and processing statistics.

Table 3.1 (cont'd)

Data Collection and Processing	BceAB-S ATPγS-bound High-res TM (EMDB-29716) (PDB 8G4C)	BceAB-S ATPγS-bound Kinked BceS (EMDB-29717) (PDB 8G4C)
Magnification	105,000	105,00
Voltage (kV)	300	300
Electron exposure (e-/Å^2)	60.5	60.5
Defocus range (μm)	0.7-2.5	0.7-2.5
Pixel size (Å)	0.872	0.872
Symmetry imposed	C1	C1
Initial particle images (no.)	455,762	455,762
Final particle images (no.)	98,858	50,073
Map resolution (Å)	3.1	3.6
FSC threshold	0.143	0.143
Refinement		
Model resolution (Å)	3.4	3.8
FSC threshold	0.5	0.5
Map sharpening *B* factor (Å^2)	-76	-67
Map-model CC		
CCmask	0.77	0.73
CCbox	0.62	0.69
CCvolume	0.73	0.70
CCpeaks	0.55	0.56
Model composition		
Non-hydrogen atoms	14498	14397
Protein residues	1802	1795
Ligands	3	2
B factors (Å^2)		
Protein	56.7	61.7
Ligand	27.0	27.8
R.m.s deviations		
Bond lengths (Å)	0.003	0.003
Bond angles (°)	0.479	0.653
Validation		
MolProbity score	1.63	1.96
Clashscore	6.03	10.57
Poor rotamers (%)	0.00	0.00
Ramachandran plot		
Favored (%)	95.69	93.66
Allowed (%)	4.31	6.34
Disallowed (%)	0.00	0.00

Interactions between BceB and BceS TM helices

To understand how BceS interacts with BceB in the transmembrane region, we combined all particles that displayed clear secondary structure for TM helices in 3D classification and refined these particles into a single volume (Fig. 3.5). Residual signal subtraction focused on the TM region was followed with a round of 3D classification without alignment, generating two distinct classes of particles with high-resolution features in the TM region. Refinement of these two classes independently produced separate 3D volumes each at ~3.4 Å overall resolution (Figs. 3.4-3.6, Table 3.1). We refer to these two reconstructions as TM-state-1 and TM-state-2. The overall structure of the BceAB-S complex in TM-state-1 and TM-state-2 is nearly identical (overall RMSD ~ 0.6 Å), with very minor shifts in the position of TM helices (Movie 3.1). For simplicity we focus on TM state-1 for the following analysis.

Within the detergent belt 14 total TM helices were clearly identified, with 10 belonging to BceB and another 4 belonging to the BceS dimer. The cryo-EM maps were of sufficient quality to build atomic models of TM_1 and TM_2 of each BceS monomer de novo (Fig. 3.4D and E). The TM helices of BceS form a 4-helix bundle like that observed for the histidine kinase NarQ from *E. coli* and the sensory rhodopsin transducer HtrII from *Natronobacterium pharaonis* (Fig. 3.7A) (16,17). The configuration of TM helices in BceS is inverted compared to NarQ and HtrII. The loop connecting TM_1 and TM_2 in BceS makes a left-handed turn such that TM_2 is positioned along the left-hand side of TM_1, whereas in NarQ and HtrII this loop makes a right-handed turn such that TM_2 is positioned along the right-hand side of TM_1 (Fig. 3.7A and B). A left-handed configuration such as that observed for BceS was previously identified in NMR structures of the isolated monomeric TM domain of *E. coli* QseC and ArcB (18).

Several types of interactions mediate dimerization of two BceS monomers (Fig. 3.8A-D). At the apex of the 4-helix BceS TM bundle near the extracellular space is a cluster of sulfur-containing residues including Met41 and Cys45. Located directly beneath this sulfur cluster, Gln19 and Gln20 from opposing BceS monomers form hydrogen bond interactions with one another (Fig. 3.8B). In the middle of the bilayer plane is a cluster of aromatic residues including Trp12, Phe16, Phe49, and Phe52 that form an extensive π-stacking interaction network (Fig. 3.8C). Directly below this π-stacking network and at the hydrophilic interface of the cytosolic leaflet of the plasma membrane is a cluster of arginine and glutamate residues including Glu8, Arg9, Arg56, and Glu60 (Fig. 3.8D) that balance the net charge within this area

and form an intricate electrostatic interaction network between BceS monomers. Immediately beneath the TM helices of BceS in the cytosolic space is a helix-turn-helix HAMP domain formed by interactions between opposing BceS monomers (Fig. 3.8A). Within the core of the HAMP domain another cluster of aromatic residues including Phe63, Tyr64, and Phe86 from opposing BceS monomers interact through π-stacking interactions (Fig. 3.8A). In total, our cryo-EM structures reveal that the intramembrane sensing histidine kinase BceS forms a classical 4-helix TM bundle and a HAMP transfer domain similar to those of other histidine kinases that contain extracellular ligand binding domains. We next focused our attention on how the BceS histidine kinase interacts with BceAB.

Although previous bacterial two-hybrid and pull-down assays demonstrated that BceS and BceB interact to form a membrane protein complex, the molecular details of interaction between these proteins remained obscure (11). A random chemical mutagenesis screen previously identified mutations in BceB that affected signaling through BceS (19). Quite strikingly this study found several mutations in the C-terminal half of BceB ($TM_{8–10}$) which reduced signaling through BceS, and only two mutations in the N-terminal half of BceB ($TM_{1–4}$). From these studies and the conformational changes we previously observed in isolated BceAB[12], it would have been reasonable to predict that BceS interacts with the C-terminal half of BceB ($TM_{8–10}$). However, in our cryo-EM structures of BceAB-S we observe the TM bundle of BceS positioned near the N-terminal region ($TM_{1–4}$) of BceB (Fig. 3.9A and B). This positioning places BceS on the opposite side of BceB as a previously identified UPP binding pocket (Fig. 3.9B) (12).

Interestingly, the interaction between BceS and BceB in the TM region is limited to the very extracellular tip of the TM helices (Fig. 3.9A and B). The total buried surface area between BceB and the two BceS monomers is only ~460 $Å^2$ near the apex of BceB-TM_3, which contacts TM_1 from one BceS monomer and TM_2 from the second BceS monomer (Fig. 3.9B and E). Although the buried protein surface area between BceB and BceS is relatively small, we identified several lipid-like densities between BceB and BceS TM helices within the bilayer plane (Fig. 3.9A-D). Unfortunately, the cryo-EM map is not of sufficient quality to unambiguously identify the specific lipids that fill the gap between BceB and BceS TM helices. Nevertheless, our cryo-EM structures clearly demonstrate that most of the interaction between BceB and BceS is mediated through protein-lipid interactions rather than direct protein–protein interaction.

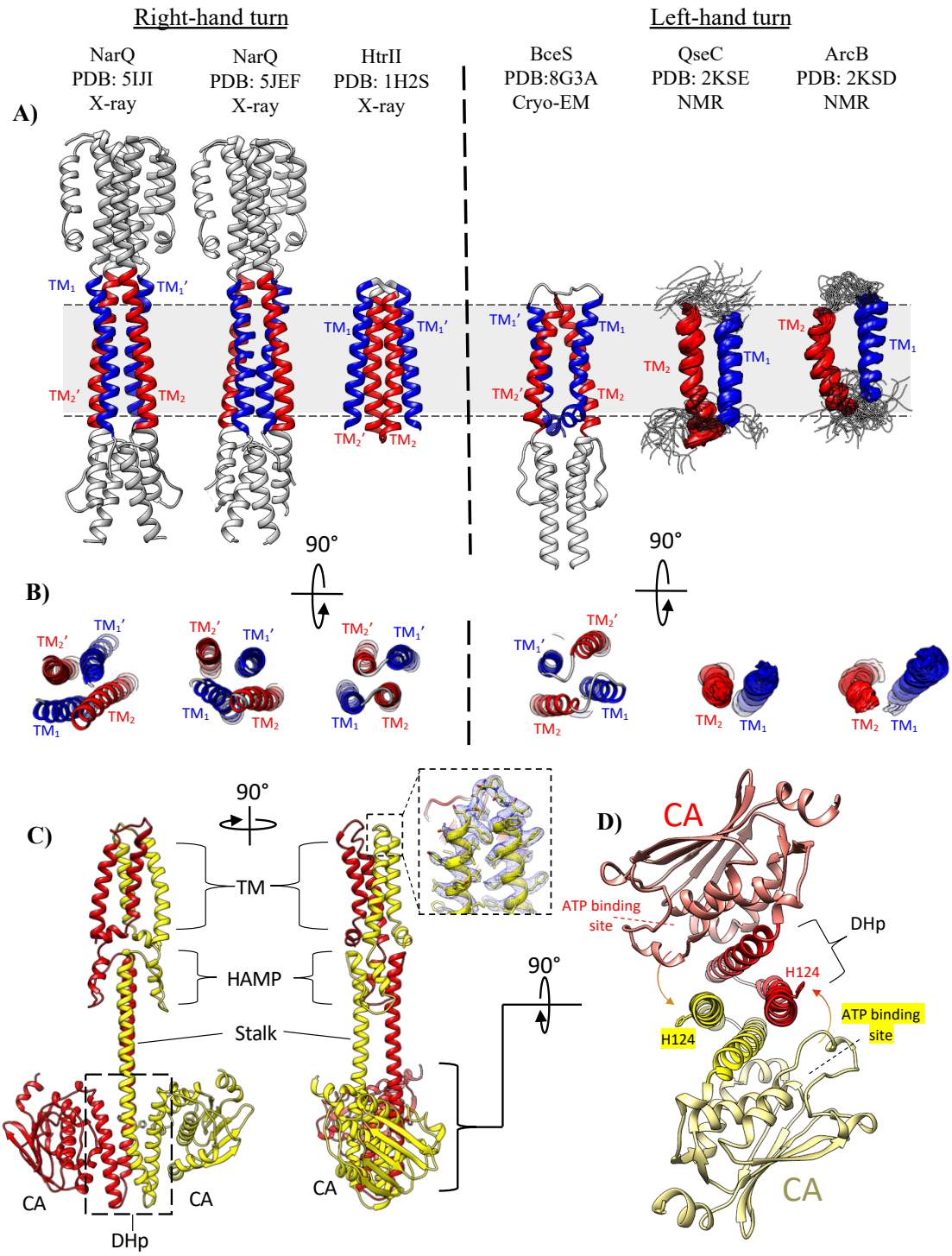

Figure 3.7: Comparison of BceS to other histidine kinases. (A) Comparison of the TM helix arrangement in BceS versus other histidine kinases of known structure. TM_1 is colored blue and TM_2 is colored red in all structures. (B) 90° rotated view of (A) showing TM helix configuration in all structures. (C) Domain architecture of BceS. Individual BceeS monomers are shown in red

Figure 3.7 (cont'd)

or yellow cartoon, with domains highlighted with black letters. The inset outlined in dashed black lines show the cryo-EM map of the TM_1-TM_2 linker in BceS. (D) View from the membrane of the DHp and CA domains in BceS. The autophosphorylated H124 residue in the DHp domain and the ATP binding sites in the CA domains are indicated. The configuration of domains in BceS indicate that autophosphorylation occurs in *trans* (indicated by arrows between ATP binding site and phosphorylated H124).

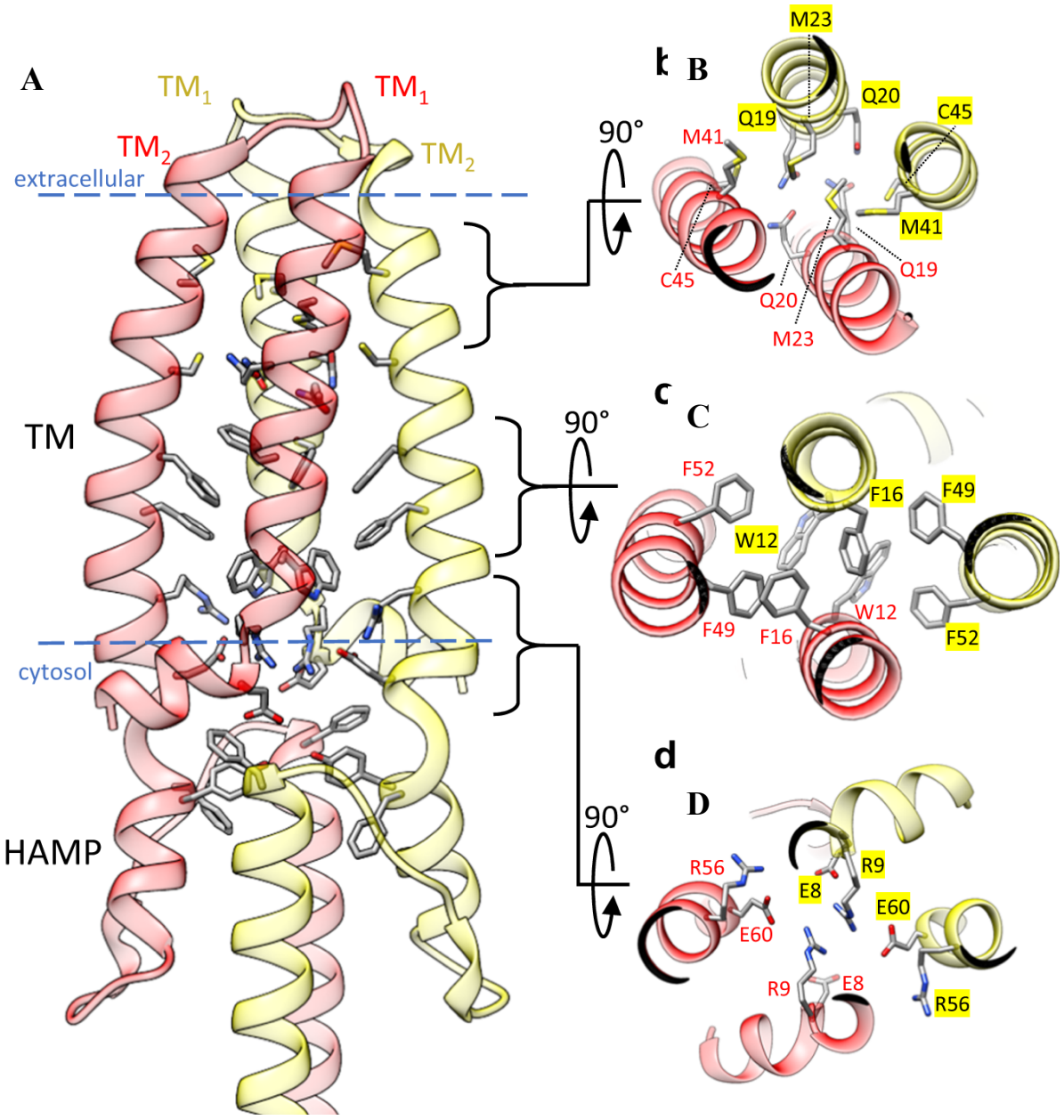

Figure 3.8: Overall configuration of the BceS TM helices and HAMP domain. Each monomer of BceS is colored either red or yellow. Blue dashed lines indicate the approximate boundary of the lipid bilayer. (B) View from the extracellular space of the tip of BceS TM helices. The core of the TM helix bundle contains a cluster of sulfur containing side-chains and hydrogen bonds between two pairs of glutamines. (C) View from the extracellular space of the middle of the BceS TM helix bundle, showing that the core of the bundle in the membrane interior contains a network of π-stacking interactions between aromatic side-chains. (D) View of the BceS TM helix bundle near the interface of the membrane and cytosol. An electrostatic network of charged residues mediates interaction between BceS TM helices.

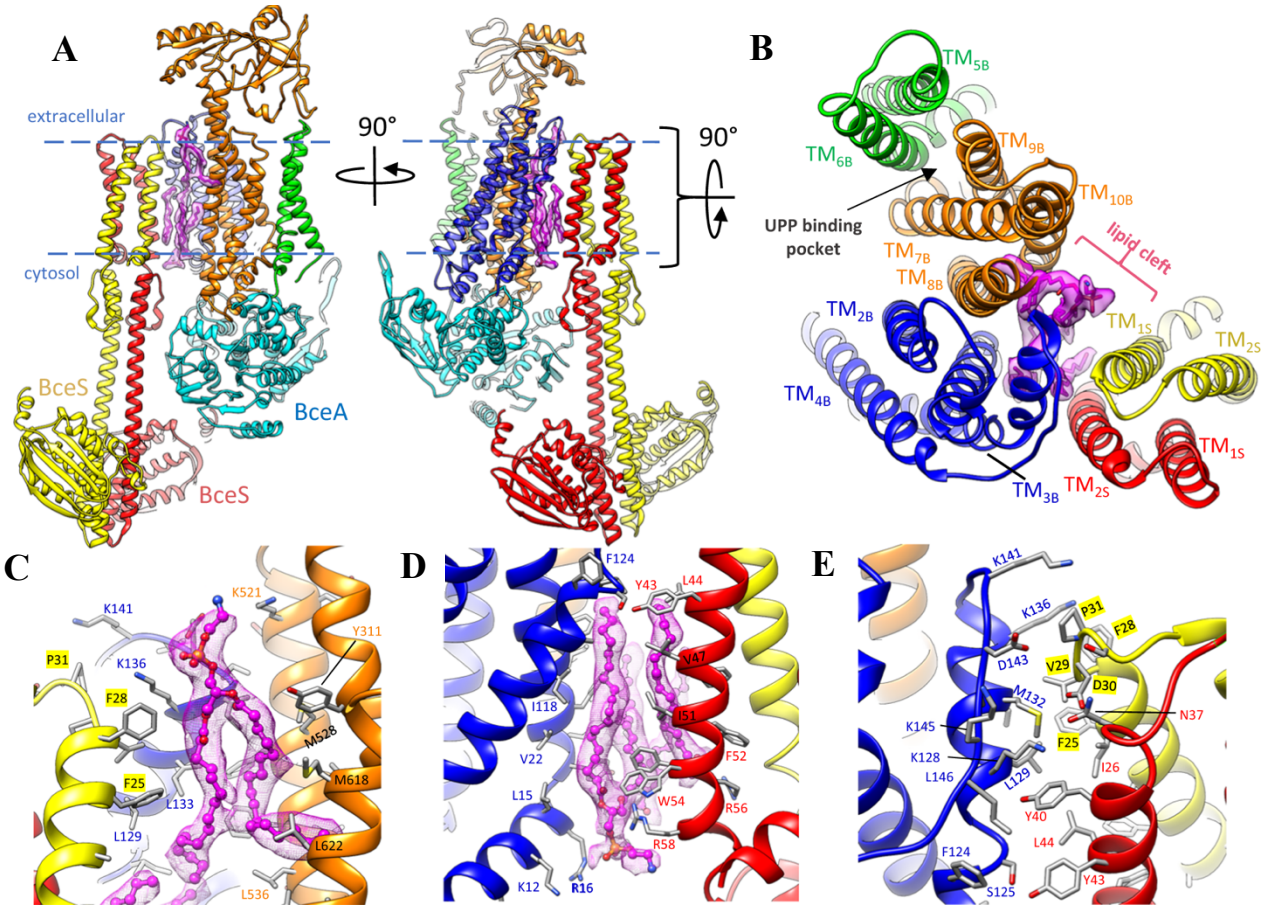

Figure 3.9: Two rotated views (A) of the atomic model of the BceAB-S complex. Individual protein chains and TM helices are colored the same as in Fig. 3.2. Purple sticks with surrounding transparent purple cryo-EM density indicate lipid molecules identified at the interface between BceB and BceS. Blue dashed lines indicate the approximate boundary of the lipid bilayer. (B) View from the extracellular space of the TM helix arrangement in the BceAB-S complex. Individual TM helices are labeled according to their number and whether they belong to BceB or BceS. Purple sticks with surrounding transparent purple cryo-EM density indicate lipid molecules that mediate interaction between BceB and BceS. The previously identified UPP binding pocket is indicated with a black arrow and is located on the opposite side of BceB as the site of BceS interaction. (C,D) Zoomed in view of lipid densities observed between BceB and BceS. Lipids are shown as magenta ball-and-stick with surrounding magenta mesh cryo-EM map. (E) Zoomed in view of the protein-protein interaction between BceB-TM_3 and BceS.

Conformational heterogeneity of BceS

Conformational flexibility of helical coiled-coils such as those found in histidine kinases is well-documented, and is proposed to underly interconversion between functional states through low energetic barriers[20,21]. Such conformational flexibility is apparent in 2D class-averages of the BceAB-S complex where the cytosolic region of BceS is often almost completely disordered (Fig. 3.10A), as well as in 3D classification of BceAB-S particles, where successive rounds of classification continually reveal multiple configurations of the BceS kinase (Fig. 3.10C). During 3D classification we routinely identified particle subsets that clearly contained all 4 BceS TM helices but showed few features for the cytosolic region of BceS below the detergent belt (Figs. 3.5 and 3.11). These results demonstrate that significant conformational flexibility in BceS begins at the HAMP domain and extends throughout the cytosolic DHp and CA domains.

We then applied 3D variability analysis (3DVA) in cryoSPARC to resolve the conformational heterogeneity in BceS, which revealed that the cytoplasmic region of BceS undergoes rotation around the axis of the stalk helices that connect the HAMP and DHp domains (Fig. 3.10B; component 1 and 2), and also translational shifts of the entire BceS cytoplasmic region relative to the BceAB transporter (Fig. 3.10B; component 2 and 3, and Movie 3.2). Much of the flexibility revealed in cryoSPARC 3DVA was also observed through standard 3D classification in Relion (Fig. 3.10C), which produced 3D classes demonstrating different conformations of BceS relative to BceAB. It is important to note that within these 3D classes the DHp and CA domains of BceS still remain poorly resolved compared to the TM regions, and subsequent 3D refinement produced reconstructions with largely disordered cytosolic regions of BceS.

Although conformational flexibility hampered near-atomic resolution reconstruction of the BceS soluble regions, we were able to separate two distinct classes of particles that reconstructed volumes showing most of the major secondary structural elements in the DHp and CA domains of BceS (Figs. 3.10D and 3.11B and D). These two volumes primarily differ in the angle of the BceS DHp/CA domains relative to the rest of the complex (Fig. 3.11F). Although BceAB and the TM/HAMP region of BceS were resolved with side-chain resolution in these reconstructions, the cytosolic DHp and CA domains of BceS had a lower local resolution, indicative of the high degree of conformational variability (Figs. 3.10D and 3.11B and D). Despite the limited resolutions in the cytosolic region, the loop between helices in the DHp domain of BceS clearly

takes a right-handed turn, placing the ATP binding site in the CA domain from one BceS monomer in proximity to His-124 of the opposite BceS monomer (Fig. 3.7C and D). Thus, BceS likely auto-phosphorylates His-124 in *trans* (20).

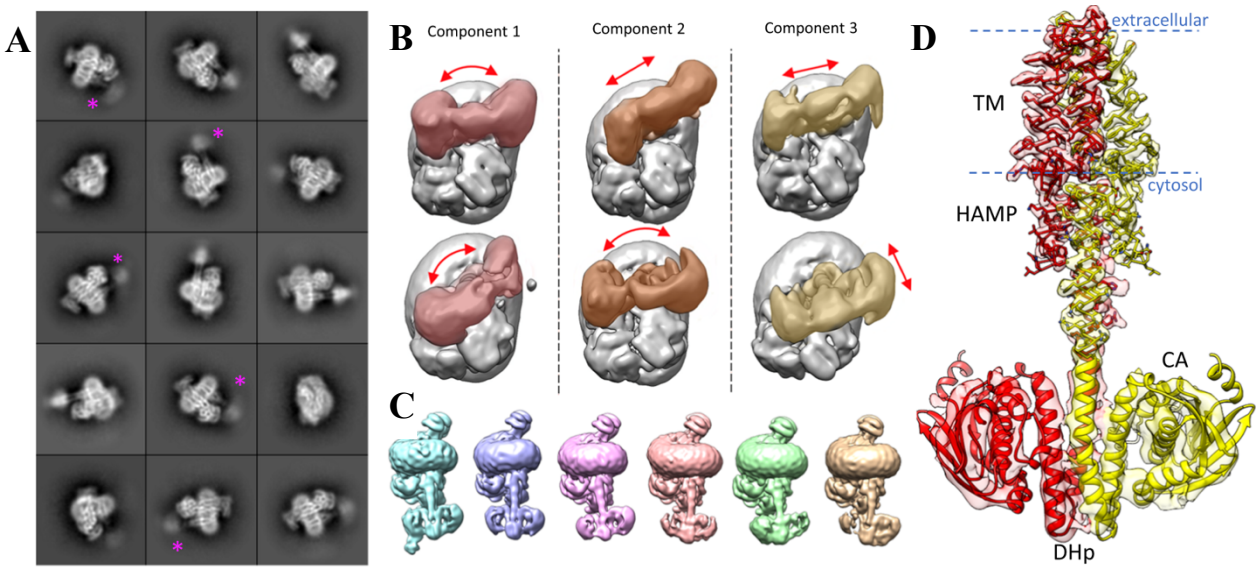

Figure 3.10: 2D class-averages (A) of detergent solubilized BceAB-S. Individual TM helices for BceS are present in the interior of the detergent micelle, while the cytoplasmic domains of BceS are often fuzzy. Purple asterisks indicate the BceS cytosolic domains in 2D averages where these domains exhibit a very large degree of structural heterogeneity. (B) The first three principal components of motion in the BceS cytosolic domains identified from 3DVA in cryoSPARC. The top and bottom rows indicate the extreme extent of motion observed in principal component. In each panel BceS is colored and BceAB and the detergent micelle are shown in grey. Red arrows indicate the direction of BceS motions observed. (C) Individual classes obtained from 3D classification of BceAB-S particles. All classes are oriented with the detergent micelle and BceAB transporter in the same position to highlight the variety of conformations that BceS can adopt within the complex. (D) View of the atomic model of BceS monomers fit into the local resolution filtered cryo-EM map of nucleotide-free BceAB-S. Near-atomic resolutions are obtained in the TM and HAMP domains, while the resolution steeply decreases entering the cytosolic DHp and CA domains due to inherent flexibility. Blue dashed lines indicate the approximate boundary of the lipid bilayer.

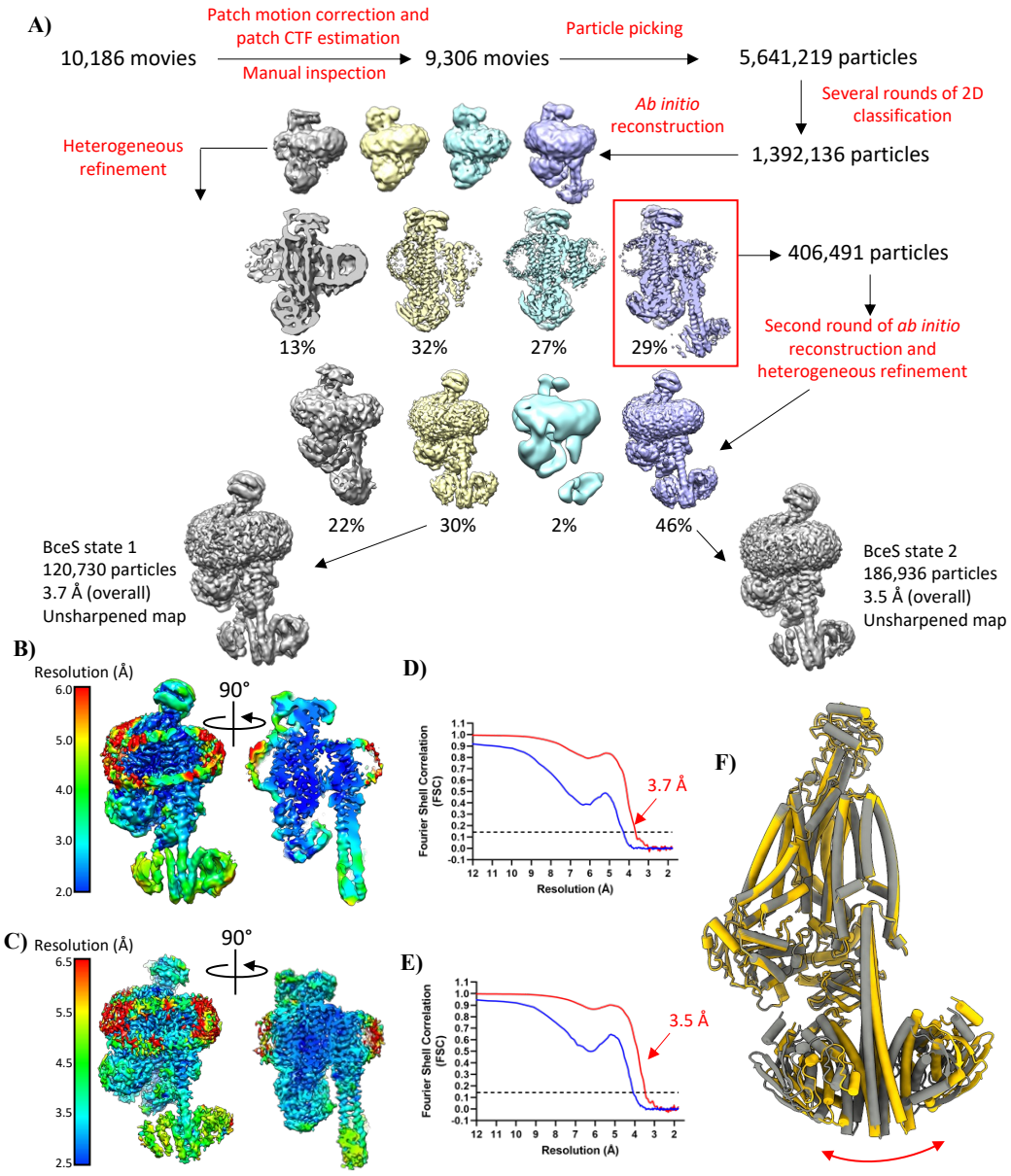

Figure 3.11: Cryo-EM data processing workflow to resolve the entirety of BceS in the nucleotide-free BceAB-S complex (A). Steps indicated in red were performed in CryoSPARC, and steps indicated in blue were performed in Relion. Local resolution map indicating varying resolution throughout the cryo-EM model for BceS state 1 (B) and BceS state 2 (C). FSC curve for BceS state 1 (D) and BcesS state 2 (E). Blue curves were generated without masking, and the red curve was generated with a tight auto-mask in CryoSPARC. Gold-standard FSC cutoff of 0.143 is indicated with a dashed black line. (F) Comparison of BceS state 1 and state 2 indicating alternate conformations of the DHp/CA domain in BceS. Red arrow indicates difference in movement of BceS between the two reconstructions.

ATP binding primes the BceAB-S complex for activation

Previous studies demonstrated that BceAB has complete control over BceS activation[14] and maintains the kinase in an inactive state in the absence of bacitracin (22). Recognition of bacitracin and ATP binding/hydrolysis by BceAB are necessary to initiate signaling through BceS (9). Based on these studies, we reasoned that ATP binding in the BceAB-S complex might drive conformational changes that prime the complex for activation upon subsequent bacitracin recognition. To investigate this hypothesis, we pursued a cryo-EM structure of wild-type BceAB-S with the non-hydrolysable ATP analog ATPγS. Initial 3D classification of the resultant dataset revealed two distinct particle populations, with one population showing a large degree of heterogeneity in the intracellular DHp and CA domains of BceS, and a second population in which the entire BceS kinase was more clearly resolved (Fig. 3.12A). Subsequent classification and refinement produced two cryo-EM maps of the ATPγS-bound BceAB-S complex, one of which was obtained at 3.1 Å overall resolution showing high resolution features BceAB and the TM and HAMP domains of BceS, but disordered BceS DHp and CA domains (Fig. 3.13B and D, Table 3.1). The second reconstruction was obtained at a slightly lower overall resolution of 3.6 Å but shows features for the entirety of BceS (Fig. 3.13C and E and Fig. 3.14A).

In both reconstructions the binding of ATPγS (Fig. 3.13G) induces the BceA nucleotide binding domains (NBDs) to transition from the highly asymmetric configuration observed in the nucleotide-free state, into a conformation that closely resembles that seen in the isolated BceAB transporter bound to ATP (Figs. 3.14A and 3.15A and C). However, close inspection reveals that the BceA subunits are not fully dimerized and ATPγS engages the Walker-A motif and Tyr13 in the A-loop of BceA, but not the signature motif in the opposing BceA monomer (Fig. 3.15C). Thus, although ATPγS induced a more symmetrical orientation of BceA monomers within the BceAB-S complex, the monomers are not positioned to support ATP hydrolysis. More importantly, the conformational shifts induced by binding of ATPγS to the BceA subunits do not affect the overall conformation of BceB. Within the ATPγS-bound BceAB-S structure, the BceB TM helix configuration closely resembles that of the nucleotide-free state, rather than the closed conformation seen with isolated BceAB bound to ATP (Fig. 3.15A and B). Thus, it appears that in the BceAB-S complex, nucleotide binding induces a conformational shift in BceAB to an intermediate state residing between the nucleotide-free and fully collapsed ATP bound conformations.

In both reconstructions of BceAB-S bound to ATPγS the TM helices and HAMP domain of BceS remain unchanged relative to their configuration in the nucleotide-free state. However, in the reconstruction where the entirety of BceS is resolved, a distinct kink is observed around residue Gly96 in the stalk helix that connects the HAMP and DHp domains of BceS (Fig. 3.14A and B). The kink is only observed in the BceS monomer with the HAMP and stalk helix positioned closest to BceAB (Fig. 3.14A). Kinking of the stalk helix causes the DHp and CA domains of both BceS monomers to rotate ~30° towards BceA from their nucleotide-free positions (Fig. 3.14B). A morph between nucleotide-free and ATPγS-bound BceAB-S structures demonstrates that movement of BceA and BceS appears to be coordinated, with kinking of the BceS stalk helix coupled to ATPγS-induced movement of BceA subunits (Movie 3.3).

Although binding of ATPγS to BceA induced a kinked alternate conformation of the stalk, the overall configuration of the DHp and CA domains within the BceS dimer remain relatively unchanged. While the limited resolution of the cryo-EM map within the BceS CA domains prevents identification of any bound ATPγS in this region, the catalytic domain is still positioned far from the phosphorylatable His124 in the DHp domain. Thus, further conformational change beyond that observed in our ATPγS bound BceAB-S structure would be required to form a Michaelis complex of BceS bound with nucleotide and poised for phosphate transfer to His124.

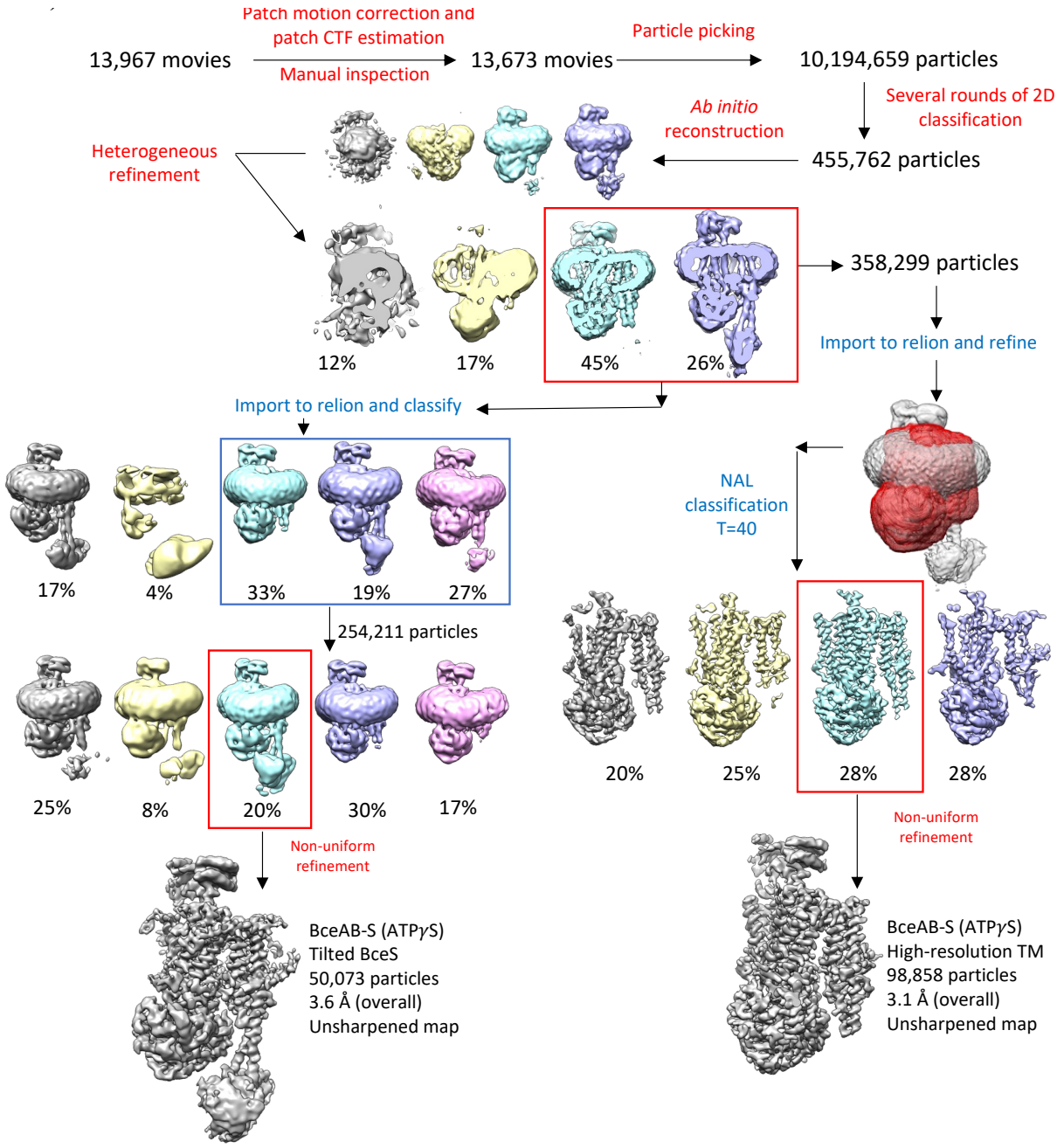

Figure 3.12: Cryo-EM data processing for ATPγS bound BceAB-S. Cryo-EM data processing workflow to resolve two different states of the BceAB-S complex bound to the nucleotide analog ATPγS. One reconstruction produced high-resolution features throughout the TM region, and the second reconstruction at a slightly lower overall resolution revealed the entirety of BceS. Steps indicated in red were performed in CryoSPARC, and steps indicated in blue were performed in Relion.

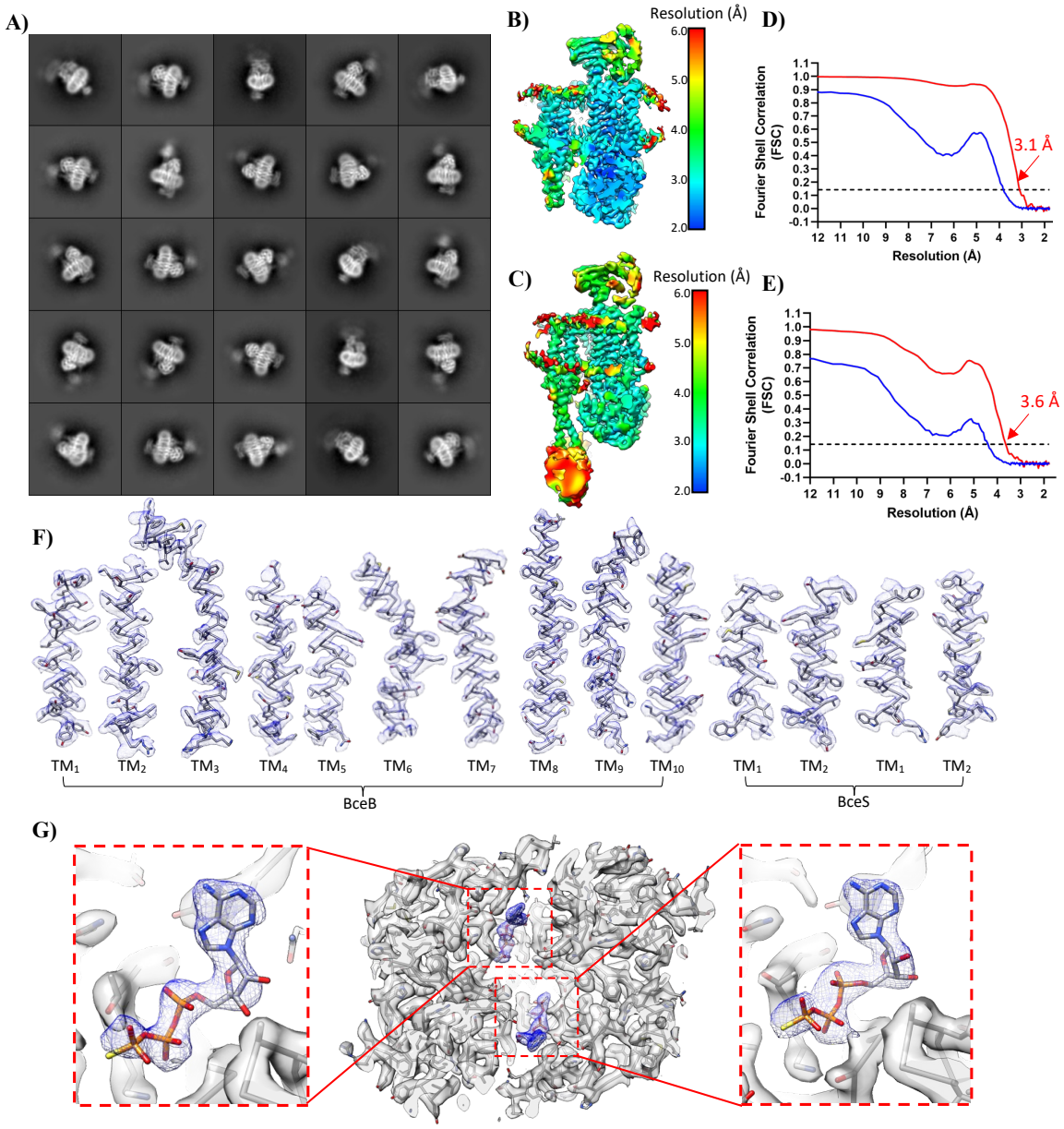

Figure 3.13: Cryo-EM for ATPγS bound BceAB-S. (A) 2D class-averages of BceAB-S particles in the presence of ATPγS. Local resolution map indicating varying resolution throughout the cryo_EM map for the reconstruction with high-resolution TM features (B) or with tilted BceS (C). FSC curve for the reconstruction with high-resolution TM features (D) or with tilted BceS (E). Blue curves were generated without masking, and the red curve was generated with a tight auto-mask in CryoSPARC. Gold-standard FSC cutoff of 0.143 is indicated with a dashed black line. (F) Representative maps for the TM helices in the ATPγS bound BceAB-S complex. (G) Cryo-EM map showing the presence of ATPγS (blue mesh) bound in the two potential ATP binding sites between monomers of BceA (transparent grey surface with grey sticks).

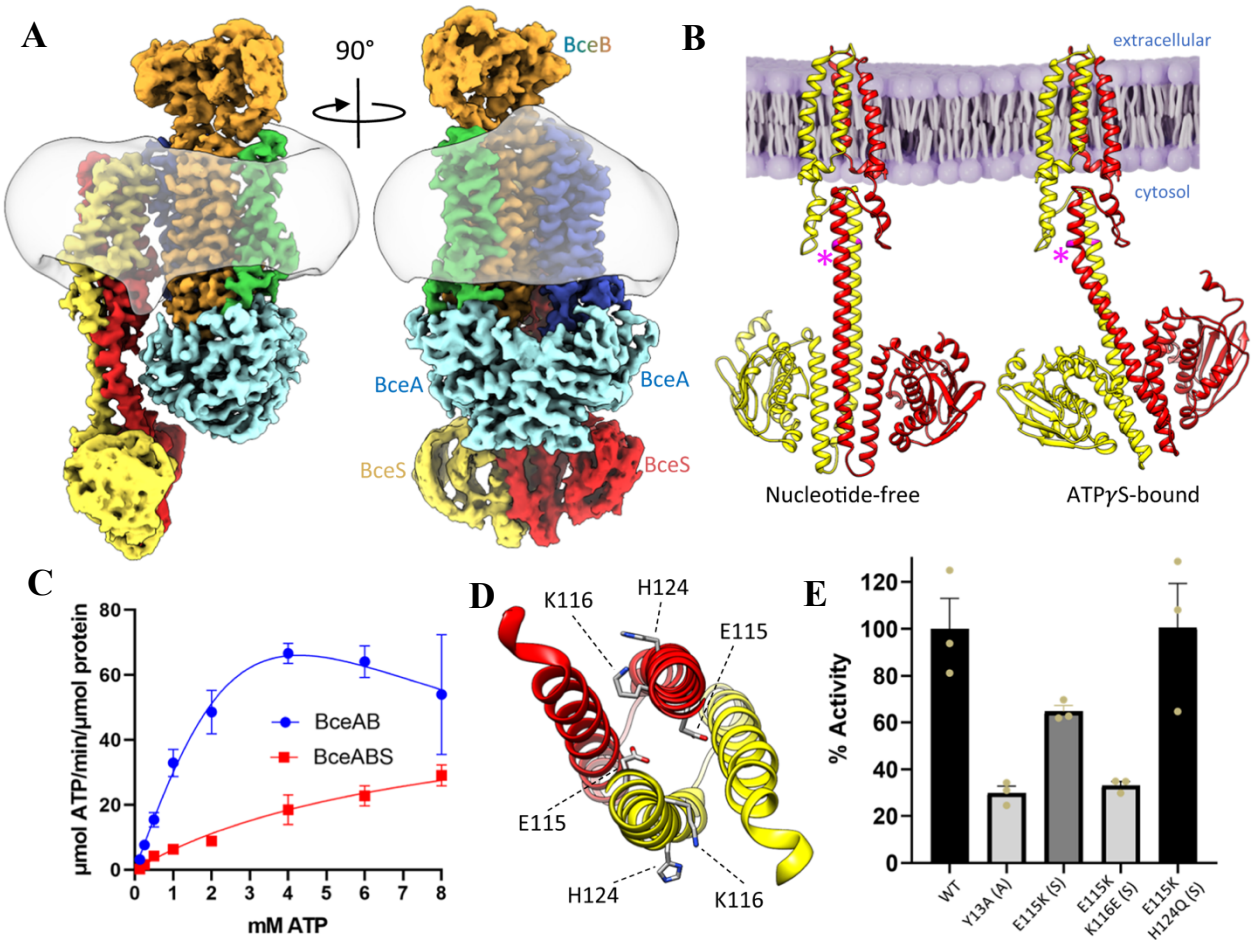

Figure 3.14: (A) Rotated views of the cryo-EM map of BceAB-S bound to ATPγS. Individual protein chains and TM helices are colored as indicated in Fig. 1. The detergent micelle is shown in transparent grey. Binding of ATPγS causes the BceA subunits (cyan) to collapse into a more tightly closed and symmetrical dimer. (B) Comparison of BceS configurations in nucleotide-free and ATPγS bound states of the BceAB-S complex. Binding of ATPγS to BceAB-S induces a ~ 30° kink in the stalk helix of one BceS monomer (pink asterisk). (C) ATPase measurements of detergent solubilized BceAB and BceAB-S complexes. Isolated BceAB exhibits higher basal ATPase activity than the complex with the BceS sensor kinase. Data points represent the mean across $n = 3$ triplicate measurements, and error bars represent standard deviation (SD) across the three measurements. (D) View of the DHp domain of BceS showing H124 that is auto-phosphorylated, and residues E115 and K116 that when substituted to charged-swap variants produce a constitutively active BceS in *B. subtilis*. (E) Comparison of maximal ATPase activity for WT and charge swap variants of the BceAB-S complex. Error bars represent standard error of the mean (SEM) across $n = 3$ triplicate measurements (shown in tan spheres).

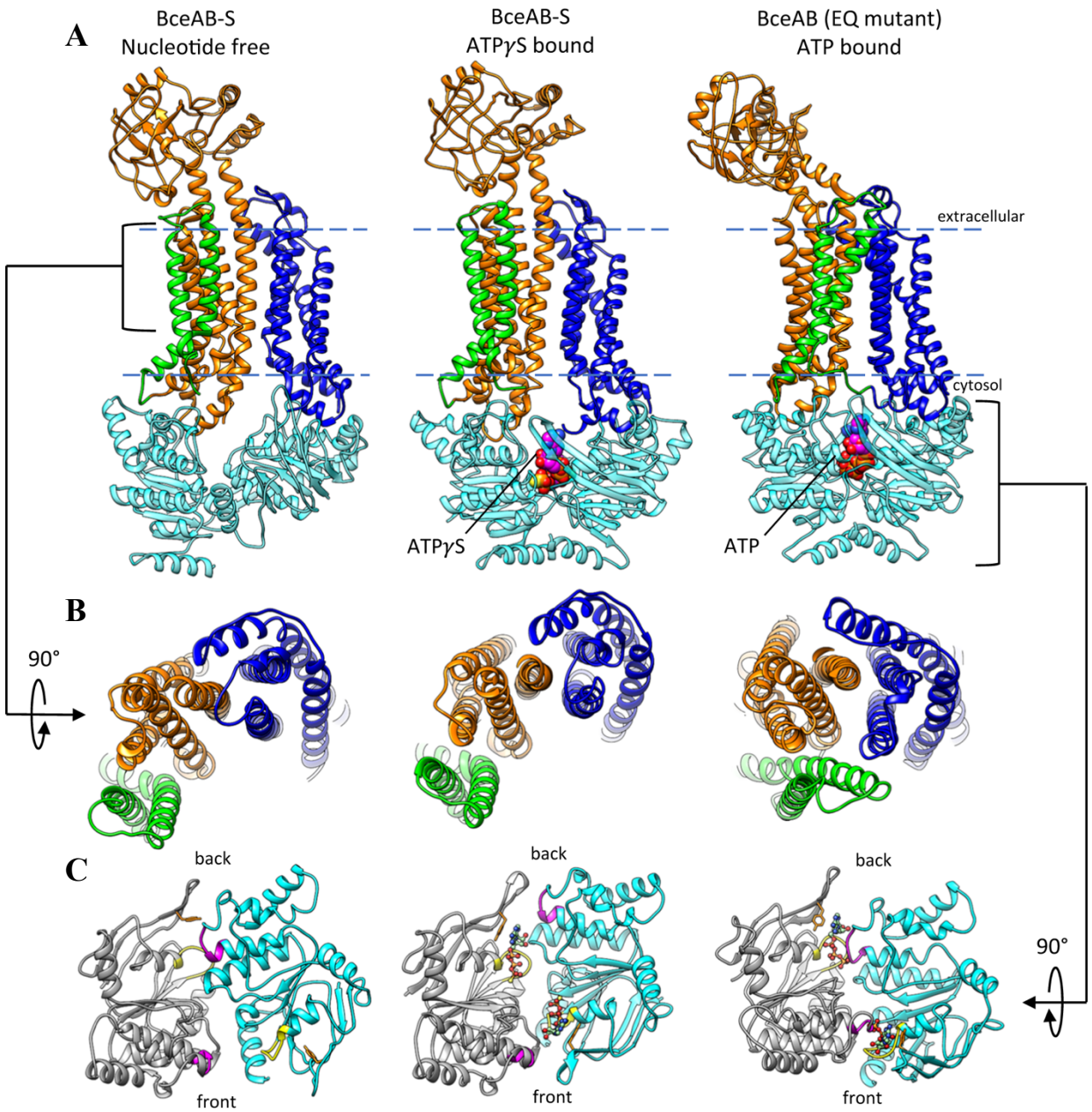

ATP site	Distance (Å)
back	20.0
front	22.9

ATP site	Distance (Å)
back	16.9
front	16.8

ATP site	Distance (Å)
back	9.5
front	9.1

Figure 3.15: (A) Comparison of the conformations adopted by BceAB either in isolation or in complex with the BceS kinase, and in different nucleotide states. BceS is omitted for clarity. Whereas binding of ATP (magenta spheres) to isolated BceAB induces closure of the TM helices, binding of ATPγS (magenta spheres) to the whole BceAB-S complex does not induce a collapse of the BceB TM helices. Blue dashed lines indicate the approximate boundary of the

Figure 3.15 (cont'd)

lipid bilayer. (B) 90° rotated view relative to **a** showing the TM helix arrangement of BceB in each structure. (C) View of the BceA NBDs in the three structures. For clarity, one BceA monomer is colored grey and the other monomer is colored cyan. The Walker A motif is colored yellow, and the ABC signature motif is colored magenta. ATPγS and ATP are shown as ball-and-sticks. (D) Distance measured between residue 47 in the Walker A motif and 146 in the ABC signature motif for the two ATP binding sites in a dimer of BceA. The front and back sites are indicated in (C).

BceS exerts enzymatic control over BceAB

As mentioned above, previous studies demonstrated that BceAB has exquisite control over BceS activation (14,15,22). To investigate the possibility that BceS exerts reciprocal regulation on the basal ATPase activity of BceAB, we performed ATPase assays on detergent solubilized and purified preparations of isolated BceAB and BceAB-S complex. The BceAB-S complex displayed significantly reduced maximal ATPase activity compared to the isolated BceAB transporter (Fig. 3.14C). This result is consistent with our structural analyses demonstrating that nucleotide binding to BceA induces full closure of the NBD dimer in the isolated BceAB transporter, but not when the latter protein is in complex with BceS (Fig. 3.15C) (12).

While the ATPase assay result in Fig. 3.14C demonstrates that BceS can throttle the basal ATPase activity of BceAB, the extent to which altered conformations or states of the BceS kinase contribute to this regulation remained unclear. Previous mutational analysis on BceS identified a critical bundle of electrostatic residues in the BceS DHp domain which can control the activation state of the kinase independent of the function of BceAB (Fig. 3.14D). In-vivo experiments in *B. subtilis* have shown that charge swap variants of Glu115 and/or Lys116 in BceS decouple BceS activation from signaling through BceAB and allow auto-phosphorylation of BceS in the absence of added bacitracin (22). To probe the role of BceS activation on reciprocal enzymatic control of BceAB, we purified BceAB-S complexes containing different combinations of these charge swap variants (with or without additional mutation of His124 in BceS) and assessed their in-vitro ATPase activity (Fig. 3.14E). The E115K variant of BceS reduced the ATPase activity of the BceAB-S complex compared to WT protein, and a E115K/K116E double charge swap variant of BceS further reduced the ATPase activity to a level comparable to that seen with an ATP binding-deficient Y13A variant of BceA. Interestingly, addition of a H124Q substitution on top of E115K resulted in BceAB-S with ATPase activity comparable to the WT complex. While it would appear from this result that autophosphorylation of His124 in BceS could be a major determinant in reciprocal regulation of BceAB ATPase activity, analysis with Phos-tag SDS-PAGE acrylamide gels or fluorescent Phos-tag gel stains[23] have thus far failed to detect in-vitro phosphorylation of BceS with any of our WT or variant complexes of BceAB-S. Nevertheless, the results of ATPase assays collectively suggest that the activation state (and/or conformational landscape) of BceS can have drastic effects on the ATPase activity of the BceAB transporter.

Discussion

Bce modules pair an ABC transporter lacking membrane transport capability with a two-component signaling system lacking a dedicated sensing domain to provide many Firmicutes a first line of defense against antimicrobial peptides that target lipid intermediates of cell wall synthesis. These modules have been proposed to utilize a flux-sensing mechanism wherein conformational cycling of the ABC transporter activates the two-component system, resulting in upregulation of the transporter to keep up with the demand for antimicrobial peptide detoxification (15,22,24). Our cryo-EM structures and biochemical data reveal how the individual components of a Bce module assemble into a functional membrane protein complex and begin to illustrate how conformational changes in the complex mediate a flux-sensing mechanism.

Our cryo-EM structures of BceAB-S demonstrate that the TM helices of the BceS sensor kinase interact with the first four TM helices of BceB (Fig. 3.2B), and that much of this interaction is mediated by membrane lipids (Fig. 3.9A and B). Previous biochemical studies demonstrated that activation of BceS by conformational cycling of BceAB is accompanied by piston-like displacements of TM_2 in BceS (22). Although we do not observe any piston-like movement of BceS TM_2 in our various cryo-EM structures, it appears that the conformational coupling between the TM domains of BceB and BceS likely involves specific interactions with membrane lipids. Further structural and biochemical analysis of the BceAB-S complex in alternate conformational states will be required to unravel precisely how conformational cycling of BceAB initiates BceS activation, and the role that membrane lipids play in this overall process.

To our knowledge, our structures of BceAB-S represent the first cryo-EM structures of a full-length membrane-embedded histidine kinase. Unlike methods such as x-ray crystallography where individual domains are observed in isolation or full-length kinases are conformationally restricted in a crystal lattice, cryo-EM can provide insight into the conformational landscape of histidine kinases. Current models of histidine kinase function favor a statistical-thermodynamic model in which signal transduction through the kinase can be thought of as a series of thermodynamically linked equilibria between conformations of individual protein domains (20). In this model the individual domains of a histidine kinase (TM, HAMP, DHp, CA, etc…) populate a landscape of thermodynamically linked independent conformational states and

dynamics. This situation is readily apparent in our cryo-EM structures of BceAB-S, where in the resting state BceS samples a wide variety of conformations (Fig. 3.10A-C). Even in the states that can be resolved through 3D classification (Fig. 3.10C) significant conformational heterogeneity is still present in the DHp and CA domains, which severely limits resolution in these regions. Our observations of BceS conformational flexibility in cryo-EM reconstructions appears highly consistent with a statistical-thermodynamic model of histidine kinase function, with the individual domains of the sensor kinase adopting a variety of conformations relative to one another.

In addition to the conformational flexibility of BceS, our structures of the BceAB-S complex reveal conformational and functional differences between the full transporter-kinase complex and BceAB alone. In a previous study with isolated BceAB, ATP binding induced full closure of the BceA NBDs and a concomitant closure of the BceB TM helices and tilting of the extracellular domain (12). In contrast, ATPγS binding within the full BceAB-S complex induced movement of the BceA subunits into a partially closed state unable to support ATP hydrolysis, without changes in the BceB TM helices (Fig. 3.15A-C). Not only do the BceAB and BceAB-S complexes adopt different conformations upon nucleotide binding, but the ATPase activity of each complex is significantly different (Fig. 3.14C). These results demonstrate that BceAB and BceS reciprocally regulate one another, with BceAB being strictly required for BceS activation, and BceS throttling the intrinsically high basal ATPase activity of BceAB to prevent futile rounds of ATP hydrolysis in the absence of antimicrobial peptides.

Together with previous biochemical studies, our cryo-EM structures begin to paint a mechanistic picture of the overall signaling process through Bce-modules (Fig. 3.16). In this model the BceAB-S complex in the nucleotide-free state (Fig. 3.16; state 1) displays asymmetric BceA subunits, and highly flexible cytosolic regions of BceS. Subsequent binding of ATP pre-loads BceA with nucleotide and brings these domains into a more symmetric configuration, but one that is still insufficient for ATP hydrolysis. Along with movement of BceA in response to nucleotide binding, BceS adopts a kinked conformation but the DHp and catalytic domains remain in a conformation insufficient to support autophosphorylation of His124 (Supplementary Fig. 3.16). This overall configuration likely represents a sensing-ready state that would be encountered in *B. subtilis* prior to challenge with bacitracin. Once UPP-bacitracin complexes are encountered, ATP hydrolysis by BceAB would be stimulated, and in turn initiate signaling and

autophosphorylation of BceS (Fig. 3.16; state 3). Previous reports suggest that this signaling involves a piston-like movement of TM_2 in BceS, and our current structural analysis suggests that signal transduction through the entire complex may also involve interactions between BceA and BceS (22). While many of the molecular details underlying bacitracin recognition and signaling activation remain to be uncovered, this model provides a plausible explanation for the tight regulation of Bce module signaling and subsequent upregulation of BceAB to rapidly respond to antimicrobial peptide induced stress.

It is important to note that under conditions of antimicrobial peptide induced stress, both BceAB and BceAB-S complexes are present within the same cell. In this situation, the differing activity levels and conformational changes of these two complexes likely reflect distinct functions. BceAB alone is most abundant under bacitracin stress, and its high activity allows for rapid removal of the antimicrobial peptide from target lipids through ATP-driven changes in BceB. BceAB-S, however, is more tightly regulated for precise and highly tuned sensing of current stress levels.

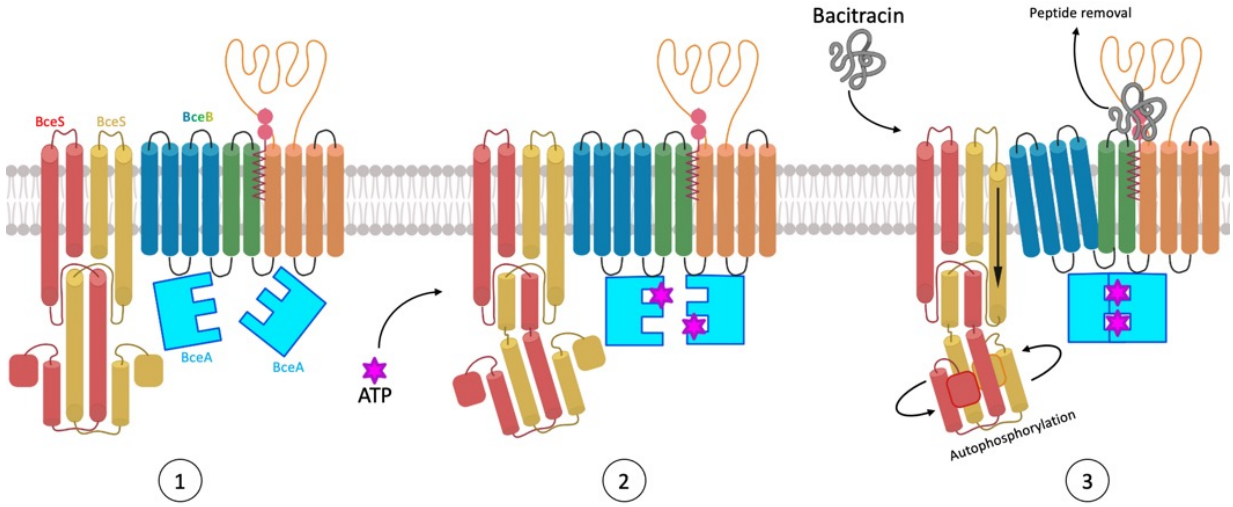

Figure 3.16: Proposed model of BceAB-S function. Cartoon diagram depicting a proposed model of steps involved in BceAB-S activation and signaling. In the resting nucleotide-free state (state 1) the BceA nucleotide binding domains adopt an asymmetric configuration. Subsequent binding of ATP (purple star) induces the BceA subunits to adopt a more symmetrical configuration (state 2), with each BceA subunit engaging ATP but not fully dimerized to support ATP hydrolysis. In state 2 the stalk helix connecting that HAMP and CA domains of BceS develops a kink. Subsequent binding of bacitracin (state 3) induces the BceA subunits to fully dimerize and initiate ATP hydrolysis, which induces a conformational change of the BceB TM helices that is in-turn sensed by BceS in the form of downward piston-like movement of BceS TM-2. The conformational changes of BceS is propagated downward through the HAMP and DHp domains, resulting in rotation of the CA domain to support autophosphorylation. During this process bacitracin is removed from the lipid target undecaprenyl pyrophosphate. ATP hydrolysis by BceA resets the complex to the resting nucleotide-free state.

Methods

Protein expression and purification

The overlapped genes encoding BceA-BceB, and the gene encoding BceS were PCR amplified from *B. subtilis* genomic DNA and assembled into a petDUET-1 vector using NEB HiFi Assembly according to the manufacturer's protocol. This procedure generated a plasmid driving production of BceB and N-terminally 6x-His tagged BceA from one T7 promoter, and BceS driven from the second T7 promoter. The expression plasmid was transformed into *E. coli* C41(DE3) cells and a starter culture from a single colony was grown at 37 °C in Luria Broth (LB) medium with 100 μg/mL ampicillin. The starter culture was used to inoculate 6 L of Terrific Broth (TB) medium with 100 μg/mL ampicillin and Antifoam-204 in baffled Fernbach flasks. Cultures were grown at 37 °C to an optical density (OD_{600}) of ~0.8 before reducing the temperature to 18 °C and inducing protein expression with 0.4 mM IPTG. After ~16 h of induction the cultures were harvested by centrifugation and resuspended in lysis buffer (25 mM Tris (pH 8), 150 mM NaCl, 10% glycerol, 5 mM β-mercaptoethanol) supplemented with 1 μg/mL pepstatin A, 1 μg/mL leupeptin, 1 μg/mL aprotinin, 0.6 mM benzamidine, and ~5,000 units of Dr. Nuclease (Syd Labs).

Bacterial cells were lysed by sonication and membranes isolated by ultracentrifugation at ~100,000 g for 1 h. Isolated membranes were resuspended in lysis buffer and solubilized by stirring for 1 h at 4 °C with lauryl maltose neopentyl glycol (LMNG) added to a final concentration of 1%. Insoluble material was removed by ultracentrifugation at 100,000 g for 1 h and the resulting supernatant was applied to Co^{3+}-Talon resin. The resin was washed with ~10 column volumes of buffer A (25 mM Tris (pH 8), 150 mM NaCl, 10 mM imidazole, 10% glycerol, and 0.005% LMNG) before eluting bound protein with buffer A containing 250 mM imidazole. The eluted protein was concentrated in a 100 kDa MWCO spin concentrator and injected onto a Superdex 200 Increase 10/300 GL column equilibrated in 25 mM Tris (pH 8), 150 mM NaCl, and 0.005% LMNG. Peak fractions corresponding to the intact BceAB-S complex were pooled, concentrated in a 100 kDa MWCO spin concentrator and used immediately for cryo-EM studies, or flash frozen in liquid nitrogen and stored at −80 °C for later use.

ATPase assay

Site-directed mutagenesis of the *bceA* and *bceS* genes was performed using a Q5 mutagenesis kit from NEB and standard manufacturers protocols (oligonucleotide primer sequences used in this study are included in the accompanying Source Data file). Plasmids encoding variants of BceAB-S were verified through Sanger sequencing at the RTSF Genomics Core at Michigan State University. Colorimetric ATPase assays were modified from a previously described protocol and performed in 96 well plates (12). To each well 2 μg of purified BceAB or 3 μg BceAB-S was added, followed by buffer containing the indicated concentration of ATP and $MgCl_2$ to create a total reaction volume of 50 μL. Samples were incubated at 37 °C for 30 min before stopping the reaction by addition of 50 μL of a 12% (w/v) SDS solution. Then 100 μL of a 1:1 mixture of 12% ascorbic acid (w/v) and 2% ammonium molybdate (w/v) was added, followed by 150 μL of a solution containing 2% sodium citrate (w/v), 2% sodium (meta)arsenite (w/v), and 2% acetic acid (v/v). Absorbance at 850 nm was measured in a Molecular Devices ID5 plate reader and converted to total ATP consumed using a standard curve generated with K_2HPO_4 solutions. The rate of ATP consumption (μmol ATP/min/μmol protein) was plotted in GraphPad Prism and curves were fit with a model of substrate inhibition Velocity = V_{max}*[ATP]/(K_m + [ATP]*(1 + [ATP]/K_i) or a standard Michaelis Menten equation Velocity = Vmax * [ATP]/(K_m + [ATP]).

Cryo-EM imaging and data processing

Grids for cryo-EM imaging were prepared on a Vitrobot Mark IV by applying 2.5 μL of purified BceAB-S at ~7 mg/mL to Quantifoil R2/2 200 mesh grids that had been glow-discharged for 45 s at 15 mA in a Pelco EasyGlow. In the case of ATPγS bound BceAB-S the purified protein complex was incubated on ice with 5 mM ATPγS and 5 mM $MgCl_2$ for 30 min before applying samples to cryo-EM grids. The grids were blotted for 5 s at 4 °C, 100% humidity, and a blot-force of 1 before being plunge frozen in liquid ethane cooled by liquid nitrogen. Frozen grids were screened for ice quality and particle distribution using EPU software on a Talos Arctica equipped with a Falcon-3 detector at the RTSF Cryo-Electron Microscopy Facility at Michigan State University. Final data collection was performed at Purdue University using Leginon[25] on a Titan Krios with a K3 direct electron detector and Gatan Quantum GIF energy filter set to a 20 eV slit width. Movies were collected in counting mode with a pixel size of 0.872 Å and a total dose of 60.5 electrons/Å^2.

Movies were corrected for beam-induced motion by performing patch motion correction in cryoSPARC, and CTF parameters were determined by patch CTF estimation in cryoSPARC (26). Micrographs with CTF fit parameters worse than 6 Å were discarded, and further manual inspection was performed to remove obviously poor micrographs. Following particle picking and several rounds of 2D classification in cryoSPARC to remove bad particles, initial models for 3D classification were constructed using ab initio reconstruction in cryoSPARC. Where indicated the particles were transferred to RELION 4.0 for further 3D classification and signal subtraction, before finally being reimported to cryoSPARC for a final round of non-uniform refinement (27,28). Resolutions of all maps were calculated using the gold-standard FSC and local resolutions were calculated in cryoSPARC.

Model building and refinement

To build atomic models into the cryo-EM maps for the nucleotide-free BceAB-S complex, we initially rigid-body docked the previous nucleotide-free BceAB transporter structure (PDB = 7TCG) and AlphaFold-predicted models of *B. subtilis* BceS monomers into the cryo-EM map using UCSF Chimera (29,30). These models were manually adjusted in COOT and refined in real-space using phenix.real_space_refine in the PHENIX software suite (31,32). Iterative rounds of real-space refinement in PHENIX and manual model adjustment in COOT were performed to optimize the overall model properties and fit to the experimental cryo-EM map.

To build atomic models of the BceAB-S complex in the ATPγS bound state, the refined nucleotide-free BceAB-S structure was first rigid body fit into the cryo-EM map as a whole using the BceB and BceS TM helices as an initial guide. Rigid body fitting of individual BceA protein chains and the cytoplasmic regions of BceS was then performed in UCSF Chimera to adjust for shifts induced by ATPγS binding. The resulting model then underwent iterative rounds of real-space refinement and manual adjustment in PHENIX and COOT as described above for the nucleotide-free complex. The initial rounds of real-space refinement in PHENIX utilized the morphing option to account for large secondary structural shifts that were not resolved through initial rigid-body docking. All models were assessed for appropriate stereochemical properties and fit to the experimental cryo-EM map using MolProbity (33). Figures were created using UCSF Chimera, UCSF ChimeraX, and BioRender.com (34).

Data Availability

Atomic coordinates and associated electron microscopy maps for the six structures reported in this publication have been deposited in the Protein Data Bank (PDB) and Electron Microscopy Data Bank (EMDB) under the following accession numbers: Nucleotide-free BceAB-S TM State 1 (PDB 8G3A, EMDB 29690), Nucleotide-free BceAB-S TM State 2 (PDB 8G3B, EMDB 29691), Nucleotide-free BceAB-S BceS State 1 (PDB 8G3F, EMDB 29694), Nucleotide-free BceAB-S BceS State 2 (PDB 8G3L, EMDB 29701), ATPγS bound BceAB-S High-res TM (PDB 8G4C, EMDB 29716), ATPγS bound BceAB-S Kinked BceS (PDB 8G4D, EMDB 29717). The initial model of BceAB used as a reference for model building is available at the PDB under the following accession number (PDB 7TCG). The AlphaFold model of BceS used as an initial template for model building is available at the AlphaFold Protein Structure Database [https://alphafold.ebi.ac.uk/entry/O35044]. Source data are provided with this paper.

Acknowledgements

Research reported in this publication was supported by the National Institute of General Medical Sciences of the National Institutes of Health under Award Number R35GM146721 to B.J.O. The content is solely the responsibility of the authors and does not necessarily represent the official views of the National Institutes of Health. Electron Microscope support at Purdue University was established under the NIH Midwest Cryo-EM Consortium grant number 1U24GM116789-01A. We would like to thank Dr. Sundharraman Subramanian for help with electron microscope operation at the RTSF Cryo-Electron Microscopy Core at Michigan State University. We are also grateful for the NIH Midwest Cryo-EM Consortium and Dr. Thomas Klose, Dr. Frank Vago, and Dr. Wen Jiang for providing microscope time and assistance with data collection at Purdue University. We would also like to thank all members of the Orlando laboratory and Dr. Robert Hausinger and Dr. Sean Crosson for careful reading of the manuscript.

REFERENCES

1. Huan, Y., Kong, Q., Mou, H. & Yi, H. Antimicrobial Peptides: Classification, Design, Application and Research Progress in Multiple Fields. *Front Microbiol* 11, 582779 (2020).

2. Wang, G., Li, X. & Wang, Z. APD3: the antimicrobial peptide database as a tool for research and education. *Nucleic Acids Res* 44, D1087-1093 (2016).

3. Breukink, E. & de Kruijff, B. Lipid II as a target for antibiotics. *Nature Reviews Drug Discovery* 5, 321-323 (2006).

4. Malin, J.J. & de Leeuw, E. Therapeutic compounds targeting Lipid II for antibacterial purposes. *Infection and drug resistance* 12, 2613-2625 (2019).

5. Assoni, L. *et al.* Resistance Mechanisms to Antimicrobial Peptides in Gram-Positive Bacteria. *Frontiers in Microbiology* 11 (2020).

6. Gebhard, S. & Mascher, T. Antimicrobial peptide sensing and detoxification modules: unravelling the regulatory circuitry of Staphylococcus aureus. *Mol Microbiol* 81, 581-587 (2011).

7. Dintner, S. *et al.* Coevolution of ABC transporters and two-component regulatory systems as resistance modules against antimicrobial peptides in Firmicutes Bacteria. *Journal of bacteriology* 193, 3851-3862 (2011).

8. Ohki, R. *et al.* The BceRS two-component regulatory system induces expression of the bacitracin transporter, BceAB, in Bacillus subtilis. *Mol Microbiol* 49, 1135-1144 (2003).

9. Rietkötter, E., Hoyer, D. & Mascher, T. Bacitracin sensing in Bacillus subtilis. *Mol Microbiol* 68, 768-785 (2008).

10. Staroń, A., Finkeisen, D.E. & Mascher, T. Peptide antibiotic sensing and detoxification modules of Bacillus subtilis. *Antimicrob Agents Chemother* 55, 515-525 (2011).

11. Dintner, S., Heermann, R., Fang, C., Jung, K. & Gebhard, S. A sensory complex consisting of an ATP-binding cassette transporter and a two-component regulatory system controls bacitracin resistance in Bacillus subtilis. *J Biol Chem* 289, 27899-27910 (2014).

12. George, N.L., Schilmiller, A.L. & Orlando, B.J. Conformational snapshots of the bacitracin sensing and resistance transporter BceAB. *Proceedings of the National Academy of Sciences of the United States of America* 119, e2123268119 (2022).

13. Kobras, C.M. *et al.* BceAB-Type Antibiotic Resistance Transporters Appear To Act by Target Protection of Cell Wall Synthesis. *Antimicrob Agents Chemother* 64 (2020).

14. Bernard, R., Guiseppi, A., Chippaux, M., Foglino, M. & Denizot, F. Resistance to bacitracin in Bacillus subtilis: unexpected requirement of the BceAB ABC transporter in the control of expression of its own structural genes. *Journal of bacteriology* 189, 8636-8642 (2007).

15. Fritz, G. *et al.* A New Way of Sensing: Need-Based Activation of Antibiotic Resistance by a Flux-Sensing Mechanism. *mBio* 6, e00975 (2015).

16. Gushchin, I. *et al.* Mechanism of transmembrane signaling by sensor histidine kinases. *Science (New York, N.Y.)* 356 (2017).

17. Moukhametzianov, R. *et al.* Development of the signal in sensory rhodopsin and its transfer to the cognate transducer. *Nature* 440, 115-119 (2006).

18. Maslennikov, I. *et al.* Membrane domain structures of three classes of histidine kinase receptors by cell-free expression and rapid NMR analysis. *Proceedings of the National Academy of Sciences of the United States of America* 107, 10902-10907 (2010).

19. Kallenberg, F., Dintner, S., Schmitz, R. & Gebhard, S. Identification of regions important for resistance and signalling within the antimicrobial peptide transporter BceAB of Bacillus subtilis. *Journal of bacteriology* 195, 3287-3297 (2013).

20. Bhate, M.P., Molnar, K.S., Goulian, M. & DeGrado, W.F. Signal transduction in histidine kinases: insights from new structures. *Structure (London, England : 1993)* 23, 981-994 (2015).

21. Diensthuber, R.P., Bommer, M., Gleichmann, T. & Möglich, A. Full-length structure of a sensor histidine kinase pinpoints coaxial coiled coils as signal transducers and modulators. *Structure (London, England : 1993)* 21, 1127-1136 (2013).

22. Koh, A., Gibbon, M.J., Van der Kamp, M.W., Pudney, C.R. & Gebhard, S. Conformation control of the histidine kinase BceS of Bacillus subtilis by its cognate ABC-transporter facilitates need-based activation of antibiotic resistance. *Mol Microbiol* 115, 157-174 (2021).

23. Kinoshita-Kikuta, E., Koike, T. & Kinoshita, E. Recent advances in the Phos-tag technique focused on the analysis of phosphoproteins in a bacterial two-component system. *J Proteomics* 252, 104429 (2022).

24. Mascher, T. Intramembrane-sensing histidine kinases: a new family of cell envelope stress sensors in Firmicutes bacteria. *FEMS microbiology letters* 264, 133-144 (2006).

25. Suloway, C. *et al.* Automated molecular microscopy: the new Leginon system. *Journal of structural biology* 151, 41-60 (2005).

26. Punjani, A., Rubinstein, J.L., Fleet, D.J. & Brubaker, M.A. cryoSPARC: algorithms for rapid unsupervised cryo-EM structure determination. *Nat Methods* 14, 290-296 (2017).

27. Scheres, S.H. RELION: implementation of a Bayesian approach to cryo-EM structure determination. *Journal of structural biology* 180, 519-530 (2012).

28. Punjani, A., Zhang, H. & Fleet, D.J. Non-uniform refinement: adaptive regularization improves single-particle cryo-EM reconstruction. *Nat Methods* 17, 1214-1221 (2020).

29. Jumper, J. *et al.* Highly accurate protein structure prediction with AlphaFold. *Nature* 596, 583-589 (2021).

30. Pettersen, E.F. *et al.* UCSF Chimera--a visualization system for exploratory research and analysis. *Journal of computational chemistry* 25, 1605-1612 (2004).

31. Emsley, P. & Cowtan, K. Coot: model-building tools for molecular graphics. *Acta crystallographica. Section D, Biological crystallography* 60, 2126-2132 (2004).

32. Adams, P.D. *et al.* PHENIX: a comprehensive Python-based system for macromolecular structure solution. *Acta crystallographica. Section D, Biological crystallography* 66, 213-221 (2010).

33. Williams, C.J. *et al.* MolProbity: More and better reference data for improved all-atom structure validation. *Protein Sci* 27, 293-315 (2018).

34. UCSF ChimeraX: Structure visualization for researchers, educators, and developers. Pettersen EF, Goddard TD, Huang CC, Meng EC, Couch GS, Croll TI, Morris JH, Ferrin TE. *Protein Sci.*2021 Jan;30(1):70-82.

CHAPTER 4: CONCLUSION AND FUTURE DIRECTIONS

This chapter is partially adapted from a review published as: **George, N. L**., Bennett, E.C. & Orlando, B. J. Guarding the Walls: The Multifaceted Roles of Bce Modules in Cell Envelope Stress Sensing and Antimicrobial Resistance. *J Bacteriol* 0:e00123-24 (2024).

Summary: What Have We Learned About Bce Modules?

Bacteria have developed diverse strategies for defending their cell envelopes from external threats. In Firmicutes, Bce modules are a widespread tool for managing cell envelope stress by combining an AMP-sensing and detoxifying transporter with a stress response coordinating two-component system. Bce modules provide specific, front-line defense for a wide variety of antimicrobial peptides and small molecule antibiotics as well as coordinate responses for heat, acid, and oxidative stress. Because of these abilities, Bce modules play important roles in virulence and the development of antibiotic resistance in a variety of pathogens, including *Staphylococcus, Streptococcus, and Enterococcus* species.

Our cryo-EM structures of the *Bacillus subtilis* BceABRS bacitracin resistance module provide the first structural insight into how what Bce module components look like, how they assemble into complexes, and the conformational dynamics they undergo. These structures also provide a new lens through which to interpret earlier data by revealing key protein features and putting mutational data in a three-dimensional context. These structures also open new research avenues to explore, especially by combining structural and biochemical studies with experiments in the bacteria that produce Bce modules, and by exploring the similarities and differences in Bce module function from species to species. By integrating interdisciplinary approaches and sharing insights across species boundaries, we will gain new insights into these multifunctional but incompletely understood systems and find new applications in the fight against antibiotic resistance. Understanding these multifunctional membrane complexes will enhance our understanding of bacterial stress sensing and may point toward new therapeutic targets for highly resistant pathogens.

What Do Structures Tell Us About Bce Mechanisms?

Our structural and biochemical studies reveal new details about Bce module function that provide insight into how these complexes mediate antimicrobial peptide resistance. In particular our work uncovers conformational changes underlying resistance and signaling as well as new layers of regulation between Bce module components.

Prior work identified the BceAB extracellular domain as critical for AMP recognition. Our structural work narrows this binding site further through identification of the lipid binding pocket between transmembrane helices 5, 6, 7, and 9 (Fig. 4.1A). This pocket sits below extracellular domain, directly beneath a series of highly variable loops including the "guard loop" determined to be important for AMP recognition in the *Staphylococcus aureus* VraFG transporter (Figure 4.1A) (1). In the structure of BceAB without ATP, the binding pocket remains open to the membrane, allowing lipid entry. If AMPs are bound to these lipids, they may engage with the extracellular domain to trigger signaling and detoxification. Structures of *B. subtilis* BceAB transporter suggest that ATP binding induces closure of the lipid binding pocket and tilting of the extracellular domain which could contribute to an upward movement of AMPs away from the membrane (2). How such conformational changes may underlie AMP release from the lipid remains to be determined, possibly by capture of AMP-bound Bce transporter structures.

The conformational changes observed upon ATP binding to BceAB also reveal key differences between Bce transporters and type VII ABC transporters such as the gram-negative FtsEX and MacAB. These "mechanotransmission" transporters all mediate function externally of the membrane, rather than transport substrates across the membrane directly. They share common features, including the FtsX-like transmembrane fold and large extracellular/periplasmic domains with similar subdomains (Porter and Sabre in MacB and BceB, Porter in FtsX) (3-5). However, Bce transporters are unique in that they consist of a single membrane subunit. This fusion of two FtsX folds results in unique conformational changes during ATP hydrolysis; while MacB is described as functioning as a "molecular bellows" that pumps antibiotics up and away from the periplasm through opening and closing of an interdomain cavity, Bce modules may work more like a "bottle opener," where transmembrane helices close the lipid binding pocket like a hand around the AMP-bound lipid "bottle" while the tilting of the extracellular domain pries off the AMP "lid"(Fig. 4.2A,C) (3). This model, effecting function through extracellular domain orientation, is somewhat similar to models of FtsEX

where ATP binding state changes the periplasmic domain conformation to extend and tilt bound EnvZ towards or away from the peptidoglycan layer (4.2B) (4,5). Another difference between Bce transporters and the gram-negative type VII transporters is that the other transporters generally interface with a third component to form a "tripartite efflux pump" that allows for transport of substrates across the outer membrane (TolC for MacAB) or enzymatic function (EnvC for FtsEX). These components allow the membrane-embedded transporter to extend their reach through the periplasm and beyond. Since the gram-positive bacteria that express Bce proteins lack an outer membrane, it is not surprising that Bce modules do not express with TolC-like proteins; they also appear to function without additional EnvC-like enzymatic extensions.

Bce kinases lack a dedicated signal sensing domain and are reliant on their transporter for function. Due to the rarity of such intramembrane histidine kinases, and that some Bce transporters are encoded in different genomic locations than their kinases, some studies of Bce modules proposed that Bce kinases function independently and sense AMPs through the membrane and/or the short extracellular loop connecting the transmembrane helices (1,6). However, our cryo-EM structures clarify Bce module architecture by showing the BceS kinase situated next to BceAB on the opposite side from the transporter's lipid binding pocket. These structures, as well as AlphaFold models of related modules show that residues in the kinase extracellular loop, including the functionally-critical equivalent of *S. aureus* GraS D35, are in contact with the top of transporter TMs 3 and 4 (6,7). This interaction may allow the kinase to sense conformational changes in the transmembrane region of the transporter (Fig. 4.1B). Given the tight control of the BceAB transporter over BceS-mediated signaling, it is surprising that the two proteins are separated by lipids through the transmembrane domains and have very few residues in contact. How activity of the transporter induces conformational change leading to kinase activation is still unclear. In addition to the BceS extracellular loop-transporter interaction, residues within the BceS HAMP domain are in proximity to the BceA nucleotide binding domains (Fig. 4.1C). It remains to be determined if interaction between these residues is functionally important, but it is plausible that such an interaction could provide a means by which the kinase could sense both the AMP binding (through the extracellular loop) and the ATP-binding (through the HAMP domain) state of the transporter.

Our work also revealed that not only is BceS regulated by its paired transporter, but the kinase exerts some control over the transporter in return. BceAB exhibits lower ATPase activity

when in complex with BceS than when expressed alone, and structures with and without ATP bound suggest that the transporter-kinase and transporter-alone complexes undergo different conformational changes during ATP binding and hydrolysis. One important but overlooked consequence of Bce module regulation is that in many species, only expression of the transporter is adjusted to cell wall stress, while two-component system expression levels stay stable (8-11). As a result, a cell under AMP-induced stress may contain both transporter-kinase and transporter-alone complexes. Higher *in vitro* ATPase activity of the *B. subtilis* BceAB transporter compared to the BceABS transporter-kinase complex support a model in which the free transporter rapidly mediates resistance, while the transporter-kinase complex functions primarily as a tightly regulated signaling complex (7). This functional division between transporter-only and transporter-kinase complexes allows the sensory complex to maintain high sensitivity and rapid response to AMPs while the isolated transporter efficiently protects the cell from damage even at low AMP concentrations (12). However, some modules, such as MbrABCD in *Streptococcus mutans,* VirABRS-AnrAB in *Listeria monocytogenes,* and BceABRS in *Streptococcus thermophilus,* do show upregulation of both the transporter and two-component system in the presence of AMPs, which could affect signaling dynamics (13-17).

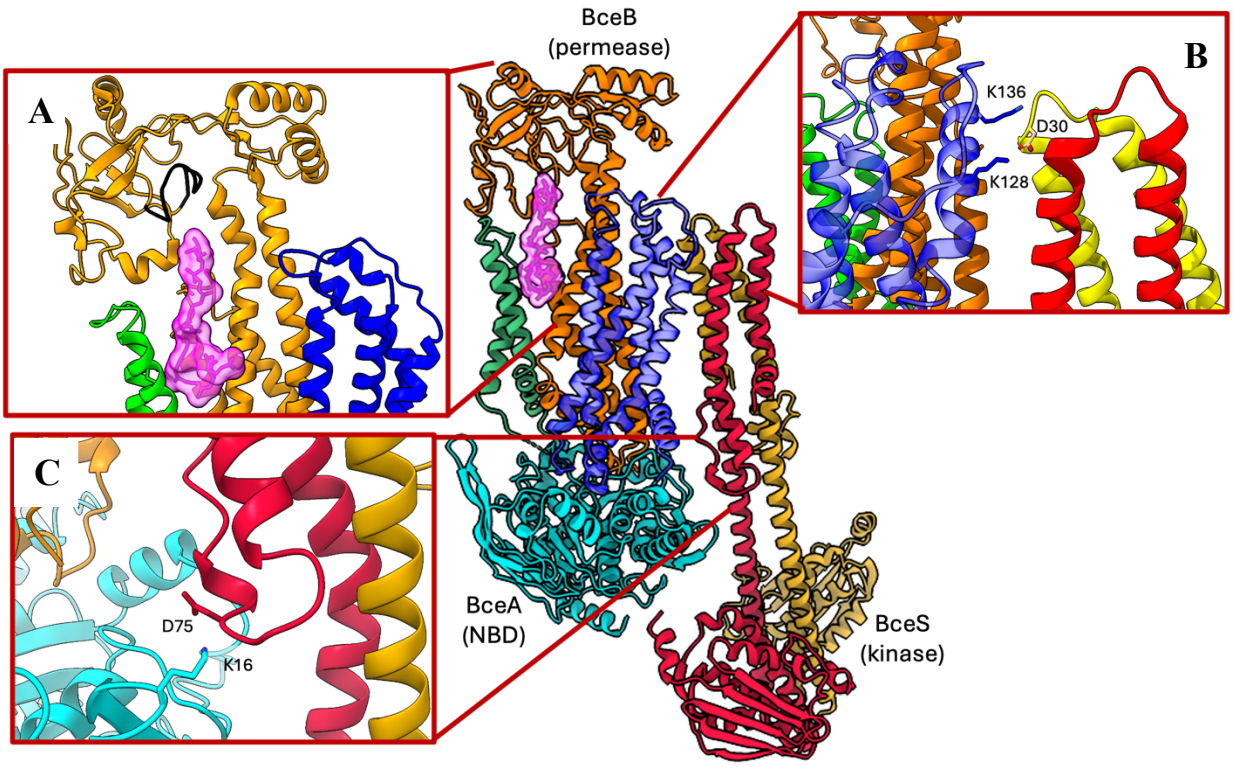

Figure 4.1: Structural features of Bce modules. Cryo-EM structure of BceABS from *B. subtilis* highlighting (A) the lipid binding pocket with lipid surface representation in pink and the extracellular domain "guard loop" in black, (B) interaction between the BceS kinase extracellular loop and BceAB transporter, and (C) residues interacting between the BceS HAMP domain and BceA. In the central structure, the kinase BceS (red and yellow) is in complex with ABC transporter BceAB (NBD = cyan, FtsX bundles = blue and orange, TMs 5 and 6 = green).

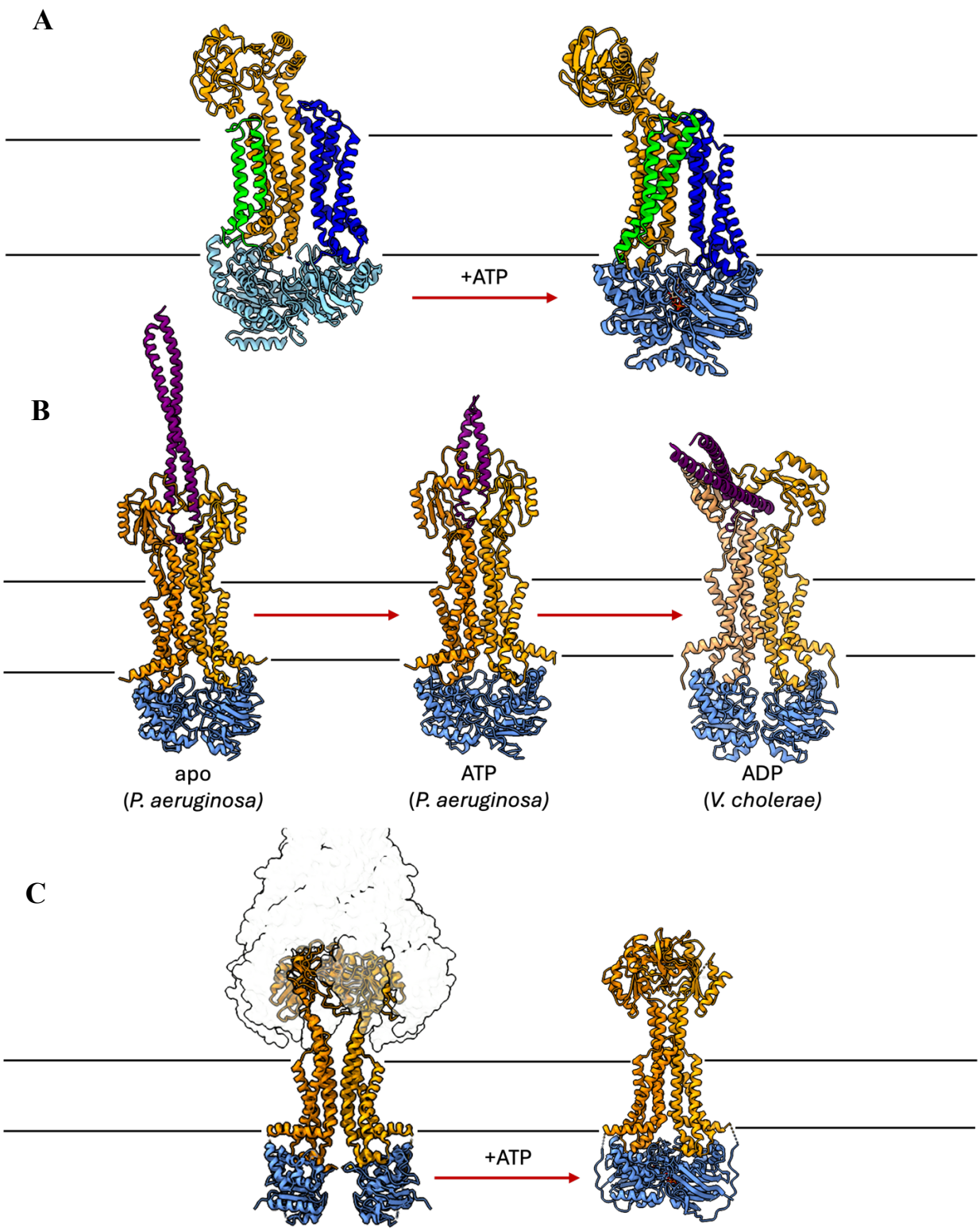

Figure 4.2: BceAB (A) conformational changes compared to gram-negative type VII ABC transporters. FtsEX (B, PDB 8I6O, 8I6S, and 8TZK), is shown with EnvZ in red. MacB (C, PDB 5NIL, 5LIL), is shown with MacA-TolC in silhouette in the structure on the left.

What Do Structures Tell us About Naturally Arising Bce Module Mutations?

Experimental studies as well as sequencing of clinical isolates have revealed many mutations that provide insight into the mechanisms of Bce module function and the evolution of resistance to new AMPs (Table 4.1). Structural data both from both our cryo-EM structures of *B. subtilis* BceAB-S and AlphaFold models of complete Bce modules helps put these results into context. By mapping previously identified mutations onto Bce structures, we can identify mutational hotspots that increase resistance and gain insight into the effect of mutations on module function.

Mutations that enhance resistance have been identified in all four Bce module proteins. Bce transporter mutations that result in resistance to novel AMPs cluster within the transmembrane helices and frequently result in increased and/or constitutive activation of the Bce two-component system (Fig. 4.3) (18-24). These results are supported by mutagenesis studies that reveal that mutations within the transmembrane helices of *B. subtilis* BceB can alter signaling sensitivity and degree of resistance (25,26). As none of these mutations appear to be near the transporter-kinase interface, it is possible that mutations within the transmembrane helices may raise or lower barriers to the transporter conformational changes driving kinase signaling. Interestingly, some mutations truncate the transporter after the first half of the transmembrane helices and are especially common in the flexible linker between TM4 and TM5. These mutations remove the extracellular domain and/or lipid binding pocket so that the transporter is unable to bind to AMPs or their target lipids. Surprisingly given the total reliance of the better-characterized Bce kinases on their transporter for activation, truncating mutants in *L. lactis* and *S. pneumoniae* appear to increase resistance to some, but not all AMPs (23,27). In *L. lactis,* loss of the second half of the YsaBC transporter increases resistance to K411 and Ent7 and decreases bacitracin resistance, with increased expression of Bce-regulated genes (23). These results suggest a tradeoff between different resistance modes; for modules such as *L. lactis* YsaBC-KinG-LlrG that upregulate additional resistance factors, sacrificing Bce transporter ligand interaction may pay off through increased two-component system activation as long as the upregulated genes are able to manage AMP stress on their own.

In addition to mutations in Bce transporters, mutations also are found within the two-component systems. Function-altering mutations have been identified in all domains of Bce histidine kinases, but mutations that increase activity cluster around the DHp domains and around the ATP binding sites of the catalytic domains (28-34). Mutations within these dynamic

regions that are associated with increased resistance likely promote the kinase active state or alter autophosphorylation/phosphotransfer kinetics to increase signaling. In addition, many mutations associated with increased resistance are found in the response regulators of Bce modules, usually in the vicinity of conserved functional motifs such as those involved in interdomain signal transduction and DNA binding (35).

An important takeaway from clinical and experimentally derived Bce module mutations is that upon exposure to new AMPs, mutations tend to arise that increase two-component system activity, rather than alter Bce transporter specificity. Few mutations have been documented in Bce transporter extracellular domains. This suggests that Bce transporters are limited in their ability to accommodate new substrates and/or that Bce-mediated regulation of other resistance determinants, especially cell wall modification genes, may play a more significant role in Bce-mediated resistance in some species than the transporters themselves. It is clear from these mutational studies that inhibitors designed to block two-component system activity, rather than targeting the transporter itself, could hold immense promise as future clinical candidates.

Species	Module	Subunit	Protein	Mutation	Reference	Function
Bacillus subtilis	BceABRS	Permease	BceB	A75T	26	Altered sensitivity, low resistance
				R83W	26	Altered sensitivity, low resistance
				G215R	26	Decreased signaling and resistance
				S219F	26	No effect on signaling, low resistance
				S219C	26	Eliminates signaling, low resistance
				G247R	26	Eliminates signaling, low resistance
				A310T	26	Decreased signaling and resistance
				S316L	26	Decreased signaling and resistance
				G525D	26	Eliminates signaling, low resistance
				G535E	26	Altered sensitivity, low resistance
				S542L	26	Altered sensitivity, low resistance
				L567P	26	Altered sensitivity
				C544Y	26	Eliminates signaling, low resistance
				M551I	26	Decreased signaling and resistance
				G609R	26	Altered sensitivity, low resistance
				M616I	26	No effect on signaling, low resistance
				V619M	26	Decreased signaling and resistance
Enterococcus faecalis	SapABRS -RapAB	Kinase	SapS	A202E	36	Associated with increased daptomycin resistance
		NBD	SapA	D219A	36	Associated with increased daptomycin resistance
Enterococcus faecium	SapABRS -RapAB	NBD	SapA	H203Y	21	Associated with increased daptomycin resistance
				G173C	21	Associated with increased daptomycin resistance

Table 4.1: Bce module mutations that may affect function identified through mutational studies, exposure to AMPs or found in environmental or clinical isolates with varying resistance.

Table 4.1 (cont'd):

Enterococcus faecium	SapABRS-RapAB	NBD	SapA	A155D	20	Associated with increased daptomycin resistance
				D143N	20	Associated with increased daptomycin resistance
				S208R	20	Associated with increased daptomycin resistance
				G15S	20	Associated with increased daptomycin resistance
		Permease	SapB	G133V	21	Associated with increased daptomycin resistance
				T156I	21	Associated with increased daptomycin resistance
				S23I	21	Associated with increased daptomycin resistance
				I576N	21	Associated with increased daptomycin resistance
				A647P	20	Associated with increased daptomycin resistance
				W503S	20	Associated with increased daptomycin resistance
				G579S	20	Associated with increased daptomycin resistance
				S171L	20	Associated with increased daptomycin resistance
Lactococcus lactis	YsaBC-KinG-LlrG	Kinase	KinG	A108D	19	Associated with increased Lcn972 resistance
			KinG	A107V	19	Associated with increased Lcn972 resistance
			KinG	V104F	19	Associated with increased Lcn972 resistance
		NBD	YsaC	S208I	22	Associated with increased bacteriocin K411 and Ent8 resistance but decreased bacitracin resistance

Table 4.1 (cont'd):

Lactococcus lactis	YsaBC-YsaBC-KinG-LlrG	NBD	YsaC	S146L	19	Associated with increased Lcn972 resistance
		Permease	YsaB	P605T/F577S	18,19	Associated with nisin resistance, but sensitive to bacitracin
				F577V	19	Associated with increased Lcn972 resistance
				I594F	19	Associated with increased Lcn972 resistance
				E190*	22	Associated with increased K411 bacteriocin resistance
				E192*	22	Associated with increased K411 bacteriocin resistance
				W433F-fs26	22	Associated with increased K411 bacteriocin resistance
				Q566*	22	Associated with increased K411 bacteriocin resistance
				A647S-fs15, C653*	22	Associated with increased K411 bacteriocin resistance
				E516*	22	Associated with increased Ent7 bacteriocin resistance
				E566*	22	Associated with increased Ent7 bacteriocin resistance
				E185*	22	Associated with increased Ent7 bacteriocin resistance
				E582*	22	Associated with increased Ent7 bacteriocin resistance
		Response regulator	LlrG	L177I	22	Associated with increased bacteriocin K411 and Ent8 resistance but decreased bacitracin resistance in absence of Bce transporter
Listeria monocytogenes	VirABRS-AnrAB	Permease	VirB	W237*	34	Associated with decreased virulence and nisin resistance
				G120D	34	Associated with decreased virulence and nisin resistance

Table 4.1 (cont'd):

Listeria monocytogenes	VirABRS-AnrAB	Permease	VirB	T117I	34	Associated with decreased virulence and nisin resistance
		Response regulator	VirR	D54*	34	Associated with decreased virulence and nisin resistance
				L48I	34	Associated with decreased virulence and nisin resistance
Staphylococcus aureus	VraDE-BraDERS	Kinase	BraS	A208E	29,37	Increases nisin and insect defensin resistance
				N130K	38	Increases nisin resistance
				N63del	39	Associated with increased vancomycin resistance
				A105T	29	Increases nisin resistance
	VraFG-GraRSX	Kinase	GraS	D35K D37K D41K	40,41	Decreases daptomycin, polymyxin B and defensin resistance and virulence
				F38A/G	40	Decreased daptomycin and polymyxin B resistance, decreased induction in acidic conditions
				P39A/G	40	Decreased daptomycin and polymyxin B resistance
				F38A/P39A	40	Decreased induction by polymyxin B
				F38G/P39G	40	Decreased induction by polymyxin B
				V66I	42	Associated with vancomycin resistance
				D97E	42	Associated with vancomycin resistance
				K109R	42	Associated with vancomycin resistance
				N118K	42	Associated with vancomycin resistance
				S176T	42	Associated with vancomycin resistance
				H265R	42	Associated with vancomycin resistance
		Response regulator	GraR	N197S	32,42	Associated with development of vancomycin resistance
				D148Q	32,42	Associated with development of vancomycin resistance

Table 4.1 (cont'd):

Staphylococcus aureus	VraFG-GraRSX	NBD	VraF	S60-I64 duplication	24	Associated with pexiganan resistance
		Permease	VraG	A576V	24	Associated with melittin resistance
				S308R	24	Associated with melittin resistance
				K380A K388A	43,44	Altered signaling, weaker association of kinase and transporter
Staphylococcus epidermidis	VraFG-GraRSX	Kinase	GraS	D35A	1	Decreased polymyxin B resistance
				T136I	31,33,45	Associated with increased vancomycin resistance
				N289Y	46	Found in VISA strains, but not VSSA strains
				A153P	46	Found in VISA strains, but not VSSA strains
				M29R	46	Found in VISA strains, but not VSSA strains
				V301E	46	Found in VISA strains, but not VSSA strains
				V304E	46	Found in VISA strains, but not VSSA strains
				R14L	46	Found in VISA strains, but not VSSA strains
				S52N	47	Associated with daptomycin resistance
		NBD	VraF	G40A	1	Decreased resistance to polymyxin B but intermediate signaling
		Permease	VraG	432-441 --> Gx10	1	Decreased polymyxin B resistance but higher induction of signaling
				d432-441	1	Higher induction of signaling
		Response regulator	GraR	N197S	31,48	Associated with increased vancomycin resistance
				S79F	48	Associated with increased vancomycin resistance
				N148E	48	Associated with increased vancomycin resistance
				F151L	46	Found in VISA strains, but not VSSA strains
Streptococcus pneumoniae	BceAB-SirRH	Permease	BceB	Q582*	27	Increases resistance to vancoresmycin but decreases resistance to bacitracin

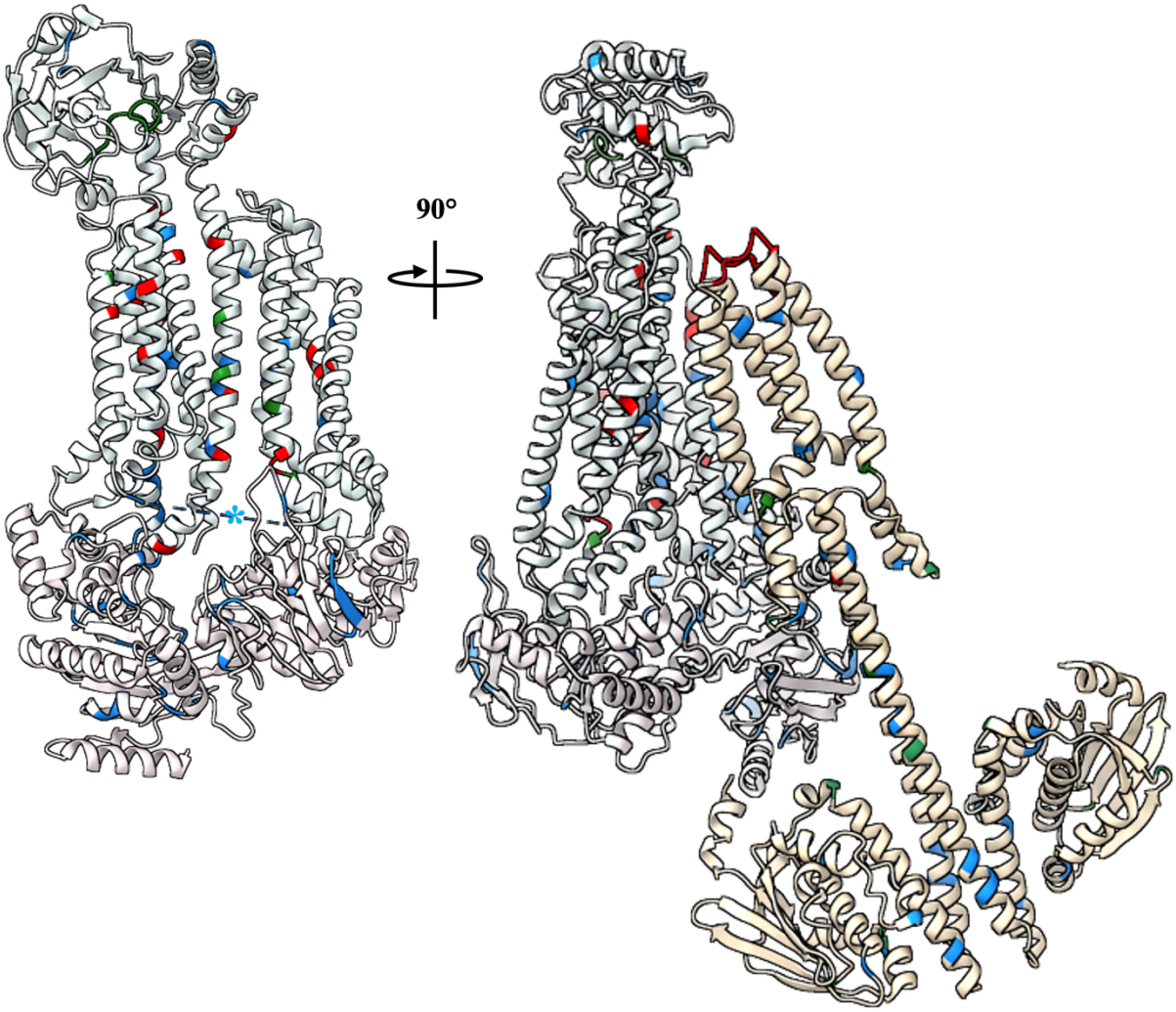

Figure 4.3: Mutations in Bce transporters and kinases. Mutations from Table 5 that are thought to increase Bce transporter/kinase function (blue), decrease function (red), or alter sensitivity or specificity (green) mapped onto the cryo-EM structure of *B. subtilis* BceABS (left: BceAB, right, BceABS). Equivalent residues in BceABS were identified by aligning AlphaFold models with the BceABS structure. The dashed line, highlighted by an asterisk (left) indicates the flexible linker in which truncations have been observed.

Future Work: Capturing Bce Modules In Action

While our published cryo-EM structures, as described in Chapters 2 and 3, provide valuable insight into conformational dynamics in Bce complexes, a critical component is missing to complete the picture of Bce module resistance and signaling. Bce modules are known to respond to structurally diverse peptides, and little is known about how specificity is maintained and how resistance is mediated to diverse peptides with multiple binding modes to UP, UPP, and lipid II. Sequence analysis of Bce modules known to have overlapping substrates is not sufficient for identifying specificity determinants as these sequences are not only highly divergent, but also likely represent a compromise between ideal binding sites for multiple peptides recognized by the same module. A solution to this conundrum may be to investigate structures of AMPs bound to Bce module transporters to identify key interactions and to make comparisons between the 3D configuration of the binding site in different transporters.

Acquisition of AMP-bound structures would be beneficial for understanding both AMP recognition and subsequent resistance and signaling-related conformational change. Initial work and plans in this area are described in detail in the Appendix. Currently there remain challenges with protein expression and lipid co-purification that must be overcome to enable structure determination. Future efforts should explore alternative strategies for expression of Bce proteins to ensure co-purification with lipids that are targeted by AMPs and to develop strategies for purifying both Bce transporter alone and Bce transporter in complex with its kinase with these lipids. This work will allow exploration of conformational change upon AMP binding in both forms of the Bce module membrane complex.

Mutational studies in *B. subtilis* would complement the *in vitro* biochemical assays and cryo-EM structures to further explore the effects of specific residues on BceABRS-mediated signaling and resistance. *B. subtilis* expressing Bce module variants can be tested for ability to signal and resist AMPs, following up on earlier studies which used *luxABCDE* under control of P_{bceA} as a transcriptional reporter to explore the substrate range of Bce modules in *B. subtilis* (49). Since the degree of signaling and degree of resistance are not perfectly linked from substrate to substrate, it will be critical to test both signaling with the *lux* reporter and resistance to each AMP tested and with each Bce module variant. Likely hotspots for peptide recognition are the highly variable, flexible loops in the extracellular domain just above the lipid binding pocket (Fig. 4.1A). In addition to comparing the effects of mutations in this region on response

to different AMPs (*B. subtilis* BceABRS responds to bacitracin, actagardine, mersacidin, and laspartomycin C to varying degrees), similar experiments could be conducted with the *B. subtilis* PsdABRS module. Both BceABRS and PsdABRS induce signaling with actagardine, but differ in their other substrates, and have no obvious shared motifs in the suspected AMP binding region (49).

The results from these studies may shed light on how signaling through Bce modules can be initiated without subsequent AMP resistance. These results may also be useful for predicting innate resistance to AMPs in Bce-expressing species as well as for the design of new therapeutics that can evade Bce module recognition.

Future Work: Exploring Signal Transduction with Bce Kinases

Bce modules also provide a unique opportunity to probe histidine kinase conformational dynamics. Due to dynamic nature of histidine kinases, most structural work to date on this protein family has involved breaking kinases into separate domains and solving structures of subsections of the proteins in isolation. However, while resolution is still limited by protein flexibility, we were able to capture the full length BceS kinase in multiple conformations in our cryo-EM structures. While intramembrane histidine kinases like Bce kinases are relatively rare, the Bce system may still be a useful model for exploring signal transduction and conformational dynamics in histidine kinases more broadly. Not only can the BceS kinase be visualized in full, but BceABS is relatively straightforward to express and has well-characterized activity in *B. subtilis,* providing multiple avenues for future research.

Our cryo-EM structures capture the proteins in absence of antimicrobial peptides, which previously published work shows are required for BceS activation (12,49,50). As expected from these earlier experiments, none of our cryo-EM data for the BceABS complex appear to show the kinase in an active state, suggesting that bacitracin binding to BceAB induces an alternative conformational state not observed in our ATP-free or ATP-bound structures that drives activation of BceS. Future work could try to capture the kinase in a phosphorylation active state, either by activating the kinase through binding AMPs to the paired transporter, or by locking the kinase in an active state through mutation. Prior publications identified an E115K K116E mutation that makes BceS constitutively active even in the absence of antimicrobial peptides, likely by stabilizing rotation in the DHp domain that bring the catalytic domains in line with the phosphorylatable histidine (Fig. 4.4A,B) (25). Initial attempts to purify BceABS E115K K116E were challenged by a higher degree of aggregation and heterogeneity than the wildtype protein, making structure determination from these samples more challenging (Fig. 4.4C-E). While this mutant may be useful for capturing an active kinase state, producing a high quality sample for cryo-EM may require modification of expression protocol and careful sample preparation. In addition, this method for capturing the active kinase disregards conformational changes above the DHp domain that initiate signaling. If an expression system to produce protein capable of binding AMPs can be developed (as described in the Appendix), a better approach to capturing active Bce kinase conformations may be to use protein bound to AMPs. This protein may stabilized in specific conformations for structural studies by either the use of nonhydrolyzable

ATP analogs or AMPs such as laspartomycin C that induce signaling but not resistance, which may induce conformational changes to activate BceS but not be removed from their target lipids by BceAB (51).

Earlier work proposed that BceS is activated through a piston-like movement of the second transmembrane helix (25). Our cryo-EM structures also reveal that only a single monomer of the BceS kinase is in contact with BceAB. With such limited contact, how are conformational changes between the transporter and kinase linked, and how is signal propagated down the kinase? In our cryo-EM structures we observed multiple layers of interaction between the kinase transmembrane helices (Fig. 3.7). These networks of interacting residues likely help transmit conformational changes down the protein and between the monomers, especially since only one monomer appears to interact directly with BceAB. Combining structures of BceS in different activation states with functional assays on cells expressing BceS with mutations in these interaction layers may provide insight into the fine-scale changes underlying signal transduction.

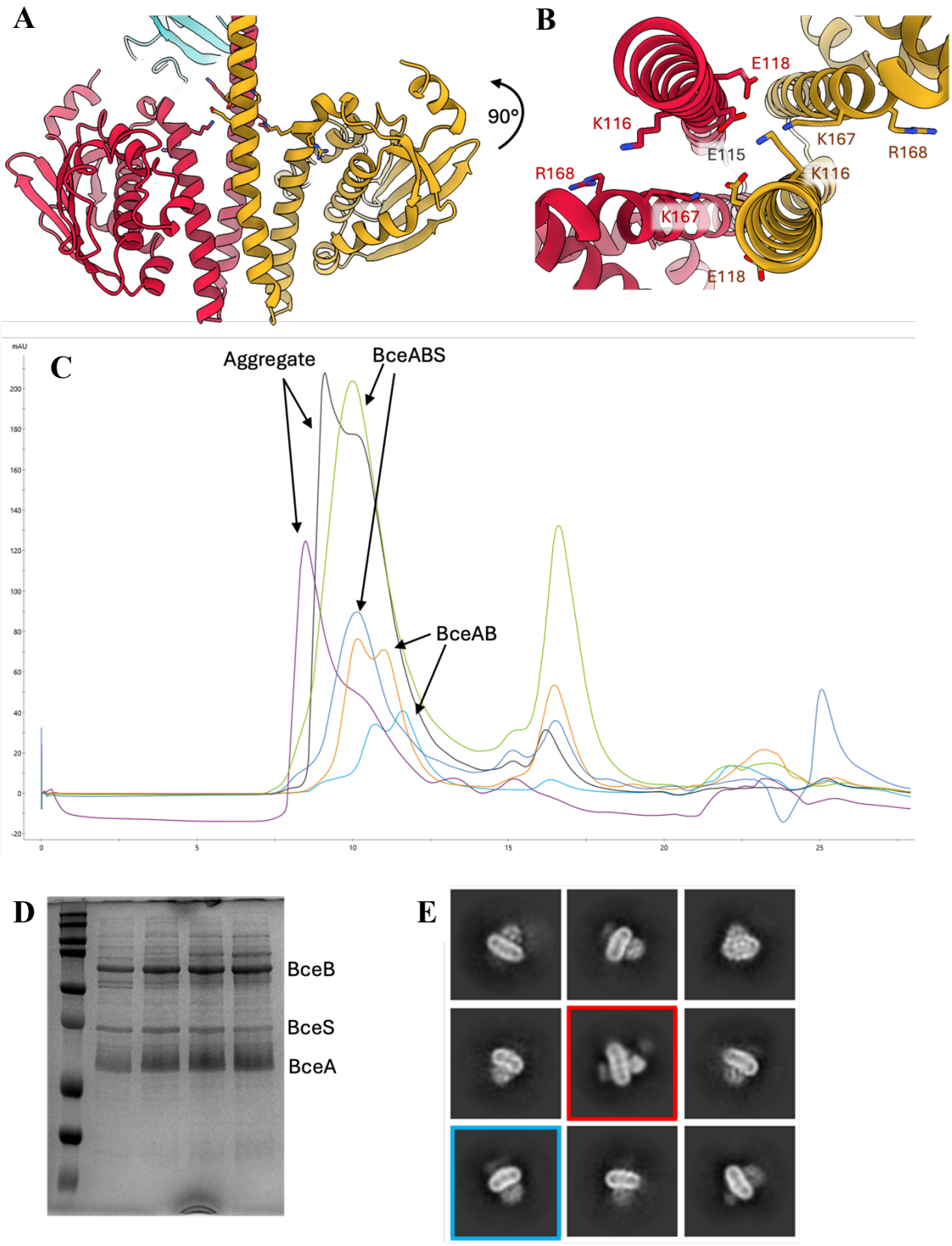

Figure 4.4: BceABS E115K K116E. Side (A) and top-down (B) views of the BceS DHp domain showing the charged residue network involved in kinase activation. The quality of BceABS E115K K116E expressed and purified in *E. coli* is more variable than wildtype BceABS, as seen in this overlay of gel filtration chromatograms (C) in which there is prep-to-prep variation in

Figure 4.4 (cont'd)

quantity of BceABS E115K K116E, BceAB without kinase, and aggregated protein. Purified BceABS E115K on SDS-PAGE appears to have a less than one-to-one ratio of BceB to BceS (D). Cryo-EM 2D averages of BceABS E115K K116E reveal heterogenous sample of both BceABS (red) and smaller micelles without obvious kinase that are likely BceAB alone (blue).

What Questions Remain?

Beyond the research areas described in the previous sections that directly follow from these studies, many other questions remain about Bce modules that may require multidisciplinary approaches to answer. A few of these potential research areas are described below:

- **How is resistance mediated by Bce transporters?** Current models of Bce transporter-mediated resistance suggest that transporters remove AMPs from their target lipids, but since Bce modules respond to a wide range of compounds, how can a single resistance mechanism accommodate AMPs of different structures and different lipid binding modes? In addition, some AMPs can induce Bce signaling but not resistance, suggesting that they can bind to Bce transporters and induce the conformational changes necessary to activate the associated kinases, but are incompatible with the AMP removal mechanism of free BceAB transporters (51). Further work needs to be done to reveal how transporters facilitate AMP removal, and for modules that regulate additional genes, to determine the relative contribution of Bce transporters themselves versus downstream regulated genes to resistance to various AMP classes.
- **What are the roles of Bce modules in bacterial communities?** Bce modules are found in diverse bacteria found in a wide variety of environments and are not restricted to pathogenic species. Little work has been done to understand what benefits Bce modules provide to bacteria outside of host-pathogen relationships. Bce modules have been linked to community behaviors such as biofilm formation and cannibalism, but this work has not yet expanded to explore interspecies interactions between AMP-producers and Bce-expressers as might occur in complex microbial communities (14,52-59). This question also intersects with broader exploration of the purpose of antibiotics in environmental settings, whether as weaponry in microbial warfare or as communication tools for coordinating community behavior (60,61). Do Bce modules protect against interspecies competition, or do they help bacteria sense their neighbors and alter their behavior to better coexist? Or both?
- **How can we use our knowledge of Bce modules to address antimicrobial resistance?** Bce modules provide a baseline level of resistance to a variety of compounds including clinically and industrially relevant AMPs and those produced by host immune systems. They also contribute to the development of resistance and coordinate virulence in

pathogens of high concern, making these complexes attractive targets for treating infections. Work is already being done to develop modified AMPs that can bypass resistance, combination therapies that target Bce modules, or inhibitors of Bce module function (62-70). Increased understanding of Bce module function and evolution will aid in these efforts to develop new treatments to highly resistant species.

Bce modules were initially identified as antimicrobial resistance systems, but we have since discovered that they play important roles in environmental stress tolerance, virulence, and multicellular behaviors. By integrating interdisciplinary approaches and sharing insights across species boundaries, we will gain new insights into these multifunctional but incompletely understood systems and find new applications in the fight against antibiotic resistance.

REFERENCES

1. Costa, S. K., Cho, J. & Cheung, A. L. GraS Sensory Activity in Staphylococcus epidermidis Is Modulated by the "Guard Loop" of VraG and the ATPase Activity of VraF. *J Bacteriol* **203**, e00178-21 (2021).

2. George, N. L., Schilmiller, A. L. & Orlando, B. J. Conformational snapshots of the bacitracin sensing and resistance transporter BceAB. *Proc National Acad Sci* **119**, e2123268119 (2022).

3. Crow, A., Greene, N. P., Kaplan, E. & Koronakis, V. Structure and mechanotransmission mechanism of the MacB ABC transporter superfamily. *Proc National Acad Sci* **114**, 12572–12577 (2017).

4. Hao, A., Suo, Y. & Lee, S.-Y. Structural insights into the FtsEX-EnvC complex regulation on septal peptidoglycan hydrolysis in Vibrio cholerae. *Structure* **32**, 188-199.e5 (2024).

5. Xu, X. *et al.* Mechanistic insights into the regulation of cell wall hydrolysis by FtsEX and EnvC at the bacterial division site. *Proc. Natl. Acad. Sci. United States Am.* **120**, e2301897120 (2023).

6. Cho, J., Manna, A. C., Snelling, H. S. & Cheung, A. L. GraS signaling in Staphylococcus aureus is regulated by a single D35 residue in the extracellular loop. *Microbiol. Spectr.* e01982-23 (2023) doi:10.1128/spectrum.01982-23.

7. George, N. L. & Orlando, B. J. Architecture of a complete Bce-type antimicrobial peptide resistance module. *Nat. Commun.* **14**, 3896 (2023).

8. Ohki, R. *et al.* A Bacitracin-Resistant Bacillus subtilis Gene Encodes a Homologue of the Membrane-Spanning Subunit of the Bacillus licheniformis ABC Transporter. *J. Bacteriol.* **185**, 51–59 (2003).

9. Ma, J. *et al.* Bacitracin resistance and enhanced virulence of Streptococcus suis via a novel efflux pump. *Bmc Vet Res* **15**, 377 (2019).

10. Kawada-Matsuo, M. *et al.* Three Distinct Two-Component Systems Are Involved in Resistance to the Class I Bacteriocins, Nukacin ISK-1 and Nisin A, in Staphylococcus aureus. *Plos One* **8**, e69455 (2013).

11. Pietiäinen, M. *et al.* Cationic antimicrobial peptides elicit a complex stress response in Bacillus subtilis that involves ECF-type sigma factors and two-component signal transduction systems. *Microbiology* **151**, 1577–1592 (2005).

12. Fritz, G. *et al.* A New Way of Sensing: Need-Based Activation of Antibiotic Resistance by a Flux-Sensing Mechanism. *Mbio* **6**, e00975-15 (2015).

13. Ouyang, J., Tian, X.-L., Versey, J., Wishart, A. & Li, Y.-H. The BceABRS Four-Component System Regulates the Bacitracin-Induced Cell Envelope Stress Response in Streptococcus mutans. *Antimicrob Agents Ch* **54**, 3895–3906 (2010).

14. Kolar, S. L. *et al.* NsaRS is a cell-envelope-stress-sensing two-component system of Staphylococcus aureus. *Microbiology* **157**, 2206–2219 (2011).

15. Gebhard, S. *et al.* Identification and Characterization of a Bacitracin Resistance Network in Enterococcus faecalis. *Antimicrob Agents Ch* **58**, 1425–1433 (2014).

16. Thevenard, B. *et al.* Response of S. thermophilus LMD-9 to bacitracin: Involvement of a BceRS/AB-like module and of the rhamnose–glucose polysaccharide synthesis pathway. *Int. J. Food Microbiol.* **177**, 89–97 (2014).

17. Camejo, A. *et al.* In Vivo Transcriptional Profiling of Listeria monocytogenes and Mutagenesis Identify New Virulence Factors Involved in Infection. *PLoS Pathog.* **5**, e1000449 (2009).

18. Campelo, A. B. *et al.* Mutations Selected After Exposure to Bacteriocin Lcn972 Activate a Bce-Like Bacitracin Resistance Module in Lactococcus lactis. *Front Microbiol* **11**, 1805 (2020).

19. López-González, M. J. *et al.* Adaptive Evolution of Industrial Lactococcus lactis Under Cell Envelope Stress Provides Phenotypic Diversity. *Front Microbiol* **9**, 2654 (2018).

20. Prater, A. G. *et al.* Daptomycin Resistance in Enterococcus faecium Can Be Delayed by Disruption of the LiaFSR Stress Response Pathway. *Antimicrob. Agents Chemother.* **65**, (2021).

21. Prater, A. G. *et al.* Environment Shapes the Accessible Daptomycin Resistance Mechanisms in Enterococcus faecium. *Antimicrob. Agents Chemother.* **63**, (2019).

22. Tymoszewska, A. & Aleksandrzak-Piekarczyk, T. The Lactococcal dgkB (yecE) and dxsA Genes for Lipid Metabolism Are Involved in the Resistance to Cell Envelope-Acting Antimicrobials. *Int J Mol Sci* **22**, 1014 (2021).

23. Tymoszewska, A. *et al.* Lactococcus lactis Resistance to Aureocin A53- and Enterocin L50-Like Bacteriocins and Membrane-Targeting Peptide Antibiotics Relies on the YsaCB-KinG-LlrG Four-Component System. *Antimicrob Agents Ch* **65**, e00921-21 (2021).

24. Shazely, B. E., Yu, G., Johnston, P. R. & Rolff, J. Resistance Evolution Against Antimicrobial Peptides in Staphylococcus aureus Alters Pharmacodynamics Beyond the MIC. *Front. Microbiol.* **11**, 103 (2020).

25. Koh, A., Gibbon, M. J., Kamp, M. W. V. der, Pudney, C. R. & Gebhard, S. Conformation control of the histidine kinase BceS of Bacillus subtilis by its cognate ABC-transporter facilitates need-based activation of antibiotic resistance. *Mol Microbiol* **115**, 157–174 (2021).

26. Kallenberg, F., Dintner, S., Schmitz, R. & Gebhard, S. Identification of Regions Important for Resistance and Signalling within the Antimicrobial Peptide Transporter BceAB of Bacillus subtilis. *J Bacteriol* **195**, 3287–3297 (2013).

27. Becker, P., Hakenbeck, R. & Henrich, B. An ABC Transporter of Streptococcus pneumoniae Involved in Susceptibility to Vancoresmycin and Bacitracin. *Antimicrob Agents Ch* **53**, 2034–2041 (2009).

28. Randall, C. P. *et al.* Acquired Nisin Resistance in Staphylococcus aureus Involves Constitutive Activation of an Intrinsic Peptide Antibiotic Detoxification Module. *Msphere* **3**, e00633-18 (2018).

29. Blake, K. L., Randall, C. P. & O'Neill, A. J. In Vitro Studies Indicate a High Resistance Potential for the Lantibiotic Nisin in Staphylococcus aureus and Define a Genetic Basis for Nisin Resistance. *Antimicrob Agents Ch* **55**, 2362–2368 (2011).

30. Cui, L., Neoh, H., Shoji, M. & Hiramatsu, K. Contribution of vraSR and graSR point mutations to vancomycin resistance in vancomycin-intermediate Staphylococcus aureus. *Antimicrob Agents Ch* **53**, 1231–4 (2009).

31. Hafer, C., Lin, Y., Kornblum, J., Lowy, F. D. & Uhlemann, A.-C. Contribution of Selected Gene Mutations to Resistance in Clinical Isolates of Vancomycin-Intermediate Staphylococcus aureus. *Antimicrob. Agents Chemother.* **56**, 5845–5851 (2012).

32. Doddangoudar, V. C., Boost, M. V., Tsang, D. N. C. & O'Donoghue, M. M. Tracking changes in the vraSR and graSR two component regulatory systems during the development and loss of vancomycin non-susceptibility in a clinical isolate. *Clin Microbiol Infec* **17**, 1268–1272 (2011).

33. Howden, B. P. *et al.* Genomic Analysis Reveals a Point Mutation in the Two-Component Sensor Gene graS That Leads to Intermediate Vancomycin Resistance in Clinical Staphylococcus aureus. *Antimicrob. Agents Chemother.* **52**, 3755–3762 (2008).

34. Wambui, J. *et al.* The Analysis of Field Strains Isolated From Food, Animal and Clinical Sources Uncovers Natural Mutations in Listeria monocytogenes Nisin Resistance Genes. *Front. Microbiol.* **11**, 549531 (2020).

35. Khosa, S., Hoeppner, A., Gohlke, H., Schmitt, L. & Smits, S. H. J. Structure of the Response Regulator NsrR from Streptococcus agalactiae, Which Is Involved in Lantibiotic Resistance. *PLoS ONE* **11**, e0149903 (2016).

36. Miller, W. R. *et al.* LiaR-independent pathways to daptomycin resistance in Enterococcus faecalis reveal a multilayer defense against cell envelope antibiotics. *Mol. Microbiol.* **111**, 811–824 (2019).

37. Makarova, O. *et al.* Genomics of experimental adaptation of Staphylococcus aureus to a natural combination of insect antimicrobial peptides. *Sci. Rep.* **8**, 15359 (2018).

38. Arii, K., Kawada-Matsuo, M., Oogai, Y., Noguchi, K. & Komatsuzawa, H. Single mutations in BraRS confer high resistance against nisin A in Staphylococcus aureus. *MicrobiologyOpen* **8**, e791 (2019).

39. Gregorio, S. D., Haim, M. S., Famiglietti, Á. M. R., Conza, J. D. & Mollerach, M. Comparative Genomics Identifies Novel Genetic Changes Associated with Oxacillin, Vancomycin and Daptomycin Susceptibility in ST100 Methicillin-Resistant Staphylococcus aureus. *Antibiotics* **12**, 372 (2023).

40. Cheung, A. L. *et al.* Role of the Staphylococcus aureus Extracellular Loop of GraS in Resistance to Distinct Human Defense Peptides in PMN and Invasive Cardiovascular infections. *Infect Immun* **89**, e00347-21 (2021).

41. Cheung, A. L. *et al.* Site-Specific Mutation of the Sensor Kinase GraS in Staphylococcus aureus Alters the Adaptive Response to Distinct Cationic Antimicrobial Peptides. *Infect Immun* **82**, 5336–5345 (2014).

42. Kang, Y. R. *et al.* Genetic alterations in methicillin-susceptible Staphylococcus aureus associated with high vancomycin minimum inhibitory concentration. *Int. J. Antimicrob. Agents* **62**, 106971 (2023).

43. Cho, J., Rigby, W. F. C. & Cheung, A. L. The thematic role of extracellular loop of VraG in activation of the membrane sensor GraS in a cystic fibrosis MRSA strain differs in nuance from the CA-MRSA strain JE2. *Plos One* **17**, e0270393 (2022).

44. Cho, J., Costa, S. K., Wierzbicki, R. M., Rigby, W. F. C. & Cheung, A. L. The extracellular loop of the membrane permease VraG interacts with GraS to sense cationic antimicrobial peptides in Staphylococcus aureus. *Plos Pathog* **17**, e1009338 (2021).

45. Hu, Q., Peng, H. & Rao, X. Molecular Events for Promotion of Vancomycin Resistance in Vancomycin Intermediate Staphylococcus aureus. *Front. Microbiol.* **7**, 1601 (2016).

46. Yoo, J. I. *et al.* Prevalence of amino acid changes in the yvqF, vraSR, graSR, and tcaRAB genes from vancomycin intermediate resistant Staphylococcus aureus. *J. Microbiol.* **51**, 160–165 (2013).

47. Li, S. *et al.* Fitness Cost of Daptomycin-Resistant Staphylococcus aureus Obtained from in Vitro Daptomycin Selection Pressure. *Front. Microbiol.* **8**, 2199 (2017).

48. Neoh, H. *et al.* Mutated Response Regulator graR Is Responsible for Phenotypic Conversion of Staphylococcus aureus from Heterogeneous Vancomycin-Intermediate Resistance to Vancomycin-Intermediate Resistance. *Antimicrob. Agents Chemother.* **52**, 45–53 (2008).

49. Staroń, A., Finkeisen, D. E. & Mascher, T. Peptide Antibiotic Sensing and Detoxification Modules of Bacillus subtilis. *Antimicrob Agents Ch* **55**, 515–525 (2011).

50. Rietkötter, E., Hoyer, D. & Mascher, T. Bacitracin sensing in Bacillus subtilis. *Mol Microbiol* **68**, 768–85 (2008).

51. Diehl, A., Wood, T. M., Gebhard, S., Martin, N. I. & Fritz, G. The Cell Envelope Stress Response of Bacillus subtilis towards Laspartomycin C. *Antibiotics* **9**, 729 (2020).

52. Boles, B. R., Thoendel, M., Roth, A. J. & Horswill, A. R. Identification of Genes Involved in Polysaccharide-Independent Staphylococcus aureus Biofilm Formation. *Plos One* **5**, e10146 (2010).

53. Shanks, R. M. Q. *et al.* Genetic Evidence for an Alternative Citrate-Dependent Biofilm Formation Pathway in Staphylococcus aureus That Is Dependent on Fibronectin Binding Proteins and the GraRS Two-Component Regulatory System. *Infect Immun* **76**, 2469–2477 (2008).

54. Tian, X.-L., Salim, H., Dong, G., Parcells, M. & Li, Y.-H. The BceABRS four-component system that is essential for cell envelope stress response is involved in sensing and response to host defence peptides and is required for the biofilm formation and fitness of Streptococcus mutans. *J Med Microbiol* **67**, 874–883 (2018).

55. Nagasawa, R., Sato, T., Nomura, N., Nakamura, T. & Senpuku, H. Potential Risk of Spreading Resistance Genes within Extracellular-DNA-Dependent Biofilms of Streptococcus mutans in Response to Cell Envelope Stress Induced by Sub-MICs of Bacitracin. *Appl. Environ. Microbiol.* **86**, (2020).

56. Yang, Y. *et al.* Role of Two-Component System Response Regulator bceR in the Antimicrobial Resistance, Virulence, Biofilm Formation, and Stress Response of Group B Streptococcus. *Front Microbiol* **10**, 10 (2019).

57. Jiang, X. *et al.* Role of the VirSR-VirAB system in biofilm formation of Listeria monocytogenes EGD-e. *Food Res. Int.* **145**, 110394 (2021).

58. Zhu, X. *et al.* A Putative ABC Transporter Is Involved in Negative Regulation of Biofilm Formation by Listeria monocytogenes. *Appl. Environ. Microbiol.* **74**, 7675–7683 (2008).

59. Höfler, C. *et al.* Cannibalism stress response in Bacillus subtilis. *Microbiology* **162**, 164–176 (2016).

60. Granato, E. T., Meiller-Legrand, T. A. & Foster, K. R. The Evolution and Ecology of Bacterial Warfare. *Curr Biol* **29**, R521–R537 (2019).

61. Spagnolo, F., Trujillo, M. & Dennehy, J. J. Why Do Antibiotics Exist? *Mbio* **12**, e01966-21 (2021).

62. Pérez-Ibarreche, M., Field, D., Ross, R. P. & Hill, C. A Bioengineered Nisin Derivative To Control Streptococcus uberis Biofilms. *Appl. Environ. Microbiol.* **87**, e00391-21 (2021).

63. Hayes, K., Field, D., Hill, C., O'Halloran, F. & Cotter, L. A novel bioengineered derivative of nisin displays enhanced antimicrobial activity against clinical Streptococcus agalactiae isolates. *J. Glob. Antimicrob. Resist.* **19**, 14–21 (2019).

64. Desmond, A., O'Halloran, F., Cotter, L., Hill, C. & Field, D. Bioengineered Nisin A Derivatives Display Enhanced Activity against Clinical Neonatal Pathogens. *Antibiotics* **11**, 1516 (2022).

65. Zaschke-Kriesche, J. *et al.* Bypassing lantibiotic resistance by an effective nisin derivative. *Bioorgan Med Chem* **27**, 3454–3462 (2019).

66. Porta, N. *et al.* Small-molecule inhibitors of nisin resistance protein NSR from the human pathogen Streptococcus agalactiae. *Bioorg. Med. Chem.* **27**, 115079 (2019).

67. El-Halfawy, O. M. *et al.* Discovery of an antivirulence compound that reverses β-lactam resistance in MRSA. *Nat Chem Biol* **16**, 143–149 (2020).

68. Watson, D. W., Iglesias, S. L., Vasarhelyi, E. M. & Heinrichs, D. E. GraXRS-Dependent Resistance of Staphylococcus aureus to Human Osteoarthritic Synovial Fluid. *mSphere* **6**, e00143-21 (2021).

69. Saputo, S., Faustoferri, R. C. & Quivey, R. G. Vitamin D Compounds Are Bactericidal against Streptococcus mutans and Target the Bacitracin-Associated Efflux System. *Antimicrob. Agents Chemother.* **62**, (2018).

70. Prieto, J. M. *et al.* Inhibiting the two-component system GraXRS with verteporfin to combat Staphylococcus aureus infections. *Sci. Rep.* **10**, 17939 (2020).

APPENDIX

Introduction

While our published cryo-EM structures described in Chapters 2 and 3 provide valuable insight into conformational dynamics in Bce complexes, a critical component is missing to complete the picture of Bce module resistance and signaling. The BceAB transporter appears to undergo different conformational changes during ATP binding and hydrolysis alone or in complex with the BceS kinase. As both complexes can exist simultaneously in the cell, we proposed that the differences in their conformational pathways reflects their distinct roles in the cell, either prioritizing signaling (BceABS) or resistance (BceAB). However, our cryo-EM structures capture the proteins in absence of antimicrobial peptides, limiting our view of the actual mechanism of AMP removal and initiation of signaling through BceS. In addition, how Bce modules distinguish between target and non-target AMPs is still poorly understood.

To address these related goals of understanding AMP binding and subsequent resistance and signaling-related conformational change, I sought to acquire a cryo-EM structure of bacitracin-bound BceAB. While these experiments were ultimately not successful, they do provide useful insights into Bce module-lipid interactions and the utility of a *B. subtilis* protein expression and purification workflow.

Cloning a Bacillus-Based Expression System

To create *B. subtilis* strains with his-tagged BceAB, Bce deletion strains were first constructed by inserting ~500 base pair genomic overlaps on either side of the kanamycin resistance gene in pUC19 (gene synthesis and cloning by Genscript). In one plasmid, overlaps extended ~500 bases to either side of *bceAB* (Δ*bceAB*), while in the other plasmid overlaps excluded *bceRS* as well as *bceAB* (Δ*bceABRS*). These plasmids were transformed into *B. subtilis* 168 by natural competence. To do this, an overnight culture of *B. subtilis* was diluted into minimal growth medium (per liter: 2g $(NH_4)_2SO_4$, 14.8g K_2HPO_4, 5.4g KH_2PO_4, 1.9g $Na_3C_6H_5O_7$, 0.2g $MgSO_4 \cdot 7H_2O$, 0.5% glycerol, 0.02% casamino acids, 1mg tryptophan) in a 100mL flask and grown for three hours at 37°C. with shaking at 200rpm. Then, cells were diluted with starvation medium (growth medium without casamino acids) and grown for an additional two hours with increased agitation (300rpm) to induce competence. 50uL of these cells were mixed with 500ng plasmid DNA before incubating for 30 min at 200rpm. After adding 500ul LB, the cells were allowed to recover and grow for two hours and then plated onto 10mg/ml kanamycin for selection. Selected colonies were tested for growth in a range of bacitracin concentrations alongside WT cells to confirm that the Bce genes were deleted. Successful transformants were frozen as glycerol stocks for later use.

To have choices for protein expression and purification, both IPTG-inducible and P_{bceA}-inducible expression strains were developed. In either case, Bce genes, with a 6xHis tag added to BceA, were cloned into the plasmid pBS1E with either the native promoter or with the IPTG-inducible $P_{hyspank}$ promoter. The pBS1E plasmid contains overlaps to *amyE* in the *B. subtilis* genome, allowing for recombination into a commonly-used *B. subtilis* genomic integration site (1). Three plasmids were created to allow expression of IPTG-induced BceAB alone, BceABRS under native promoters, or BceAB under its native promoter without BceABRS. These plasmids were transformed into *B. subtilis bceAB::*kan or *bceABRS::*kan and transformants selected for with 1ug/ml erythromycin and 25ug/ml lincomycin erythromycin combined with lincomycin. To confirm these results, successful colonies were spotted onto LB/starch plates and grown overnight at 37°C. Plates were then stained with iodine to look for starch consumption. Colonies that grew in the presence of antibiotics but did not show starch hydrolysis were frozen as glycerol stocks to use for expression.

Purifying BceAB from B. subtilis

To express BceAB under its native promoter, *B. subtilis bceAB:*kan *amyE::his-bceAB* were grown in LB to OD ~0.6 and induced with 40ug/ml bacitracin. This concentration of bacitracin has been shown to induce near-maximum expression of BceAB but does not impair growth (2). Cells were grown at 37°C for four hours. Protein purification followed the same protocol as described previously for *E. coli* BceAB expression, with two minor changes: first, the concentration of protease inhibitors in the lysis buffer was doubled (*B. subtilis* 168 expresses several secreted proteases), and second, the cells were incubated with lysozyme for one hour at room temperature prior to sonication to break down the cell walls.

Eight liters of *B. subtilis* yielded about a quarter as much BceAB protein as standard *E. coli* expression. To have enough for experimental purposes, the volume of cells used in subsequent expressions was increased, up to 32L per purification. All cell pellets were combined during resuspension and processed together. Protein from *B. subtilis* expressed under the native promoter was of high purity and homogeneity (Fig. 5.1A). Interestingly, BceA is expressed in excess in *B. subtilis* similarly to expression in *E. coli*. In addition, very little BceAB-S complex was produced, as would be expected under a regulatory system where BceS levels do not increase even under AMP stress. This observation supports our model in which the BceABS complex and BceAB complex exist side-by-side and play separate roles in the cell. A similar process was followed for IPTG-induced BceAB. Initial expressions used 0.7mM IPTG for induction as used in *E. coli* expression. The yield from these expressions was about half that of the P_{bceA}-induced expressions, and protein was much less homogenous, with an increased aggregate peak on gel filtration (Fig. 5.1B).

To confirm that the purified protein was properly folded and functional, the ATPase activity of the bacitracin-induced *B. subtilis* protein was tested. The *B. subtilis* protein showed comparable ATPase activity to that seen from *E. coli*-purified protein (Fig. 5.1C). Upon addition of bacitracin, however, no change in ATPase activity was observed (Fig. 5.1D). This assay was conducted without zinc, which is required for maximal bacitracin activity, because we previously observed that zinc inhibits BceAB ATPase activity. Bacitracin can, however use magnesium, which is present in the ATPase buffer, instead of zinc with lower activity (3). These results suggested that bacitracin is unable to bind to *B. subtilis* BceAB protein, potentially because of a lack of compatible lipid.

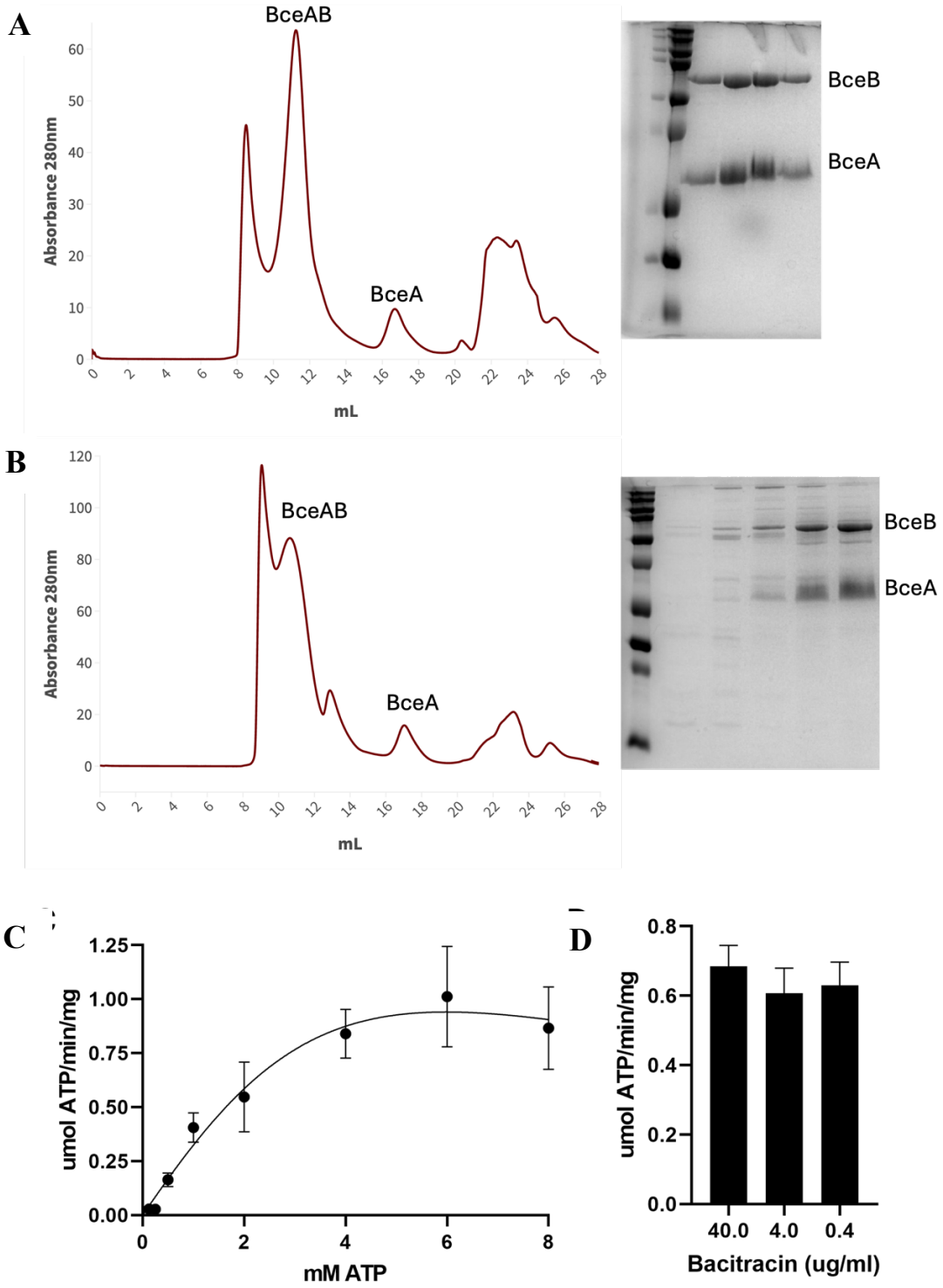

Figure 5.1: Purification of BceAB from *B. subtilis*. Gel filtration profile and SDS-PAGE gel of purified BceAB induced with bacitracin (A). Gel filtration profile and SDS-PAGE gel of purified BceAB induced with IPTG (B). BceAB from *B. subtilis* is active in *in vitro* ATPase assays (C). BceAB from *B. subtilis* shows no significant change in activity upon addition of bacitracin (D).

BceAB Purified from Bacillus Does Not Contain UPP

Co-purifying lipids were identified in BceAB from both bacitracin-induced and IPTG-induced expressions with the help of Tony Schilmiller at the RTSF Mass Spectrometry and Metabolomics Core through similar methods as described in Chapter 2. The bacitracin-induced protein was determined to contain undecaprenyl lipids, as expected for expression under native conditions. Unexpectedly, however, the undecaprenyl lipids observed were undecaprenol and undecaprenyl monophosphate, not the undecaprenyl pyrophosphate to which bacitracin binds. IPTG-induced protein, on the other hand, did not appear to contain undecaprenyl lipids. It is unclear if this difference is due to the induction method, or due to protein quality, as the IPTG-induced sample was less homogenous than the bacitracin-induced sample and produced in smaller amounts. It is possible that the amount of well-folded, lipid-containing BceAB was much lower for this expression than for the bacitracin induction expression. If the amount of lipid-containing protein was lower than estimated, this may have challenged lipid identification. Each sample was only tested once; testing another purification from a larger volume of cells, ideally after optimizing expression conditions is needed to confirm and clarify these results.

Conclusions and Future Work

These initial forays into expressing Bce proteins for use in structural studies failed to produce a structure but did produce useful insights into protein expression in *B. subtilis* and identified future avenues to explore the role of undecaprenyl lipids in Bce mechanisms.

The first takeaway from this project is that Bce proteins are expressed under native conditions at high enough levels to be used for biochemical characterization. Protein expressed under the native Bce promoter was similarly pure and homogenous as the *E. coli* protein. These results are important because our experience with *E. coli* protein containing an arabinose-modified lipid that cannot be bound by bacitracin indicates that expression in a native membrane environment may be critical for in vitro characterization of AMP binding and Bce module function in the presence of AMPs. The ability to purify Bce modules from the native source in useable quantities even with minimal optimization opens possibilities for conducting these experiments. While the volume of cells needed per expression is much higher compared to working in *E. coli* (24-30L vs 8-16L), further optimization of induction and expression conditions may reduce the disparity between systems. In addition, *B. subtilis* could be used to express Bce module proteins from other species to allow *in vitro* characterization of Bce modules expressed in an easy-to-work with bacterial system. *B. subtilis* is already being used to explore the function of other heterologously-expressed cell wall stress components (4).

In addition, the Bce promoter may be useful for expression of non-Bce proteins in *B. subtilis.* This promoter is highly sensitive to bacitracin concentrations across multiple orders of magnitude and allows for high-level production of proteins (2). Similar systems, LIKE, SURE, and NICE, have been developed using the bacitracin-inducible *liaI,* nisin-inducible *nisA*, and subtilin-inducible *spaS* promoters for protein expression (5-7). In some cases, these AMP-induced expression systems may perform better than gram-positive IPTG-inducible promoters (8). The Bce promoter, exhibiting similar behavior to those used in existing expression systems, expands the options for protein expression in gram-positive bacteria.

Interestingly, neither bacitracin-induced nor IPTG-induced Bce protein contained undecaprenyl pyrophosphate. While the results with the IPTG induced protein are likely explained by poor sample quality, the bacitracin protein is more challenging to interpret. Undecaprenyl pyrophosphate is required for bacitracin induction of Bce signaling and expression, so how could significant quantities of BceAB be produced without this lipid? One

possibility is that UPP is lost during solubilization of BceAB from the cell membranes, which is done in absence of bacitracin. This may also explain the results with the IPTG-induced protein, which was never exposed to bacitracin. Future preparations of BceAB from *B. subtilis* could include bacitracin during membrane solubilization to try to increase the amount of undecaprenyl pyrophosphate captured with BceAB during this critical step. Another possibility is that the presence of undecaprenyl phosphate, but not undecaprenyl pyrophosphate in *B. subtilis* BceAB indicates a new element of Bce-related resistance: dephosphorylation of lipids to remove bound AMPs and push the lipids forward through the lipid II cycle. Such a mechanism, possibly involving additional protein components, diverges significantly from the current models of Bce-mediated resistance. Confirmation of these initial mass spectrometry results with additional samples will be required to guide future work in this area.

If further exploration of the *B. subtilis* expression system by including bacitracin during protein solubilization fails to produce undecaprenyl pyrophosphate-containing BceAB, another route to an AMP-bound structure is to express the protein with bacitracin and then form a complex with an AMP such as laspartomycin C which is known to bind undecaprenyl monophosphate (9). Alternatively, it may be possible to develop modified *E. coli* lacking the ability to make the arabinose lipid that often co-purifies with BceAB. In *E. coli,* arabinose is attached to undecaprenyl phosphate by the enzyme ArnC as part of a pathway leading to lipid A modification for polymyxin resistance (10). Deletion of *arnC* might allow purification of BceAB with an AMP-compatible lipid. One potential challenge with using modified *E. coli* is that gram-negative bacteria possess lower (~10-fold less) levels of lipid II intermediates compared to gram-positive bacteria, limiting opportunities for overexpressed BceAB to encounter its substrate (11).

Finally, these initial *B. subtilis* expression experiments have focused on the production of BceAB without BceS. Since BceS is under a low-level constitutive promoter, producing the full BceABS complex for structural studies in *B. subtilis* would require changing to an inducible promoter, likely the IPTG-inducible $P_{hyspank}$. Using the IPTG-inducible system may be preferable to the bacitracin-induction system because of the feedback built into the Bce system. While additional optimization may be required to purify the BceABS complex from *B. subtilis*, this work may allow capture of the complex in new conformations to elucidate how signaling is initiated in the Bce module.

REFERENCES

1. Popp, P. F., Dotzler, M., Radeck, J., Bartels, J. & Mascher, T. The Bacillus BioBrick Box 2.0: expanding the genetic toolbox for the standardized work with Bacillus subtilis. *Sci Rep-uk* **7**, 15058 (2017).

2. Fritz, G. *et al.* A New Way of Sensing: Need-Based Activation of Antibiotic Resistance by a Flux-Sensing Mechanism. *Mbio* **6**, e00975-15 (2015).

3. Storm, D. R. & Strominger, J. L. Complex Formation between Bacitracin Peptides and Isoprenyl Pyrophosphates THE SPECIFICITY OF LIPID-PEPTIDE INTERACTIONS. *J Biol Chem* **248**, 3940–3945 (1973).

4. Fang, C., Stiegeler, E., Cook, G. M., Mascher, T. & Gebhard, S. Bacillus subtilis as a Platform for Molecular Characterisation of Regulatory Mechanisms of Enterococcus faecalis Resistance against Cell Wall Antibiotics. *Plos One* **9**, e93169 (2014).

5. Toymentseva, A. A., Schrecke, K., Sharipova, M. R. & Mascher, T. The LIKE system, a novel protein expression toolbox for Bacillus subtilis based on the liaI promoter. *Microb Cell Fact* **11**, 143–143 (2012).

6. Zhou, X. X., Li, W. F., Ma, G. X. & Pan, Y. J. The nisin-controlled gene expression system: Construction, application and improvements. *Biotechnol Adv* **24**, 285–295 (2006).

7. Bongers, R. S., Veening, J.-W., Wieringen, M. V., Kuipers, O. P. & Kleerebezem, M. Development and Characterization of a Subtilin-Regulated Expression System in Bacillus subtilis : Strict Control of Gene Expression by Addition of Subtilin. *Appl. Environ. Microbiol.* **71**, 8818–8824 (2005).

8. Vavrová, Ľ., Muchová, K. & Barák, I. Comparison of different Bacillus subtilis expression systems. *Res Microbiol* **161**, 791–797 (2010).

9. Diehl, A., Wood, T. M., Gebhard, S., Martin, N. I. & Fritz, G. The Cell Envelope Stress Response of Bacillus subtilis towards Laspartomycin C. *Antibiotics* **9**, 729 (2020).

10. Breazeale, S. D., Ribeiro, A. A., McClerren, A. L. & Raetz, C. R. H. A Formyltransferase Required for Polymyxin Resistance in Escherichia coli and the Modification of Lipid A with 4-Amino-4-deoxy-l-arabinose IDENTIFICATION AND FUNCTION OF UDP-4-DEOXY-4-FORMAMIDO-l-ARABINOSE. *J Biol Chem* **280**, 14154–14167 (2005).

11. Piepenbreier, H., Diehl, A. & Fritz, G. Minimal exposure of lipid II cycle intermediates triggers cell wall antibiotic resistance. *Nat Commun* **10**, 2733 (2019).